Physics – Uspekhi **40** (5) 445 – 476 (1997)

REVIEWS OF TOPICAL PROBLEMS PACS numbers: **71.27.+a**, **74.90.+n**, 75.10.Lp

Strongly correlated electrons: the $t-J$ model

Yu A Izyumov

Contents

Abstract. **A systematic study is made of the $t-J$ model as a working model for copper oxide high-T_c superconductors. The main focus is on the near-half-filling region (low hole concentrations) relevant to these materials. The theory of the magnetic polaron, which is a charge carrier traveling in an antiferromagnetic matrix, and the theory of antiferromagnetic ordering are discussed in a unified framework. The spin liquid state beyond the antiferromagnetic phase is examined. The Hamiltonian parameters – hole concentration phase diagram for the model is described and compared with that for the Hubbard model in the strong correlation limit. Two extensions of the $t-J$ model, the $t-t'-J$ model and the three-center interaction model, are discussed. Mostly analytic strong correlation techniques are employed in this review.**

Yu A Izyumov Institute of Metal Physics, Ural Division, Russian Academy of Sciences, ul. S Kovalevskoĭ 18, 620219 Ekaterinburg, Russia
Tel. (7-3432) 74 41 93
Fax (7-3432) 74 52 44
E-mail: izyumov@ifm.e-burg.su

Received 30 September 1996
Uspekhi Fizicheskikh Nauk **167** (5) 465 – 497 (1997)
Translated by E M Yankovsky; edited by S N Gorin

1. Introduction

1.1 Two fundamental models in the theory of strongly correlated systems

For more than thirty years the Hubbard model [1] was the main model in the theory of metallic magnetic materials. Initially it was introduced to describe magnetism in transition d metals and their compounds in an effort to overcome the contradictions between the itinerant (band) nature of d electrons and the presence of localized magnetic moments in such systems. Actually, as was shown by Hubbard [2], the applicability range of the model proved to be much broader: the model made it possible, among other things, to describe the metal – insulator phase transition initiated by changes in the Hamiltonian parameters. The simplest single-band Hubbard model contains two such parameters: the width W of the initial band and the magnitude U of the Coulomb repulsion between two electrons at the same site. It occurred that for sufficiently large $U \geqslant U_c \sim W$ the ground state of the system is an insulator state, while for $U < U_c$ it is a metallic state. The reason is that for large U the appearance of two electrons at the same site is energetically unfavorable and the initial band splits into two Hubbard sub-bands with a gap at the band center. Thus, when the band is half-filled, the Fermi level is in the gap, and the ground state is an insulator state. The electrons become localized at the lattice sites and behave like localized magnetic moments with spin $S = 1/2$. An indirect exchange interaction arises between

such electrons, so that the system in the insulator state is an antiferromagnet.

Of course, at deviations from the half-filled state of the band the system acquires finite conductivity, but clearly, there exists a strong interaction between the charge carriers and the magnetic order, which may initiate deviations from the Fermi-liquid behavior of the electron system. All these effects — the metal–insulator phase transition, the emergence of localized magnetic moments, and the deviations from the Fermi-liquid behavior — are manifestations of strong correlations existing in the system, i.e., the tendency of electrons to avoid each other. Systems with $U \gtrsim W$ have become known as strongly correlated electron systems (SCES). The described behavior of the system with the variation of the on-site Coulomb repulsion has been corroborated by theoretical work on the Hubbard model (see Ref. [3]), and the interested reader can find the analysis of the properties of narrow-band magnetic materials based on this model in many sources (e.g., see Ref. [4]).

The success of the Hubbard model is due to its simplicity, and at the same time, to its rich content. The model Hamiltonian can be estimated by the criterion usually applied to true works of art: 'it contains everything that is needed and nothing superfluous'. Indeed, the Hamiltonian

$$H = -t\sum_{ij\sigma} C_{i\sigma}^{\dagger} C_{j\sigma} + U\sum_{i} n_{i\uparrow} n_{i\downarrow} \qquad (1.1)$$

contains a kinetic term describing the electron motion from site to site and the energy of repulsion at a single site. Here $C_{i\sigma}$ ($C_{i\sigma}^{\dagger}$) is the Fermi annihilation (creation) operator for an electron at site i with spin σ, and $n_{i\sigma} = C_{i\sigma}^{\dagger} C_{i\sigma}$ is the number of electrons at a site with a given spin. The kinetic term is written in the nearest-neighbor approximation for the transition matrix element, so that in this case the initial-band width is $W = 2zt$, where z is the number of nearest neighbors.

In the limit $U \gg W$ in second-order perturbation theory in W/U, we obtain (see Section 2.1) the following effective Hamiltonian:

$$H = -t\sum_{ij\sigma}(1 - n_{i\bar{\sigma}}) C_{i\sigma}^{\dagger} C_{j\sigma}(1 - n_{j\bar{\sigma}}) + J\sum_{ij} \mathbf{S}_i \mathbf{S}_j\,, \qquad (1.2)$$

where $J = 2t^2/U$ is the indirect exchange integral [5], and $n_i = \sum_{\sigma} n_{i\sigma}$ is the number of electrons at site i. The factors $1 - n_{i\bar{\sigma}}$ reflect the fact that an electron with spin σ is forbidden to be at a site with another electron (with spin $\bar{\sigma} \equiv -\sigma$). Thus, the Hubbard model in the $U \gg W$ limit describes the motion of electrons from one unoccupied site to another. The exclusion of states with electron pairs at a site ('doublons') is, in effect, equivalent to the appearance of an indirect exchange interaction of electrons at neighboring sites with an exchange integral of the antiferromagnetic sign.

The model with Hamiltonian (1.2) is the famous t–J model. It is the limiting case of the Hubbard model with $U \gg W$, but it is sometimes regarded (without the $-n_i n_j/4$ term) as a separate phenomenological model, in which the parameters t and J are independent. The model was developed to describe electron motion in an antiferromagnetic matrix. It has gained popularity in recent years after Anderson [6] suggested that the electron properties of high-T_c superconductors of the metal-oxide group are described by Hamiltonian (1.2). To see that this is indeed the case we must discuss in detail the electron structure of high-T_c compounds.

1.2 t–J Model as the basic electron model for high-T_c superconductors of the copper-oxide group

An important structural element of all high-T_c copper-oxide compounds are the CuO_2 planes, with which the superconducting properties are associated. Depending on composition, the unit cell of a high-T_c compound may contain one, two, or three such planes, with the transition temperature (the highest T_c for the given class of compounds) increasing with the number of these planes. The distance between neighboring planes is much greater than the spacing between the nearest-neighbor copper atoms in a plane, which is the cause of a large anisotropy in the properties, including the superconducting properties. In particular, the correlation length ξ (the size of the Cooper pair) in the plane is severalfold larger than the same quantity in the direction perpendicular to the plane (e.g., see Ref. [7]). A unique feature of these materials is the very small value of ξ. For instance, inside a plane ξ is three to four times larger than the lattice parameter, while in the perpendicular direction it is smaller than the distance between the planes. This suggests that the charge carriers within a plane are strongly isolated from those in other planes and that the electronic states in such planes are two-dimensional.

All electronic properties are strongly dependent on doping. For two classes of compounds, the lanthanum system ($La_{2-x}Sr_xCuO_{4-y}$) and the yttrium–barium system ($YBa_2Cu_3O_{6+x}$), the transition temperature T_c and other physical characteristics depend on the strontium or oxygen content. What is remarkable is that the initial systems without dopants, La_2CuO_4 and $YBa_2Cu_3O_6$, are insulators and antiferromagnets. As the concentration x grows, the Néel temperature T_N sharply drops, and the substances become metals, although their conductivity is poor. Superconductivity emerges at higher values of x, outside the magnetically ordered phase (Figs 1 and 2). Measurements of the Hall constant show that the charge carriers are holes in all classes of high-T_c compounds with the exception of the neodymium system, where electrons are the charge carriers. It has been established that the holes emerging as a result of doping are formed in the CuO_2 planes at copper and oxygen atoms, and it is these holes that are the charge carriers.

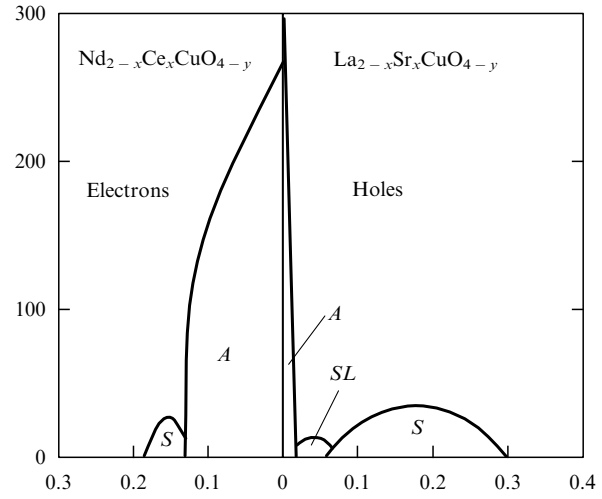

Figure 1. Phase diagram for the lanthanum and neodymium systems in high-T_c materials. The phases are denoted as follows: A is the antiferromagnetic phase, S is the superconducting phase, and SL is the spin-liquid phase.

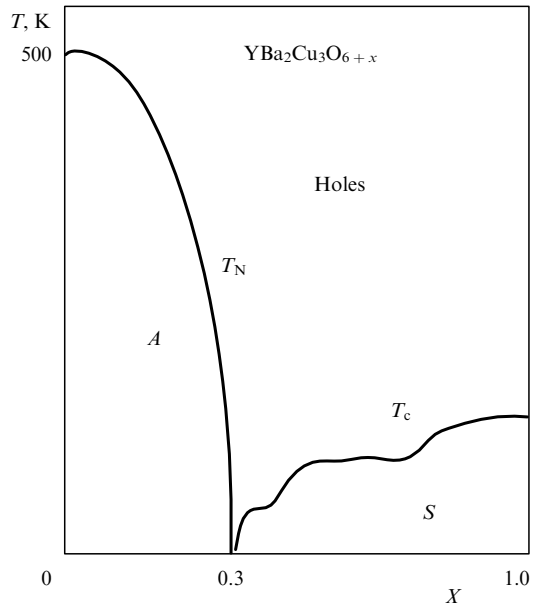

Figure 2. Phase diagram for the yttrium – barium system.

Lately an important problem in this field of research has been resolved: high-T_c superconductivity in compounds of the metal-oxide group has been found to be related to certain features in the behavior of such systems in the normal phase. These features consist in the deviation of the electron properties from those of a Fermi liquid. It appears that the magnetic susceptibility and the Hall constant are temperature-dependent, contrary to the predictions of the theory of an ordinary Fermi liquid. Moreover, all classes of high-T_c materials with hole conductivity and compositions that allow high-T_c superconductivity exhibit a linear growth of the electrical conductivity with T within a broad temperature range above T_c.

As the phase diagrams in Figs 1 and 2 show, the superconducting state emerges near the antiferromagnetic phase. In the yttrium – barium system the regions of antiferromagnetism and superconductivity are adjacent, while in the lanthanum system the two are separated by a region without long-range magnetic order but with strong quantum fluctuations. This region became known as the spin-liquid region. We observe, therefore, the ordinary interrelationship between magnetic order and superconductivity: the two avoid each other. At the same time, experiments in inelastic magnetic scattering of neutrons in the lanthanum and yttrium – barium systems indicate that there are strong magnetic fluctuations for a broad range of doping levels outside the antiferromagnetic phase, a range that even penetrates the superconducting-phase region. This, obviously, is an indication of how important antiferromagnetic fluctuations are in the mechanism of high-T_c superconductivity.

Comparing these features of high-T_c materials with what was said in Section 1.1 about the Hubbard model, we see that the model has the potential to describe the main electronic properties of high-T_c compounds. The estimates of the parameters U and W extracted from the experimental data on high-T_c compounds show that we are dealing with strong correlations, $U \gg W$, so that the $t-J$ model with Hamiltonian (1.2) can be applied to such materials (Anderson was the first to point out this possibility). Understanding the properties of high-T_c materials requires studying the two-dimensional $t-J$ model near the half-filled band state. This explains the huge body of theoretical research in this field (several hundred papers devoted to this problem have been published since 1987).

The case of a half-filled band [meaning the band corresponding to the model Hamiltonian (1.2)] leads to an insulator state with localized magnetic moments ($S = 1/2$) corresponding to the d^9 state of the copper ions in the CuO_2 planes. Upon doping, a fraction of the copper atoms lose one electron each, so that hole type charge carriers are created. Strictly speaking, holes are created upon doping not only at copper atoms but also at oxygen atoms. These holes form what is known as Zhang – Rice singlets [8] centered at copper sites, and it is such singlets that Hamiltonian (1.2) of the $t-J$ model refers to, so that the $C_{i\sigma}$ and $C_{i\sigma}^{\dagger}$ operators annihilate and create such a singlet at site i.

1.3 Difficulties encountered in theoretical studies of the $t-J$-model

Despite the simple structure of Hamiltonian (1.2), what complicates matters considerably is the presence of the factors $1 - n_{i\bar{\sigma}}$ in the kinetic term, factors that exclude 'doublons' from the picture. Although the exchange term is small compared to the kinetic term (because $J/t \sim t/U \ll 1$), it is difficult to use the latter as a zeroth approximation since there are no known approaches to solving this problem even in the $U \to \infty$ limit. For this reason the literature contains a large number of papers devoted to various methods of reducing the problem to simplified models, but the validity of these methods is questionable (or at least is not obvious). The kinetic term in (1.2) can be expressed in terms of the operators $X_i^{\sigma 0} \equiv C_{i\sigma}^{\dagger}(1 - n_{i\bar{\sigma}})$ and $X_i^{0\sigma} \equiv C_{i\sigma}(1 - n_{i\bar{\sigma}})$, which coincide with the ordinary Fermi operators only at sites without a second electron. The numerous attempts to calculate the various physical properties in the $t-J$ model, such as the elementary excitation spectrum, the density of states, and the characteristics of the magnetic states of the system, are associated with the representation of the X operators, with their complicated commutation relations, by products of Fermi and Bose operators with simple commutation relations. This method became known as the auxiliary boson or fermion method. The price for introducing the well-known second-quantization Fermi and Bose operators is extremely high: one must allow for certain constraints to ensure that the appearance of unavoidable non-physical states is excluded. Physically the constraints are equivalent to the initial condition of exclusion of 'doublon' states. Thus, the auxiliary particle method shifts the initial difficulties of the problem to another place, and sometimes this proves useful. Because such a representation of X operators lacks uniqueness, it is difficult to compare the results and to estimate the adopted approximation.

This explains the presence of other approaches to solving the same problems. Among these are the mean-field approximations, although for the $t-J$ model the formulation of such an approach is not as trivial (in view of the specific features of the Hamiltonian) as it is for ordinary Fermi systems with a weak Coulomb interaction. In this situation numerical methods of the quantum Monte Carlo (QMC) type or the exact diagonalization of small clusters become important. In the most important two-dimensional case modern computers can perform such calculations well. It appears that small

clusters (e.g., 4×4) provide stable results with an increasing number of sites in the cluster, so that they reflect the physics of an infinite lattice. The numerical methods used in studying the $t-J$ model, on the one hand, are extremely informative, and on the other, make it possible to monitor the approximations in analytic calculations. As a result, there has been considerable progress in understanding the physics of systems described by the $t-J$ model.

But what quantities must one calculate in the $t-J$ model and what problems must the model solve? The central problem is finding the quasiparticle spectrum. Since low hole concentrations are important, the problem reduces to that of a single hole moving in an antiferromagnetic matrix. Since, as noted earlier, there is strong interaction between the charge and spin degrees of freedom, a hole distorts the antiferromagnetic structure within a certain neighborhood of radius R_p. Long-range magnetic order disappears if the distorted regions associated with different holes overlap. Here the critical hole concentration δ_c can easily be estimated: for a two-dimensional lattice, obviously, $\delta_c \sim a^2/R_p^2$, where a is the lattice parameter. Figures 1 and 2 show that for high-T_c materials the antiferromagnetic phase occupies a small region, with the result that $\delta_c \ll 1$, which implies that R_p amounts to several lattice parameters. The above reasoning implies that the charge carrier in the $t-J$ model near half-filling can only be a complex particle such as a hole surrounded by a region of destroyed antiferromagnetic order, or a magnetic polaron. The detailed theoretical analysis in Sections 3 and 4 supports this picture and gives all the quasiparticle characteristics: the dispersion law, the damping, and the spatial size R_p. The reader will also see that the structure of the quasiparticle states is closely related to that of the antiferromagnetic phase at a given hole concentration. The objective of the theory is to calculate the critical concentration δ_c and the Néel temperature T_N as functions of the hole concentration. Section 5 is devoted to this aspect of the problem. Analysis becomes difficult when one examines the region $\delta > \delta_c$, where antiferromagnetic correlations are absent and the spin-liquid state sets in. What is needed here is an approach based on the theory of gage fields (Section 6). Finally, in Section 7 we briefly discuss the general structure of the phase diagram for the $t-J$ model and compare it with that of the phase diagram for the Hubbard model in the $U \gg W$ limit. This, in a nutshell, is the plan of the review.

The reader could notice that the superconductivity aspects of the model are ignored entirely. The earlier approaches to this problem can be found in review [9]. Since that review was published, there has been considerable progress in understanding the problem and the role that spin fluctuations play in the formation of high-T_c superconductivity. This requires a separate review. The reader must bear in mind that the research in superconductivity is based on studies of the properties of the $t-J$ model in the normal phase. The present review generalizes the results of this research.

Another aspect worth noting is that the present review does not touch on approaches based on numerical methods, since there is a comprehensive review [7] specially devoted to this problem, a review that also compares in detail the theoretical results and the experimental data on high-T_c compounds, and the interested reader is advised to study that review. We note once more that our goal was to describe the studies of the $t-J$ model by analytic methods, just as we did in the case of the Hubbard model in review [3]. Together the two reviews, [3] and the present one, make it possible to determine the status of current studies of the problem of strongly correlated systems.

2. Formulation of the model

2.1 Deriving the $t-J$-model Hamiltonian from the Hubbard-model Hamiltonian

The $t-J$ model was proposed in Refs [10–12], and the effective Hamiltonian (1.2) was derived by a number of researchers (see Refs [11,12]) from the Hubbard Hamiltonian in the $U \gg W$ limit. Thus, the two energy parameters in the $t-J$ model obey the following inequality: $J \ll t$. Below we derive the Hamiltonian of the $t-J$ model by a new method, which clarifies the position of the model in the hierarchy of models of the SCES theory.

A convenient formalism in the $U \gg W$ limit is that of Hubbard X operators [13]. The operator X_i^{pq} is specified at each site and describes the transitions between the four possible states $|\sigma\rangle$, $|2\rangle$, and $|0\rangle$ with a single electron at a site (with spins $\sigma = \uparrow, \downarrow$), with two electrons, and without an electron, respectively. The ordinary electron operators are linear combinations of two Fermi X operators:

$$C_{i\sigma}^{\dagger} = X_i^{\sigma 0} + \sigma X_i^{2\bar{\sigma}}, \qquad C_{i\sigma} = X_i^{0\sigma} + \sigma X_i^{\bar{\sigma}2}. \tag{2.1}$$

We see that a single-particle state is formed via the creation of an electron from the vacuum state or the appearance of a second electron at a site that already contains an electron. The operators $X_i^{\sigma 0}$ and $X_i^{2\sigma}$ generate one- and two-electron states, and these states form the upper and lower Hubbard subbands, respectively. The X operators can be expressed in terms of the electron operators as follows:

$$\begin{aligned}
&X_i^{\sigma 0} = C_{i\sigma}^{\dagger}(1 - n_{i\bar{\sigma}}), \qquad X_i^{2\sigma} = \sigma C_{i\bar{\sigma}}^{\dagger} n_{i\sigma},\\
&X_i^{\sigma\bar{\sigma}} = C_{i\sigma}^{\dagger} C_{i\bar{\sigma}}, \qquad X_i^{20} = \sigma C_{i\bar{\sigma}}^{\dagger} C_{i\sigma}^{\dagger},\\
&X_i^{00} = (1 - n_{i\uparrow})(1 - n_{i\downarrow}),\\
&X_i^{\sigma\sigma} = n_{i\sigma}(1 - n_{i\bar{\sigma}}), \qquad X_i^{22} = n_{i\uparrow} n_{i\downarrow}.
\end{aligned} \tag{2.2}$$

The above formulas make it possible to derive the effective model Hamiltonian in the $U \gg W$ limit when the Coulomb term is taken as the zeroth-order Hamiltonian and the kinetic term is considered a perturbation. In terms of the X operators, the Hubbard model Hamiltonian (1.1) can be written as the sum of three terms:

$$\begin{aligned}
H = H_1 + H_1' + H_0 \equiv &-t \sum_{ij\sigma} \left(X_i^{\sigma 0} X_j^{0\sigma} + X_i^{2\bar{\sigma}} X_j^{\bar{\sigma}2} \right)\\
&- t \sum_{ij\sigma} \sigma \left(X_i^{\sigma 0} X_j^{\bar{\sigma}2} + X_i^{2\bar{\sigma}} X_j^{0\sigma} \right) + U \sum_i X_i^{22}.
\end{aligned} \tag{2.3}$$

Let us now apply a canonical transformation to the Hamiltonian,

$$H \to \tilde{H} = e^S H e^{-S} = H + [S, H] + \frac{1}{2}[S, [S, H]] + \ldots$$

with the operator

$$S = \xi \sum_{ijs} s \left(X_i^{s0} X_j^{\bar{s}2} - X_i^{2\bar{s}} X_j^{0s} \right)$$

containing an arbitrary parameter ξ. The parameter is fixed by the condition that

$$H_1' + [S, H_0] = 0$$

which excludes all band-to-band terms from the Hamiltonian; this yields $\xi = -t/U$. Since we have adopted the condition that $U \gg W$, we can limit ourselves to the terms in the Hamiltonian that are second-order in t/U, with the result that

$$\tilde{H} = H_0 + H_1 + [S, H_1] + \frac{1}{2}[S, H_1'] .$$

Calculating the commutators, we see that the term $[S, H_1]$ allows for band-to-band transitions only in the second order in t/U, and can be discarded. Thus, we arrive at the following effective Hamiltonian:

$$\tilde{H} = -t\sum_{ij\sigma} X_i^{\sigma 0} X_j^{0\sigma} + \frac{t^2}{U}\sum_{ij\sigma}(X_i^{\sigma\bar{\sigma}} X_j^{\bar{\sigma}\sigma} - X_i^{\sigma\sigma} X_j^{\bar{\sigma}\bar{\sigma}}) + \frac{t^2}{U}\sum_{ijl\sigma}(X_i^{\bar{\sigma}0} X_l^{\sigma\bar{\sigma}} X_j^{0\sigma} - X_i^{\sigma 0} X_l^{\bar{\sigma}\bar{\sigma}} X_j^{0\sigma}) + H_2 , \quad (2.4)$$

where H_2 is the part of the Hamiltonian that allows for states with two electrons at a site:

$$H_2 = U\sum_i X_i^{22} - t\sum_{ij\sigma} X_i^{2\bar{\sigma}} X_j^{\bar{\sigma}2} . \quad (2.5)$$

The second term in (2.4) can be expressed in terms of the spin operator $\mathbf{S}_i$,

$$\mathbf{S}_i = \frac{1}{2}\sum_{\sigma\sigma'} C_{i\sigma}^{\dagger} \boldsymbol{\tau}_{\sigma\sigma'} C_{i\sigma'} , \quad (2.6)$$

where $\boldsymbol{\tau}$ is a vector composed of Pauli matrices. In particular, for the circular $S_i^{\pm} = S_i^x \pm iS_i^y$ and longitudinal S_i^z projections of the spin vector we have

$$S_i^+ = C_{i\uparrow}^{\dagger} C_{i\downarrow} = X_i^{+-}, \qquad S_i^- = C_{i\downarrow}^{\dagger} C_{i\uparrow} = X_i^{-+} ,$$
$$S_i^z = \frac{1}{2}(C_{i\uparrow}^{\dagger} C_{i\uparrow} - C_{i\downarrow}^{\dagger} C_{i\downarrow}) = \frac{1}{2}(X_i^{++} - X_i^{--}) . \quad (2.7)$$

Thus, the effective Hamiltonian (2.4) can be written as

$$\tilde{H} = -t\sum_{ij\sigma} X_i^{\sigma 0} X_j^{0\sigma} + J\sum_{ij}\left(\mathbf{S}_i\mathbf{S}_j - \frac{1}{4} n_i n_j\right) + \frac{1}{2} J\sum_{ijl\sigma}(X_i^{\bar{\sigma}0} X_l^{\sigma\bar{\sigma}} X_j^{0\sigma} - X_i^{\sigma 0} X_l^{\bar{\sigma}\bar{\sigma}} X_j^{0\sigma}) + H_2 , \quad (2.8)$$

where $J = 2t^2/U$ is the effective exchange integral, and $n_i = n_{i\uparrow} + n_{i\downarrow}$ is the operator of the number of electrons at site i.

The sum of the first two terms on the right-hand side of Eqn (2.8) comprises the Hamiltonian of the $t-J$ model. Thus, going from the effective Hamiltonian (2.8) to that of the $t-J$ model requires dropping the term H_2 (i.e., projecting the Hamiltonian onto the lower Hubbard sub-band) and ignoring the term that depends on three sites. Note that in the three-site term the sites i and j are the nearest neighbors of the third site l but are not necessarily each other's nearest neighbors. The triple term describes a transition from site i to site j with or without an electron spin flip, with an electron spin flip at the third site l in the first case or without a spin flip in the second. In such transitions the matrix element is not t but a much smaller quantity of order t^2/U.

Thus, projecting the effective Hamiltonian (2.8) onto the space of states describing the lower Hubbard sub-band and discarding the triple term, we arrive at the Hamiltonian

$$H = -t\sum_{ij\sigma} X_i^{\sigma 0} X_j^{0\sigma} + J\sum_{ij}\left(\mathbf{S}_i\mathbf{S}_j - \frac{1}{4} n_i n_j\right) . \quad (2.9)$$

In deriving this Hamiltonian we imposed no restrictions on the electron concentration. For an almost half-filled band, we have $\langle n_i \rangle \approx 1$, and the $n_i n_j$ in (2.9) is often dropped. There is also another way of writing Hamiltonian (2.9) in which, instead of spin operators, only X operators are used:

$$H = -t\sum_{ij\sigma} X_i^{\sigma 0} X_j^{0\sigma} + \frac{1}{2} J\sum_{ij\sigma}(X_i^{\sigma\bar{\sigma}} X_j^{\bar{\sigma}\sigma} - X_i^{\sigma\sigma} X_j^{\bar{\sigma}\bar{\sigma}}) . \quad (2.10)$$

This is exactly the sum of the first two terms on the right-hand side of expression (2.4) for the effective Hamiltonian.

2.2 Representation in terms of auxiliary particles

Since X operators obey complicated commutation relations, there have been many attempts to represent them in the form of a product of ordinary Fermi and Bose creation and annihilation operators, e.g., $X_i^{0\sigma} = f_i b_{i\sigma}$. This provides a number of technical advantages but introduces a considerable difficulty, namely, the need to allow for constraints that ensure the absence of non-physical states unavoidably introduced by these representations. Such representations are ambiguous and are classified primarily by the operator to which the spin label of the X operator representing the creation and annihilation of a physical electron is attached. If the spin label is attached to a Bose operator, the corresponding representation is called a slave-fermion representation, while if the label is attached to a Fermi operator, the representation is called slave-boson.

Note, for the sake of reference, that in addition to the mentioned slave-fermion [14–17] and slave-boson [15–19] representations, a number of new representations [20–27] have lately been proposed. For instance, Chang [25] introduced a representation that employs, in addition to slave-fermion and slave-boson operators, the Goldstein–Primakoff representation well-known in the theory of magnetism. Le Guillou and Ragoucy [26] did a special study of the problem of the sum rules that are valid for different types of representation. Other representations have been employed, and we consider these below. The ambiguity in representing the X operators by Fermi and Bose operators reflects the multitude of representations of the algebra of X operators and the reason why it is often difficult to verify the validity of the various representations.

Of special interest is the slave-fermion representation in which the spin operator for $S = 1/2$ is used instead of the Bose operators. The first to suggest such an approach were Richard and Yushankhai [20], and their results were improved in Refs [21–24] by a rigorous derivation of the Hamiltonian of the $t-J$ model in this new representation. Since we use this approach in analyzing the magnetic-polaron problem, let us discuss it in greater detail. The idea consists in the following. When a band is half-filled, all sites have localized electrons with spin $S = 1/2$; however, in the

presence of holes one can expect that $S = 0$ at some sites. Therefore, we have a lattice filled by spins of different magnitudes. This fact can be expressed by the following equality for the number of electrons at a site, which is either 0 or 1:

$$C_{i\uparrow}^{\dagger} C_{i\uparrow} + C_{i\downarrow}^{\dagger} C_{i\downarrow} = 1 - h_i^{\dagger} h_i \,, \tag{2.11}$$

where $h_i^{\dagger} h_i$ is the operator of the number of holes (unoccupied sites), whose eigenvalues are 0 and 1. Actually the operators $S_i^{\pm}$ and S_i^z in (2.7) are not spin operators, since although they obey the same commutation relations as spin operators

$$\left[S_i^+, S_j^-\right] = 2S_i^z \delta_{ij}, \qquad \left[S_i^z, S_j^{\pm}\right] = \pm S_i^{\pm} \delta_{ij} \,, \tag{2.12}$$

they do not yield a correct expression for the square of spin:

$$\mathbf{S}_i \mathbf{S}_i = \frac{3}{4}(n_{i\uparrow} + n_{i\downarrow} - n_{i\uparrow} n_{i\downarrow}) \approx \frac{3}{4}(n_{i\uparrow} + n_{i\downarrow}) = \frac{3}{4}(1 - h_i^{\dagger} h_i) \,.$$

This combination is equal to 3/4 for a site occupied by a single electron and to 0 for a site carrying a hole. In other words, Eqns (2.7) define spin operators with a variable value of S, equal to 1/2 or 0. At the same time, we can introduce spin operators $\mathbf{s}_i$ with $s = 1/2$ for each site (we call these pseudospin operators). Since for these operators we can always write $\mathbf{s}_i \mathbf{s}_i = 3/4$, the following relationship exists between the operators of the physical spin $\mathbf{S}_i$ and the pseudospin $\mathbf{s}_i$:

$$\mathbf{S}_i = \mathbf{s}_i (1 - h_i^{\dagger} h_i) \,, \tag{2.13}$$

where the Fermi operators h_i and $h_i^{\dagger}$ commute with the operators $\mathbf{s}_i$. In view of the projection properties of the operator $(1 - h_i^{\dagger} h_i)^2 = 1 - h_i^{\dagger} h_i$, the commutation relations (2.12) for the spin are also valid here.

The kinetic term in Hamiltonian (2.9) can be expressed in terms of the Fermi hole operators and the pseudospin operators. As a result, the Hamiltonian of the t–J model, (1.2) or (2.9), in the new representation assumes the form

$$H = t \sum_{ij} 2 h_i^{\dagger} h_j \left(\mathbf{s}_i \mathbf{s}_j + \frac{1}{4}\right) + J \sum_{ij} (1 - h_i^{\dagger} h_i) \left(\mathbf{s}_i \mathbf{s}_j - \frac{1}{4}\right) (1 - h_j^{\dagger} h_j) \,. \tag{2.14}$$

It describes the interaction of holes and pseudospins. In contrast to the initial Hamiltonian (1.2), a pseudospin of magnitude $s = 1/2$ is placed at each site. In representation (2.14), the spin and charge degrees of freedom are separated. This representation proves convenient in discussing the aspects of the interaction of the charge carriers in the model and the various states of the spin system. Note that Hamiltonian (2.14) was introduced by Wang and Rice [21], and was postulated earlier by Khaliullin [22].

Hamiltonian (2.14) describes the t–J model for $n < 1$, when the lower Hubbard sub-band is less than half-filled and holes are the carriers. For $n > 1$ the upper sub-band begins to fill, and the electrons which fill it serve as carriers. The number of electrons at a site is given by the following relationship:

$$C_{i\uparrow}^{\dagger} C_{i\uparrow} + C_{i\downarrow}^{\dagger} C_{i\downarrow} = 1 + d_i^{\dagger} d_i \,, \tag{2.15}$$

where d_i is the Fermi operator generating a state with two electrons at a site. In this case the physical spin $\mathbf{S}_i$ is related to the pseudospin $\mathbf{s}_i$ as follows: $\mathbf{S}_i = (1 - d_i^{\dagger} d_i)\mathbf{s}_i$. Here, instead of (2.14), we have the Hamiltonian

$$H = -t \sum_{ij} 2 d_i^{\dagger} d_j \left(\mathbf{s}_i \mathbf{s}_j + \frac{1}{4}\right) + J \sum_{ij} (1 - d_i^{\dagger} d_i) \left(\mathbf{s}_i \mathbf{s}_j - \frac{1}{4}\right) (1 - d_j^{\dagger} d_j) \,. \tag{2.16}$$

The difference in the sign in front of the first term on the right-hand sides of Eqns (2.14) and (2.16) reflects the electron – hole symmetry of the Hubbard model.

Recently Wang [23] developed a slave-fermion representation for the total Hubbard Hamiltonian (1.1). In this case, in addition to the hole creation operators $h_i^{\dagger}$, one must introduce the 'doublon' creation operators $d_i^{\dagger}$. The Hamiltonian has the form of [23]

$$\begin{aligned} H = {} & t \sum_{ij} 2 h_i^{\dagger} h_j (1 - d_i^{\dagger} d_i)(1 - d_j^{\dagger} d_j) \left(\mathbf{s}_i \mathbf{s}_j + \frac{1}{4}\right) \\ & - t \sum_{ij} 2 d_i^{\dagger} d_j (1 - h_i^{\dagger} h_i)(1 - h_j^{\dagger} h_j) \left(\mathbf{s}_i \mathbf{s}_j + \frac{1}{4}\right) \\ & + U \sum_i d_i^{\dagger} d_i - t \sum_{ij} (1 - d_i^{\dagger} d_i)(1 - h_j^{\dagger} h_j) \\ & \times (e_i d_j P_{ij} + d_j^{\dagger} e_i^{\dagger} P_{ij}^{\dagger}) \,, \end{aligned} \tag{2.17}$$

where

$$P_{ij} = \left(\frac{1}{2} + s_i^z\right) s_j^- + \left(\frac{1}{2} - s_j^z\right) s_i^+ - \left(\frac{1}{2} + s_j^z\right) s_i^- - \left(\frac{1}{2} - s_i^z\right) s_j^+ . \tag{2.18}$$

Note that (2.17) is invariant with respect to time reversal, since in this case $s_i^z \to -s_i^z$ and $s_i^{\pm} \to -s_i^{\mp}$.

In contrast to the other slave-fermion [14–17] and slave-boson [18–23] representations, which require the taking into account of several complicated constraints, representation (2.17) contains only one local constraint $h_i^{\dagger} h_i d_i^{\dagger} d_i = 0$, which is automatically satisfied in the $U \gg W$ limit. Moreover, (2.17) contains no constraint on the relationship between the spin and charge degrees of freedom. In the $U \gg W$ limit one can apply a canonical transformation and readily obtain the effective Hamiltonian. For $n < 1$, we obtain Hamiltonian (2.14) of the t–J model with an additional term

$$-\frac{1}{4} J \sum_{ijl} h_i h_j^{\dagger} (1 - h_l^{\dagger} h_l) P_{il} P_{jl}^{\dagger} \,, \tag{2.19}$$

where i and j are different sites that are the nearest neighbors of site l. Clearly,

$$\begin{aligned} P_{il} P_{jl}^{\dagger} = {} & \frac{1}{4} + \mathbf{s}_i \mathbf{s}_j - \mathbf{s}_i \mathbf{s}_l - \mathbf{s}_j \mathbf{s}_l + s_j^z (s_i^+ s_l^- - s_i^- s_l^+) \\ & + s_i^z (s_l^+ s_j^- - s_l^- s_j^+) - s_l^z (s_i^+ s_j^- - s_i^- s_j^+) \,. \end{aligned} \tag{2.20}$$

The additional three-particle term in (2.20) corresponds to the three-particle term in Hamiltonian (2.8) expressed in terms of X operators. It describes the transfer of a hole between nearest neighbors. Although the corresponding matrix element $\propto J \ll t$, the importance of the triple term rapidly increases

with hole concentration. In Section 4 we use the pseudospin representation of the $t-J$ model to study the magnetic-polaron problem.

3. Hole in an antiferromagnetic matrix

3.1 The retraceable-path approximation

The problem of describing the behavior of an isolated hole in a quantum antiferromagnet was formulated long before high-T_c compounds were discovered [28–30]. Bulaevskiĭ, Khomskiĭ, and Nagaev [28, 29] and Brinkman and Rice [30] laid the foundation for the theory of many-body quantum systems (a hole plus a Néel state of the matrix). Recent years have seen extensive research in this field. The approaches proposed in Refs [28–30] have made it possible to interpret the physics of the problem in simple terms.

Let us examine Fig. 3, which depicts the state of a system for two positions of a hole: the initial position (a) and the final position (b). When the hole travels over a distance of an integral number l of lattice parameters through the antiferromagnetic matrix, the spins form a 'wrong' pattern (in relation to the Néel state), with the result that the exchange energy of the system increases by an amount of the order of lJ. This makes the process in which the hole leaves its initial position, where the Néel order is maintained everywhere, energetically unfavorable; as a result, the hole becomes autolocalized. Figure 3 shows that the hole may be interpreted as a particle moving in a linear potential. In the continuum limit the problem reduces, obviously, to solving the Schrödinger equation for a particle in a linear potential, which is simply the Airy equation. Its eigenvalue spectrum is well-known — it consists of a system of discrete levels with separations of the order of $(J/t)^{2/3}t$ [29]. The lowest level is located near the bottom of the initial band and corresponds to the ground state of the localized hole, called a quasi-oscillator in Ref. [28]. Note that in our discussion we assume the Ising approximation of the exchange interaction to be valid, $J(\mathbf{S}_i\mathbf{S}_j) \to JS_i^zS_j^z$, which means that the ground state of the entire matrix is a Néel state. The transverse part of the exchange Hamiltonian, $J(S_i^xS_j^x + S_i^yS_j^y)$, initiates spin deviations, which allow the hole to move. Thus, a discrete quasi-oscillator level spreads out to form a band. Determining the position and width of the band, or more precisely, the dispersion law and the decay of the single-particle state, constitutes the main problem.

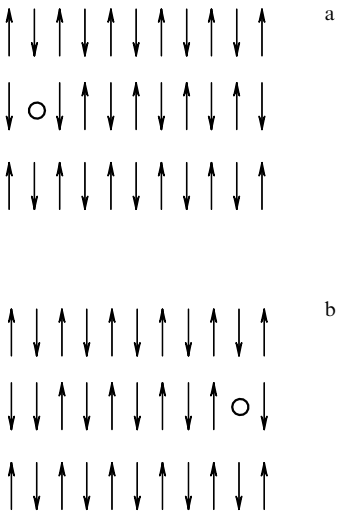

Figure 3. Motion of a hole in an antiferromagnetic matrix accompanied by violation of spin order.

Let us examine the Green's function of a hole moving in a matrix with a certain configuration of spins s (the ensemble of spins at all the lattice sites) [30]

$$G_{ij}^s(\omega) = \sum_\sigma \left\langle s \left| C_{i\sigma}^\dagger \frac{1}{\omega - H} C_{j\sigma} \right| s \right\rangle . \tag{3.1}$$

Knowing the diagonal elements, we can calculate the density of single-particle states

$$\rho^s(\omega) = -\frac{1}{\pi}\sum_i \operatorname{Im} G_{ii}^s(\omega) . \tag{3.2}$$

Employing the identity

$$\frac{1}{\omega - H} = \frac{1}{\omega}\sum_{n=0}^{\infty}\left(\frac{H}{\omega}\right)^n , \tag{3.3}$$

we can write $G_{ii}^s(\omega)$ in the form of a series

$$G_{ii}^s(\omega) = \frac{1}{\omega} + \frac{1}{\omega}\sum_{n=2}^{\infty} A_{in}^s \left(\frac{t}{\omega}\right)^n . \tag{3.4}$$

The coefficients A_{in}^s give the number of paths that the hole can follow starting from site i and hopping n times in such a way that after it returns to the initial site the spin configuration of the matrix is the same as at the beginning.

In writing (3.4) we allowed only for the kinetic term in the Hamiltonian, which corresponds to the limit $U \to \infty$. Thus, calculating the Green's function reduces to finding all the possible paths and coefficients A_{in}^s. These coefficients have long been tabulated for various types of lattices in connection with the problem of phase transitions in the Ising and Heisenberg models. Analysis of these results shows, for instance, that for a cubic lattice, self-avoiding paths, i.e., those along which the hole travels to a certain site and back (a retraceable path), contribute the most; this remains valid for any spin configuration s. The contributions from all such paths for a hypercubic lattice with z nearest neighbors to (3.4) lead to the following result [30]:

$$G_{ii}(\omega) = \frac{1}{\omega}\left\{1 - \frac{z}{2(z-1)}\left[1 - \sqrt{1 - \frac{4(z-1)t^2}{\omega^2}}\right]\right\}^{-1} . \tag{3.5}$$

This expression is real for frequencies $|\omega| > 2\sqrt{z-1}\,t \equiv \eta z t$, but in the interval

$$-zt\eta < \omega < zt\eta \tag{3.6}$$

there exists a finite density of states corresponding to a continuous spectrum. Since the frequency interval is narrower than that for free electrons, a correlation narrowing of the band occurs. This is, of course, an interesting effect, but the corresponding approximation (the retraceable-path approximation) is still purely heuristic. Recently a physical substantiation of this approximation was given in by Metzner et al. [31] in their studies of a space that in the limit has an infinite number of dimensions.

3.2 The limit of a space of infinite dimensionality

The limit $d \to \infty$ is of great importance to the SCES theory. In this limit, the equations of the theory become extremely simple and can be considered as the true-mean-field approximation for such systems (see review [3]). Methods have also been developed for obtaining systematic corrections of the order of $1/d$, which make it possible to examine systems with a finite number d of spatial dimensions. Before passing to the limit $d \to \infty$, we must first scale the parameters of the system. In particular, for Hamiltonian (1.2) of the t–J model we must put

$$t = \frac{t^*}{\sqrt{z}}\,, \qquad J = \frac{J^*}{z}\,, \tag{3.7}$$

where $t^* = \text{const}$ and $J^* = \text{const}$ [31]. For a hypercubic lattice, $z = 2d$ tends to infinity as $d \to \infty$. This scaling makes it possible to calculate the mean kinetic and exchange energies per lattice site, which remain finite as $d \to \infty$. It is well known (see [32]) that in this limit the initial electron spectrum is Gaussian, i.e.,

$$\rho(\omega) = \frac{1}{\sqrt{2\pi}t^*} \exp\left(-\frac{\omega^2}{2t^{*2}}\right). \tag{3.8}$$

The two quantities t^* and J^* serve as natural scales for the kinetic and exchange energies in the system.

Metzner et al. [31] and Strack and Vollhardt [33] used the $d \to \infty$ limit for the t–J model. The basic problem still amounts to calculating the Green's function of a hole using representation (3.4). To this end, we must calculate the contributions from the various paths along which the particles travel in the lattice. In the $d \gg 1$ limit, the various paths can be classified according to powers of $1/d$. As a result, we find that in the $d \to \infty$ limit the only graphs that survive are of the form of loop trees along which a particle can travel only once.

According to representation (3.4), the paths along which the particle travels must be such that after the particle returns to the initial point the spin configuration of the matrix does not change. It can be shown that for a Néel ground state the presence of closed loops traversed only once changes the spin configuration of the matrix, with the result that they contribute nothing to $G_{ii}(\omega)$. We are therefore left with contributions from retraceable paths. The sum of all such contributions can be written as follows (for details see [33]):

$$G_{ii}(\omega) = \cfrac{1}{\omega - t^{*2}\cfrac{1}{\omega - \cfrac{J^*}{2} - t^{*2}\cfrac{1}{\omega - 2\cfrac{J^*}{2} - t^{*2}\cfrac{1}{\omega - 3\cfrac{J^*}{2} - t^{*2}\ldots}}}}\,. \tag{3.9}$$

This non-terminating continued fraction is equivalent to the functional equation

$$G_{ii}(\omega) = \frac{1}{\omega - t^{*2}G_{ii}(\omega - J^*/2)}\,. \tag{3.10}$$

At $J^* = 0$ the equation becomes quadratic and leads to the following result:

$$G_{ii}(\omega) = \frac{\omega}{2t^{*2}}\left(1 - \sqrt{1 - \frac{4t^{*2}}{\omega^2}}\right), \tag{3.11}$$

$$\rho(\omega) = \frac{1}{2\pi t^{*2}}\sqrt{4t^{*2} - \omega^2}\,, \qquad |\omega| < 2t^*\,. \tag{3.12}$$

Equation (3.11) coincides with Eqn (3.5) in the limit $z \to \infty$ if we substitute $t = \sqrt{z}\,t^*$. Thus, the result obtained in the retraceable-path approximation proves to be exact in the $d \to \infty$ limit. This correspondence clarifies the physical meaning of this approximation.

Let us take the more general case, where $J^* \neq 0$. The solution of Eqn (3.10) can be expressed in terms of Bessel functions of the first kind, $\mathcal{J}_\nu(x)$, with [34]

$$G_{ii}(\omega) = \frac{1}{t^*}\sum_{n=1}^{\infty}\left[\frac{1}{x - j_{\nu-1,n}} + \frac{1}{x + j_{\nu-1,n}}\right], \tag{3.13}$$

where $x = 4t^*/J^*$, $\nu = -2\omega/J^*$, and $j_{\nu,n}$ are the zeros of the function $x^\nu \mathcal{J}_\nu(x)$. Thus, the poles of the Green's function can be found by solving the following equations: $x \pm j_{\nu-1,n} = 0$. For large ν these can be solved exactly, with the position of the poles near the bottom of the band given by the expression

$$\omega_n = -2t^* - \frac{J^*}{2} - a_n t^*\left(\frac{J^*}{2t^*}\right)^{2/3}, \tag{3.14}$$

where a_n are zeros of the Airy function. For the first values of n we have

$$a_1 = -2.33\,, \qquad a_2 = -4.08\,, \qquad a_3 = -5.52\,, \ldots \tag{3.15}$$

Formula (3.14) shows that there are discrete levels near the bottom ($\omega = -2t^*$) of the initial band, and the level separation is of the order of $(J^*/t^*)^{2/3}t^*$. The density of states calculated by formula (3.2) is depicted in Fig. 4. We see that for finite J^*, there is indeed a system of discrete peaks; at $J^* = 0$ the peaks merge, and their envelope is depicted in Fig. 4 by a dashed curve.

Earlier the $(J^*/t^*)^{2/3}$ dependence for the positions of the discrete levels was obtained by Bulaevskiĭ et al. [29] in the

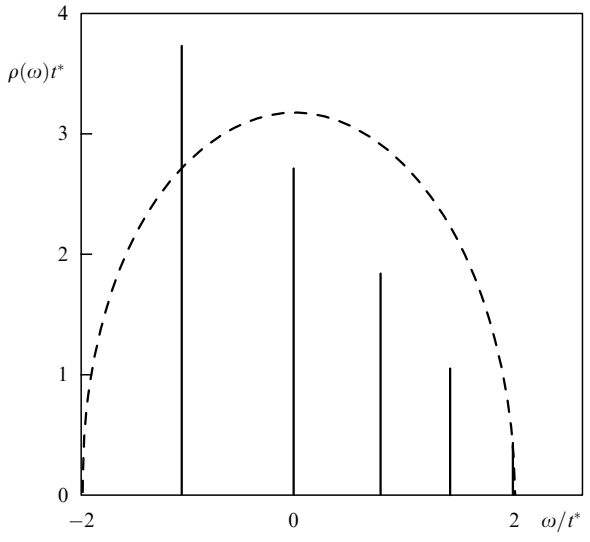

Figure 4. Density of states for a hole in an antiferromagnetic matrix in the $d = \infty$ limit for $J^*/t^* = 0$ (the dashed curve) and $J^*/t^* = 0.1$ (the solid line) [33].

continuum approximation, in which the problem of a hole in an antiferromagnetic matrix reduces in the three-dimensional case to solving the Schrödinger equation with a linear potential

$$t\Delta\psi + \frac{J^*}{2} r\psi = \left(E + 2t^* + \frac{J^*}{2}\right)\psi . \qquad (3.16)$$

Here r is the distance from the hole to point $\mathbf{r}$, and $2t^* + J^*/2$ determines the point from which energy is measured (the bottom of the continuous band). For the orbital angular moment $l = 0$ the Airy equation (3.16) has the quantities (3.14) obtained in the $d \to \infty$ limit as its eigenvalues. Thus, the continuum approximation [29] is exact in the limit of an infinite-dimensional space for large values of ω/J^*.

The continuum approximation uses only the Ising part of the exchange Hamiltonian. The transverse part would seem to smear the discrete levels (3.14). However, as the methods of exact diagonalization of small clusters in a square lattice show [35], this is not the case: the hole spectrum retains its discrete nature. On the other hand, the results of examining the $d \to \infty$ limit in the theory [33] with the complete exchange Hamiltonian lead to the discrete spectrum (3.14). This means that in such a limit the transverse part of the exchange interaction is irrelevant. It turns out that even at $d = 2$ the main features of the behavior of the model in the $d \to \infty$ limit are retained, i.e., the spectrum of a hole in an antiferromagnetic matrix is discrete. Matching the results for the $d \to \infty$ limit with those for finite d would require developing a method by which the corrections would be taken into account systematically in powers of the parameter $1/d$.

Allowance for first-order corrections often leads to nonphysical results (a negative density of states) [36], which suggests that an infinite series in powers of $1/d$ must be taken into account. One way to resolve the problem in this manner is to obtain self-consistent equations for the Green's function. Reasoning along similar lines, Brinkman and Rice [30] obtained, for the particular case of $J^* = 0$, the following expression for the Green's function:

$$G_{ii}(\omega) = \frac{\omega(1 - 1/d) - \sqrt{\omega^2 - 4t^{*2}(1 - 1/2d)}}{2t^{*2} - \omega^2/d} , \qquad (3.17)$$

which incorporates the $1/d$-corrections to separate terms in the numerator and denominator. If we substitute $t^* = \sqrt{2d}\, t$ into (3.17), we see that (3.17) coincides with (3.5) obtained in the retraceable-path approximation, which suggests that in the case of a finite-dimensional space the approximation is equivalent to the self-consistent approach with $1/d$-corrections in the theory with $d = \infty$. In this way we have determined the status of the heuristic approximation that allows only for retraceable paths. It would be interesting to go beyond the scope of this approximation, say, in discussing spin-wave excitations of a quantum antiferromagnet with embedded holes.

We have discussed the results of studies of the behavior of a hole in an antiferromagnetic matrix. Similar research for other spin configurations in the $d \to \infty$ limit was done by Metzner et al. [31]. It appears that in a ferromagnetic matrix a particle moves freely and that the corresponding density of states is given by the Gaussian function (3.8). This means that the $d = \infty$ approximation does not take into account the contribution of large ferromagnetic clusters, which lead to long Lifshitz tails in the density of states [37]. Nevertheless, the Green's function obtained in the $d = \infty$ approximation obeys all the necessary sum rules, as does the conductivity $\sigma(\omega)$ calculated in this approximation [36].

Now let us go back to the problem of a hole moving in an antiferromagnetic matrix. In the Ising approximation for the exchange interaction, the hole spectrum is determined by (3.14), with the hole remaining immobile. The ground state corresponds to the lower level $n = 1$, located at a distance of the order of $(J^*/t^*)^{2/3} t^*$ from the bottom of the initial spectrum. The transverse terms in the exchange interaction can generate spin waves, and because the hole interacts with these waves, it acquires a finite mass and begins to move. This motion through the lattice manifests itself in the broadening of the first discrete level. The width of the band attributed to the generation of spin waves must be of the order of the exchange interaction, with the result that the presence of the next discrete levels cannot significantly affect the hole motion in the lower band, since $J^* \ll t^*$. This suggests that the hole moving through the lattice because of deformations in the Néel structure (spin-wave excitation) becomes a magnetic polaron and forms a band of quasiparticle states with a width of the order of J^*. The higher discrete levels broaden because of spin waves and form an incoherent spectrum in an energy range of the order of the width of the initial band. In Section 4 we show that such a structure of quasiparticle states emerges as a result of the motion of a hole in an antiferromagnetic matrix.

4. The magnetic polaron

4.1 The effective Hamiltonian of a hole moving in an antiferromagnetic matrix

The fact that a quasiparticle spectrum for a hole in an antiferromagnetic matrix actually exists was demonstrated by a number of researchers (see Refs [38–45]) who used numerical methods of exact diagonalization of small clusters in two-dimensional space ($d = 2$). In the low-energy region (measured from the bottom of the hole band) the spectrum exhibits a characteristic peak distinctly separated from the broad incoherent part of the spectrum of width $(6-7)t$. The coherent propagation of a quasiparticle is described by a dispersion relation that has minima at the points $\mathbf{k} = (\pm\pi/2, \pm\pi/2)$ lying at the edge of the Brillouin zone for an antiferromagnetic Néel lattice.

Kane et al. [47] were the first to corroborate this picture of the quasiparticle spectrum analytically. The method of self-consistent perturbation theory they used has been since developed by other researchers (see Refs [48–53]). It is based on deriving an effective Hamiltonian for an antiferromagnetic matrix containing a single hole. When the band is exactly half-filled, the Hamiltonian of the $t-J$ model reduces to a Heisenberg Hamiltonian with antiferromagnetic exchange interaction, whose weakly excited states are described by spin waves. The loss of a single electron induces a local perturbation of the spectrum of the magnetic matrix, which must be described by an effective interaction between the hole and the spin waves. To derive the corresponding effective Hamiltonian we use the slave-fermion representation [46, 54] of the electron operators in Hamiltonian (1.2). Below, we demonstrate some of the steps in transforming the Hamiltonian.

We assume that the matrix spins are Néel-ordered, so that we have two sublattices with the spins either 'up' or 'down' on

each of them. At this point it is convenient to rotate the local system of coordinates connected with the sites of the $\downarrow$-sublattice through 180° with respect to the $\mathbf{x}$ axis. The operators at the sites of the $\downarrow$-sublattice are then transformed as

$$S_j^{\pm} \to S_j^{\mp}\,, \qquad S_j^z \to -S_j^z\,, \qquad C_{j\sigma} \to C_{j\bar{\sigma}}\,, \tag{4.1}$$

which leads to the following transformation of the Hamiltonian (1.2):

$$H \to -t\sum_{ij\sigma} \tilde{C}_{i\sigma}^{\dagger}\tilde{C}_{j\bar{\sigma}} + J\sum_{ij}\left[\frac{1}{2}\,(S_i^+ S_j^+ + S_i^- S_j^-) - S_i^z S_j^z - \frac{1}{4}\,n_i n_j\right], \tag{4.2}$$

where $\tilde{C}_{i\sigma} \equiv C_{i\sigma}(1 - n_{i\bar{\sigma}}) = X_i^{0\sigma}$. This canonical transformation transforms the Néel state into a ferromagnetic state with the spins directed up, so that now there is no need to distinguish between the sublattices. Next, we go from the electron ($\tilde{C}_{i\sigma}$) and spin ($\mathbf{S}_i$) operators to the spinless Fermi operators h_i and pseudospin operators $\mathbf{s}_i$ via the following formulas [50]:

$$\tilde{C}_{i\uparrow} = h_i^{\dagger}\left(\frac{1}{2} + s_i^z\right), \qquad \tilde{C}_{i\downarrow} = h_i^{\dagger} s_i^+\,, \qquad \mathbf{S}_i = \mathbf{s}_i h_i h_i^{\dagger}\,. \tag{4.3}$$

In this representation the Hamiltonian of the t–J model assumes the form

$$H = t\sum_{ij} h_i^{\dagger} h_j\left[\left(\frac{1}{2} + s_i^z\right)s_j^- + \left(\frac{1}{2} + s_j^z\right)s_i^+\right] + J\sum_{ij} h_i h_i^{\dagger} h_j h_j^{\dagger}\left[\frac{1}{2}\,(s_i^+ s_j^+ + s_i^- s_j^-) - s_i^z s_j^z\right]. \tag{4.4}$$

The third step in deriving the effective Hamiltonian consists in using the Goldstein–Primakoff representation for spin operators, a representation that expresses these operators in terms of the Bose operators $b_i^{\dagger}$ and b_i of spin deviations. For spin $s = 1/2$ we have

$$s_i^+ = \sqrt{1 - b_i^{\dagger} b_i}\, b_i \approx b_i\,, \qquad s_i^- = b_i^{\dagger}\sqrt{1 - b_i^{\dagger} b_i} \approx b_i^{\dagger}\,,$$
$$s_i^z = \frac{1}{2} - b_i^{\dagger} b_i\,.$$

The linear approximation in (4.4) provides a good description of the spin dynamics of an antiferromagnet at low temperatures, since the average value of the spin deviations at a site is small: $\langle b_i^{\dagger} b_i\rangle \ll 1$. We employ this approximation and replace the hole number operator in the second term on the right-hand side of Eqn (4.4) with its expectation value

$$h_i h_i^{\dagger} = 1 - h_i^{\dagger} h_i \to 1 - \langle h_i^{\dagger} h_i\rangle \equiv 1 - \delta\,,$$

where δ is the hole concentration. Hamiltonian (4.4) can then be written as

$$H = t\sum_{ij} h_i^{\dagger} h_j (b_i + b_j^{\dagger}) + J\sum_{ij}\left[\frac{1}{2}\,(b_i^{\dagger} b_j^{\dagger} + b_i b_j) + b_i^{\dagger} b_i + b_j^{\dagger} b_j\right] \tag{4.5}$$

[we have dropped the constant term, since it only shifts the energy origin, and have replaced $J(1 - \delta^2)$ by J to simplify the notation]. After expanding the operators in a Fourier series and applying the canonical transformation

$$b_{\mathbf{q}} = u_{\mathbf{q}}\beta_{\mathbf{q}} + v_{\mathbf{q}}\,\beta_{-\mathbf{q}}^{\dagger} \tag{4.6}$$

to the new Bose operators $\beta_{\mathbf{q}}$, we arrive at the final expression for the effective Hamiltonian [47]

$$H = \sum_{\mathbf{q}} \omega_{\mathbf{q}}^0\,\beta_{\mathbf{q}}^{\dagger}\beta_{\mathbf{q}} - \mu\sum_{\mathbf{k}} h_{\mathbf{k}}^{\dagger} h_{\mathbf{k}} + \sum_{\mathbf{kq}}\left[\mathcal{M}_{\mathbf{q}}(\mathbf{k}) h_{\mathbf{k}}^{\dagger} h_{\mathbf{k}-\mathbf{q}}\,\beta_{\mathbf{q}} + \text{c.c.}\right], \tag{4.7}$$

which contains a term with the chemical potential. Here,

$$\mathcal{M}_{\mathbf{q}}(\mathbf{k}) = zt(u_{\mathbf{q}}\gamma_{\mathbf{k}-\mathbf{q}} + v_{\mathbf{q}}\gamma_{\mathbf{k}}) \tag{4.8}$$

is the hole–spin-wave interaction amplitude, and

$$u_{\mathbf{q}} = \left[\frac{1 + \sqrt{1 - \gamma_{\mathbf{q}}^2}}{2\sqrt{1 - \gamma_{\mathbf{q}}^2}}\right]^{1/2}, \qquad v_{\mathbf{q}} = -\operatorname{sign}\gamma_{\mathbf{q}}\left[\frac{1 - \sqrt{1 - \gamma_{\mathbf{q}}^2}}{2\sqrt{1 - \gamma_{\mathbf{q}}^2}}\right]^{1/2},$$
$$\gamma_{\mathbf{q}} = \frac{2}{z}\sum_{\alpha=1}^{z/2}\cos q_{\alpha}\,, \qquad \omega_{\mathbf{q}}^0 = \frac{1}{2}\,zJ\sqrt{1 - \gamma_{\mathbf{q}}^2}\,.$$

We see that in the case of a half-filled band the Hamiltonian of the t–J model reduces to the spin-wave Hamiltonian of a Néel antiferromagnet interacting with spinless fermions, which are holes. This closely resembles the polaron problem, but also has a dramatic difference: Hamiltonian (4.7) has no initial term of the type $\sum_{\mathbf{k}} \varepsilon_{\mathbf{k}} h_{\mathbf{k}}^{\dagger} h_{\mathbf{k}}$ for holes. The kinetic term of the t–J model becomes a term describing fermion–magnon coupling. Since the interaction amplitude $t \gg J$, we are dealing with strong coupling.

Due to the presence of an interaction term a fermion acquires a self-energy. We will see later that the self-energy has a dispersion and corresponds to a quasiparticle, which can be called a magnetic polaron. Note that the interaction amplitude vanishes at $\mathbf{q} = 0$ and $\mathbf{q} = (\pi, \pi, \ldots)$ but becomes large at intermediate values of the momentum transfer $\mathbf{q}$. This implies that the interaction between a hole and short-wavelength spin waves plays an important role in the magnetic-polaron problem. This means that the magnetic polaron is well-localized in space.

4.2 The Green's function for holes

Hamiltonian (4.7) for a single hole in an antiferromagnetic matrix was first derived by Kane et al. [47], who also calculated the Green's function for holes at absolute zero using the self-consistent perturbation theory. Analytic results were obtained only in the pole approximation, where the contributions of incoherent states are ignored. The results confirm the expected structure of the spectrum of hole states described in Section 4.1. To describe the system analytically at finite temperatures and finite (but low) hole concentrations, we introduce (following [49]) a retarded Green's function

$$\left\langle\!\left\langle h_{\mathbf{k}}(t)\middle| h_{\mathbf{k}}^{\dagger}(t')\right\rangle\!\right\rangle = -\mathrm{i}\Theta(t - t')\left\langle\left\{h_{\mathbf{k}}(t), h_{\mathbf{k}}^{\dagger}(t')\right\}\right\rangle, \tag{4.9}$$

where $\Theta(\tau)$ is the step function, equal to 0 for $\tau < 0$ and to 1 for $\tau > 0$, and $\{\ldots,\ldots\}$ stands for an anticommutator. Its Fourier transform in the variable $t - t'$

$$G(\mathbf{k},\omega) \equiv \langle\langle h_{\mathbf{k}} | h_{\mathbf{k}}^{\dagger}\rangle\rangle_{\omega} = \int_{-\infty}^{\infty} \mathrm{d}(t-t')\, \exp\left[\mathrm{i}\omega(t-t')\right] \langle\langle h_{\mathbf{k}}(t) | h_{\mathbf{k}}^{\dagger}(t')\rangle\rangle$$

with an infinitesimal positive imaginary addition $\mathrm{i}\delta$ to ω makes it possible to calculate the spectral density of the hole states

$$A(\mathbf{k},\omega) = -\frac{1}{\pi}\,\mathrm{Im}\, G(\mathbf{k},\omega)\,. \tag{4.10}$$

Now we can easily write the equations of motion for the Green's function by first differentiating (4.9) with respect to t and then with respect to t' [56]. After a Fourier transformation with respect to $t - t'$ we arrive at a pair of coupled equations

$$(\omega+\mu)G(\mathbf{k},\omega) = 1 + \sum_{\mathbf{q}} \langle\langle h_{\mathbf{k}-\mathbf{q}} B(\mathbf{k},\mathbf{q}) | h_{\mathbf{k}}^{\dagger}\rangle\rangle_{\omega}\,, \tag{4.11}$$

$$(\omega+\mu)\langle\langle h_{\mathbf{k}-\mathbf{q}} B(\mathbf{k},\mathbf{q}) | h_{\mathbf{k}}^{\dagger}\rangle\rangle_{\omega} = \sum_{\mathbf{q}'} \langle\langle h_{\mathbf{k}-\mathbf{q}} B(\mathbf{k},\mathbf{q}) | h_{\mathbf{k}-\mathbf{q}'}^{\dagger} B^{\dagger}(\mathbf{k},\mathbf{q}')\rangle\rangle_{\omega}\,, \tag{4.12}$$

where

$$B(\mathbf{k},\mathbf{q}) = \mathcal{M}_{\mathbf{q}}(\mathbf{k}+\mathbf{q})\beta_{\mathbf{q}} + \mathcal{M}'_{\mathbf{q}}(\mathbf{k})\beta_{-\mathbf{q}}^{\dagger}\,.$$

Here $\mathcal{M}_{\mathbf{q}}(\mathbf{k})$ is defined in (4.8) and $\mathcal{M}'_{\mathbf{q}}(\mathbf{k}) = zt(u_{\mathbf{q}}\gamma_{\mathbf{k}} + v_{\mathbf{q}}\gamma_{\mathbf{k}-\mathbf{q}})$. Substituting (4.12) into (4.11) and introducing the zeroth hole Green's function $G_0(\mathbf{k},\omega) = (\omega+\mu)^{-1}$, we obtain the equation

$$G(\mathbf{k},\omega) = G_0(\mathbf{k},\omega) + G_0(\mathbf{k},\omega)T(\mathbf{k},\omega)G_0(\mathbf{k},\omega)\,, \tag{4.13}$$

where the scattering matrix $T(\mathbf{k},\omega)$ is a higher-order Green's function

$$T(\mathbf{k},\omega) = \sum_{\mathbf{q}\mathbf{q}'} \langle\langle h_{\mathbf{k}-\mathbf{q}} B(\mathbf{k},\mathbf{q}) | h_{\mathbf{k}-\mathbf{q}'}^{\dagger} B^{\dagger}(\mathbf{k},\mathbf{q}')\rangle\rangle_{\omega}\,. \tag{4.14}$$

Comparing Eqn (4.13) with the Dyson equation

$$G(\mathbf{k},\omega) = G_0(\mathbf{k},\omega) + G_0(\mathbf{k},\omega)\Sigma(\mathbf{k},\omega)G(\mathbf{k},\omega)\,,$$

we find the relation between the T matrix and the self-energy part Σ

$$T = \Sigma + \Sigma G_0 T\,.$$

We see that Σ is the irreducible part of the scattering matrix:

$$\Sigma(\mathbf{k},\omega) = T_{\mathrm{irr}}(\mathbf{k},\omega)\,. \tag{4.15}$$

It can be calculated by simply decoupling the correlation functions in (4.14):

$$\langle h_{\mathbf{k}-\mathbf{q}'}^{\dagger} B^{\dagger}(\mathbf{k},\mathbf{q}') h_{\mathbf{k}-\mathbf{q}}(t) B(\mathbf{k},\mathbf{q};t)\rangle \approx \delta_{\mathbf{q}\mathbf{q}'}\langle h_{\mathbf{k}-\mathbf{q}}^{\dagger} h_{\mathbf{k}-\mathbf{q}}(t)\rangle\langle B^{\dagger}(\mathbf{k},\mathbf{q}) B(\mathbf{k},\mathbf{q};t)\rangle\,.$$

Now we can use the spectral theorem to express the single-particle correlators of the fermion and boson operators in terms of the corresponding Green's functions. As a result, we arrive at the following expression for the self-energy part of the hole:

$$\Sigma(\mathbf{k},\omega) = \sum_{\mathbf{q}} \int \frac{\mathrm{d}\omega_1}{\pi}\,\frac{\mathrm{d}\omega_2}{\pi} \times \frac{\exp\left[\beta(\omega_1+\omega_2)\right]+1}{\left[\exp(\beta\omega_1)+1\right]\left[\exp(\beta\omega_2)-1\right]}\,\frac{\mathrm{Im}\langle\langle h_{\mathbf{k}-\mathbf{q}} | h_{\mathbf{k}-\mathbf{q}}^{\dagger}\rangle\rangle_{\omega_1}}{\omega-\omega_1-\omega_2+\mathrm{i}\delta} \times \left\{\mathcal{M}_{\mathbf{q}}^{2}(\mathbf{k})\,\mathrm{Im}\,\langle\langle \beta_{\mathbf{q}} | \beta_{\mathbf{q}}^{\dagger}\rangle\rangle_{\omega_2} + \mathcal{M}_{\mathbf{q}}'^{2}(\mathbf{k})\,\mathrm{Im}\,\langle\langle \beta_{-\mathbf{q}}^{\dagger} | \beta_{-\mathbf{q}}\rangle\rangle_{\omega_2}\right\}. \tag{4.16}$$

If we ignore the self-energy parts in the spin-wave Green's function $\langle\langle \beta_{\mathbf{q}} | \beta_{\mathbf{q}}^{\dagger}\rangle\rangle_{\omega}$, we have

$$-\frac{1}{\pi}\,\mathrm{Im}\,\langle\langle \beta_{\mathbf{q}} | \beta_{\mathbf{q}}^{\dagger}\rangle\rangle_{\omega} = \delta(\omega-\omega_{\mathbf{q}}^{0})\,,$$

$$-\frac{1}{\pi}\,\mathrm{Im}\,\langle\langle \beta_{-\mathbf{q}}^{\dagger} | \beta_{-\mathbf{q}}\rangle\rangle_{\omega} = -\delta(\omega+\omega_{\mathbf{q}}^{0})\,.$$

We substitute this into (4.16) and write the self-energy part of the holes in the following form [49]:

$$\Sigma(\mathbf{k},\omega) = \sum_{\mathbf{q}} \mathcal{M}_{\mathbf{q}}^{2}(\mathbf{k}) \int \mathrm{d}\varepsilon\, \frac{A(\mathbf{k}-\mathbf{q},\varepsilon)}{\omega-\varepsilon-\omega_{\mathbf{q}}^{0}+\mathrm{i}\delta}\left[1-f(\varepsilon)+N(\omega_{\mathbf{q}}^{0})\right] + \sum_{\mathbf{q}} \mathcal{M}_{\mathbf{q}}'^{2}(\mathbf{k}) \int \mathrm{d}\varepsilon\, \frac{A(\mathbf{k}-\mathbf{q},\varepsilon)}{\omega-\varepsilon+\omega_{\mathbf{q}}^{0}+\mathrm{i}\delta}\left[f(\varepsilon)+N(\omega_{\mathbf{q}}^{0})\right]. \tag{4.17}$$

Here,

$$f(\varepsilon) = \frac{1}{\exp(\beta\varepsilon)+1}\,, \qquad N(\omega) = \frac{1}{\exp(\beta\omega)-1}\,.$$

Since, according to (4.10), the spectral density is determined by the exact hole Green's function, the latter can be found from Eqn (4.17) in a self-consistent manner. To make this equation complete, we must augment it by the chemical potential equation

$$\delta = \frac{1}{N}\sum_{\mathbf{k}} \int \mathrm{d}\varepsilon\, A(\mathbf{k},\varepsilon) f(\varepsilon)\,. \tag{4.18}$$

Plakida et al. [49] found that at $T = 0$ formula (4.17) transforms into the well-known result [47, 48] obtained for causal Green's functions by summing a certain class of diagrams. From the point of view of perturbation theory, the results of Refs [47, 48] and Eqn (4.17) correspond to the self-consistent Born approximation (SCBA). If we substitute the spectral density of the corresponding initial Green's function into the right-hand side of Eqn (4.17), we obtain the Born approximation corresponding to the second order in the interaction amplitude. SCBA amounts to replacing the initial spectral density by the exact spectral density, which is absolutely necessary for our magnetic-polaron problem, since the interaction amplitude contains no small parameter.

The first and second terms on the right-hand side of Eqn (4.17) correspond to magnon emission and absorption by the hole.

4.3 Results of numerical calculations

Numerical solution of the system of equations (4.17) and (4.18) allowing for (4.10) and the Dyson equation was carried out for a cluster on a 16-by-16 square lattice ($z = 4$) [48, 49]. The results for a single hole at $T = 0$ are in full agreement with those obtained earlier by Martinez and Horsch [48]. Below, we display the results for the spectral density at absolute zero for two values of hole concentration and two values of the wave vector, $(\pi/2, \pi/2)$ and $(0, 0)$, at the center and edge of the magnetic Brillouin zone (Fig. 5).

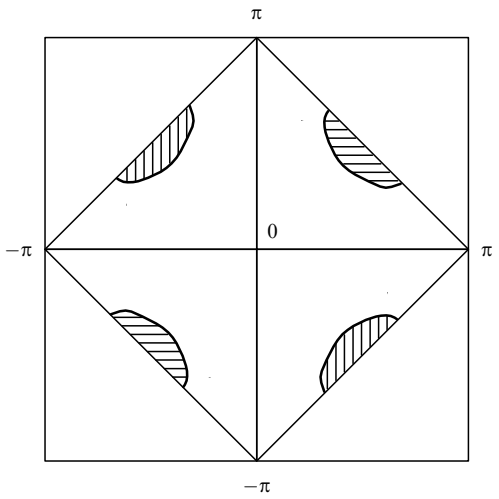

Figure 5. The Brillouin zone for a square lattice (hatched areas) and for an antiferromagnetic Néel structure (solid line).

For both values of $\mathbf{k}$, Fig. 6 clearly demonstrates a narrow quasiparticle peak at $\omega = 0$ and a broad incoherent background extending to energies of about $7t$. The finite width of the quasiparticle peak is due to the finiteness of the imaginary addition η to the frequency, which in the present calculation is set equal to $0.01t$. The results correspond to the following form of the hole density of states:

$$A(\mathbf{k}, \omega) = Z_{\mathbf{k}} \delta\big(\omega - E(\mathbf{k}) + \mu\big) + A_{\text{inc}}(\mathbf{k}, \omega)\,, \qquad (4.19)$$

where $Z_{\mathbf{k}}$ is the intensity of the quasiparticle state (defined as the integral over the peak's area), and $A_{\text{inc}}(\mathbf{k}, \omega)$ is the incoherent part of the spectrum. At $\mathbf{k} = (\pi/2, \pi/2)$ and $\delta = 3\%$, we have $Z_{\mathbf{k}} \approx 0.353$, which is somewhat larger than the value $Z_{\mathbf{k}} = 0.329$ for an extremely low hole concentration, corresponding to an isolated impurity. As the concentration rises to 10%, the spectrum for the state with $\mathbf{k} = \mathbf{0}$ acquires new features: at $\omega < 0$, there appears a region of incoherent states, and the peak's intensity decreases accordingly. But at $\mathbf{k} = (\pi/2, \pi/2)$ the intensity of the coherent peak hardly changes. It grows to a value $Z_{\mathbf{k}} = 0.369$. The insignificant increase in the peak's height is retained on a further increase in concentration: $Z_{\mathbf{k}} = 0.373$ at $\delta = 10\%$. The calculations made for different values of $\mathbf{k}$ suggest that the point $\mathbf{k} = (\pi/2, \pi/2)$ corresponds to the minimum in energy, and for this reason we must study the quasiparticle peak at $\mathbf{k} = (\pi/2, \pi/2)$ in greater detail. Figure 7 depicts the calculated dispersion curves of an isolated hole for different values of the exchange integral J [39] (Fig. 7a). The main feature of the obtained solution is the presence of a local maximum at point $(0, \pi)$ and an absolute minimum at point $(\pi/2, \pi/2)$. The presence of a minimum on the ΓM line is clearly visible,

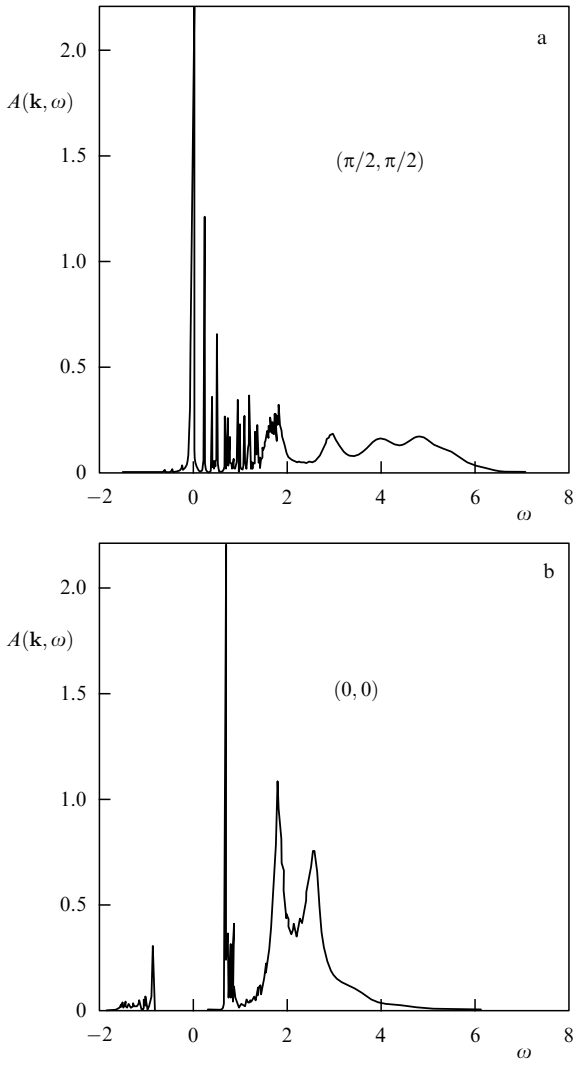

Figure 6. Spectral function $A(\mathbf{k}, \omega)$ for $J/t = 0.4$, $T = 0$, and $\delta = 3\%$ at $\mathbf{k} = (\pi/2, \pi/2)$ (a) and $\mathbf{k} = (0, 0)$ (b). All energies here and in what follows are expressed in units of t; frequencies are measured from the chemical potential μ [49].

but the minimum proves to be a saddle point if one takes into account the dispersion in the direction perpendicular to this line. The minimum at point $(\pi/2, \pi/2)$ corresponds to one of the four pockets of the Fermi surface. The numerical results in Fig. 7a were approximated by the function

$$E(\mathbf{k}) = \varepsilon_0 + x_1(\cos k_x + \cos k_y)^2 + x_2(\cos 2k_x + \cos 2k_y)\,, \qquad (4.20)$$

which corresponds to electron transfer between nearest neighbors and next-nearest neighbors in the same Néel sublattice. The adjustable coefficients increase with J/t up to values of the order of unity. For instance, at $J/t = 0.3$ we find that $\varepsilon_0/t = -2.305$, $x_1/t = 0.131$, and $x_2/t = 0.027$. The dispersion relation shows that the hole forms a band at the lower edge of the initial band, and the width of this 'hole' band is of the order of the exchange interaction, as expected. The results expressed by a dispersion curve are equivalent to a pattern of equal-energy lines in Fig. 8, with closed sections of the Fermi surface (pockets) centered at points $(\pm\pi/2, \pm\pi/2)$ clearly visible.

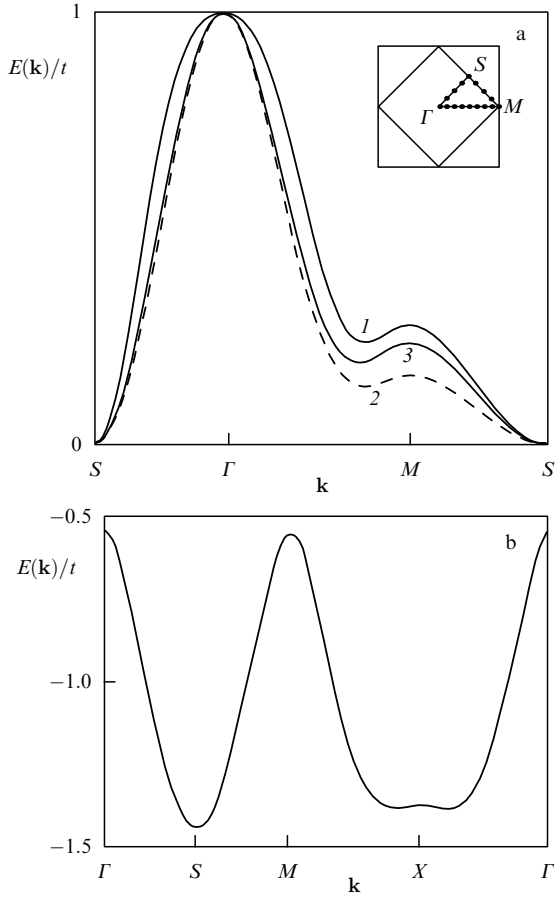

Figure 7. Dispersion curves for a magnetic polaron: (a) calculated in SCBA at $J/t = 0.01$ (curve *1*), $J/t = 0.8$ (curve *2*), and in the limit of large J (curve *3*) [39]; and (b) calculated in the ordinary magnetic-polaron theory at $J/t = 0.4$ [68].

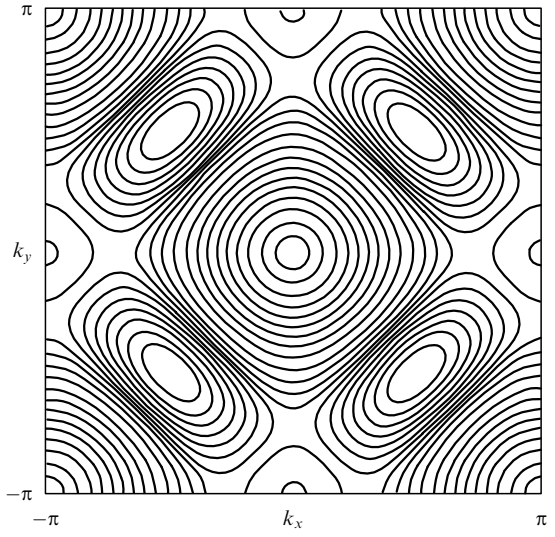

Figure 8. Constant-energy curves in the limit of large values of J [39].

Let us now return to the paper of Plakida et al. [49], where calculations were also made for finite temperatures. First we note that the quasiparticle peak $\omega_{\mathrm{QP}}(\mathbf{k}^*) = E(\mathbf{k}^*) - \mu$ at point $\mathbf{k}^* = (\pi/2, \pi/2)$ shifts toward higher frequencies linearly with rising concentration:

$$\omega_{\mathrm{QP}}(\mathbf{k}^*) \approx -1.5\delta J \qquad (\delta > 1.5\,\%)\,,$$

and that $\omega_{\mathrm{QP}}(\mathbf{k}^*) < 0$. The quantity $\mu - E(\mathbf{k}^*)$ should be identified with the quasiparticle Fermi energy. We define the temperature of degeneracy of the quasiparticle gas as

$$T_{\mathrm{d}} = \mu - E(\mathbf{k}^*) = 1.5\delta J \tag{4.21}$$

(the Boltzmann constant is set to unity). The behavior of the quasiparticle gas for $T \ll T_{\mathrm{d}}$ is expected to be different from that for $T > T_{\mathrm{d}}$.

Analysis of the calculations made for different temperatures shows no significant changes in the shape of the spectrum up to $T \sim T_{\mathrm{d}}$. At a fixed δ the only temperature effect is a uniform shift in $A(\mathbf{k}, \omega)$ toward higher values of ω for all values of $\mathbf{k}$. It particular, it appears that the quasiparticle peak at $\mathbf{k} = \mathbf{k}^*$ is close to $\omega_{\mathrm{QP}} = 0$ for $T \lesssim T_{\mathrm{d}}$. At higher temperatures the sharp structure of the spectrum evens out, but the quasiparticle peaks remain and only lower slightly as T increases. The pattern is repeated for other hole concentrations. It appears, therefore, that in a broad range of hole concentrations and temperatures the spectral density $A(\mathbf{k}, \omega)$ for the state $\mathbf{k} = \mathbf{k}^*$ contains a quasiparticle peak whose intensity changes only slightly as δ and T grow. The peak moves toward higher frequencies as the temperature increases.

Now let us study the momentum distribution function of frequencies

$$N(\mathbf{k}) = \int \mathrm{d}\omega\, A(\mathbf{k}, \omega) f(\omega)\,. \tag{4.22}$$

Generally, coherent and incoherent states with $\omega < 0$ contribute to this function (the chemical potential μ is zero on the adopted energy scale). To understand the nature of the incoherent contribution to $A(\mathbf{k}, \omega)$ it is advisable to analyze the imaginary part of the self-energy of the holes,

$$\Gamma(\mathbf{k}, \omega) = -\mathrm{Im}\,\Sigma(\mathbf{k}, \omega)\,.$$

The results of calculations of this imaginary part for a 3% hole concentration are depicted in Fig. 9. Using (4.10), we can write

$$A(\mathbf{k}, \omega) = \frac{1}{\pi} \frac{\Gamma(\mathbf{k}, \omega)}{\left[\omega - \mathrm{Re}\,\Sigma(\mathbf{k}, \omega) + \mu\right]^2 + \left[\Gamma(\mathbf{k}, \omega)\right]^2}\,. \tag{4.23}$$

The position of the peak of this function of ω (the smaller the Γ, the sharper the peak) can be found from the equation

$$E(\mathbf{k}) = \mathrm{Re}\,\Sigma\big(\mathbf{k}, E(\mathbf{k})\big) - \mu\,. \tag{4.24}$$

For the state $\mathbf{k} = \mathbf{k}^*$ the value of $E(\mathbf{k}^*) - \mu$ at $\delta = 3\%$ is close to zero, and in this neighborhood, as Fig. 9 clearly demonstrates, $\Gamma = 0$, with the result that (4.23) reduces to the function $Z_{\mathbf{k}^*}\delta\big(\omega - \omega_{\mathrm{QP}}(\mathbf{k}^*)\big)$, where

$$Z_{\mathbf{k}} = \left[1 - \frac{\partial}{\partial\omega}\,\mathrm{Re}\,\Sigma(\mathbf{k}, \omega)\bigg|_{\omega = E(\mathbf{k})}\right]^{-1}. \tag{4.25}$$

On the other hand, in the region where $\omega > \omega_{\mathrm{QP}}(\mathbf{k})$ we have $\Gamma(\mathbf{k}, \omega) \gg \left|\omega - \mathrm{Re}\,\Sigma(\mathbf{k}, \omega) + \mu\right|$, so that (4.23) yields the

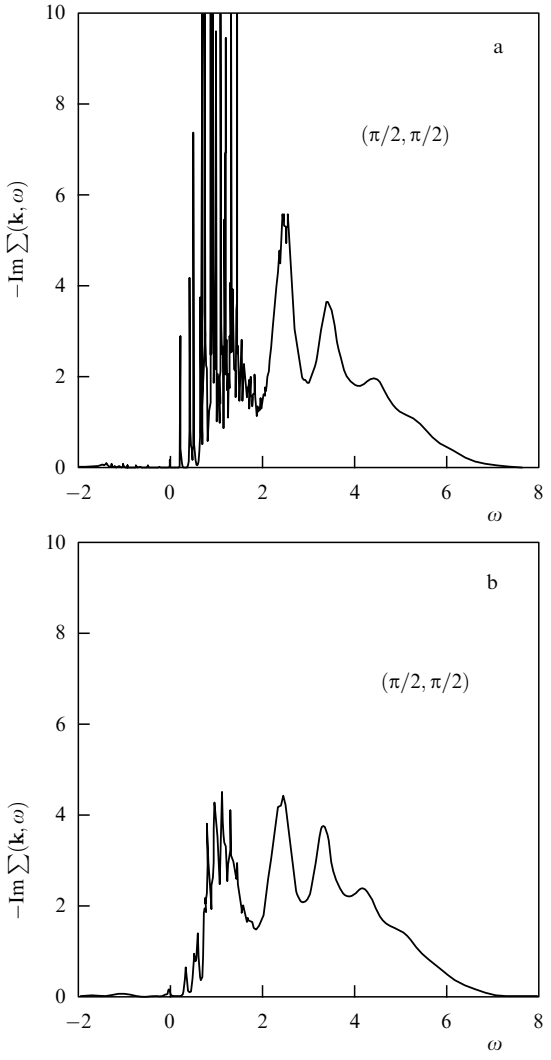

Figure 9. Imaginary part of the self-energy of the holes for $\delta = 3\%$ at $T = 0$ (a) and at $T = 0.1t$ (b) [49].

following approximate expression for the spectral density of incoherent states:

$$A_{\mathrm{inc}}(\mathbf{k}, \omega) \approx \frac{1}{\pi \Gamma(\mathbf{k}, \omega)} \,. \tag{4.26}$$

Now let us go back to expression (4.22) for $N(\mathbf{k})$. For points that are far from $\mathbf{k}^*$ the quasiparticle peaks are in the $\omega > 0$ range, with the result that $N(\mathbf{k})$ is determined by the contribution of incoherent states with $\omega < 0$, with an integral contribution of such states of order δ (Fig. 6b). Thus, far from $\mathbf{k}^*$ we have $N(\mathbf{k}) \sim \delta \ll 1$. For the point $\mathbf{k} = \mathbf{k}^*$ there can be no contribution when $\omega < 0$, but on the other hand, there is a quasiparticle peak in the $\omega < 0$ range (see Fig. 6). This peak determines that $N(\mathbf{k}) \approx Z_{\mathbf{k}}$ near $\mathbf{k} = \mathbf{k}^*$. Outside the neighborhood of point $\mathbf{k}^*$ we have $\omega_{\mathrm{QP}}(\mathbf{k}) > 0$, with the result that $N(\mathbf{k})$ becomes small. This reasoning suggests that the quasiparticles in $\mathbf{k}$-space are distributed near four pockets centered at $(\pm\pi/2, \pm\pi/2)$. The integral volume of each pocket must be of order δ.

The $N(\mathbf{k})$ distribution for a 3% hole concentration at $T = 0$ is depicted in Fig. 10. The absence of a jump in $N(\mathbf{k})$ at the Fermi surface is due to the finiteness of the imaginary addition η used in calculations. At a 10% hole concentration,

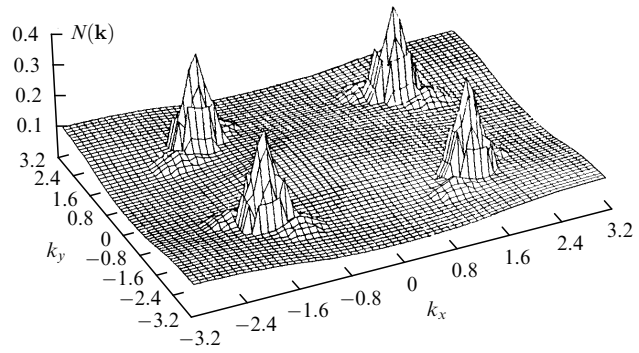

Figure 10. Hole distribution function $N(\mathbf{k})$ in the $\mathbf{k}$-space for $\delta = 3\%$ at $T = 0$ [49].

the distribution undergoes a dramatic change: the ridge in $N(\mathbf{k})$ along the boundaries of the magnetic Brillouin zone grows. At $\delta = 20\%$, this ridge is retained, but there are also peaks near the $(\pi, 0)$ type points, with the background of incoherent states not changing significantly. Thus, as the hole concentration grows, the states forming pockets in the neighborhood of the point $(\pi/2, \pi/2)$ tend to form pockets in the neighborhood of the $(\pi, 0)$ type points.

At finite temperatures the coherent peaks in $N(\mathbf{k})$ become much lower. For instance, calculations with $\delta = 3\%$ at $T \approx 0.017t > T_{\mathrm{d}}$ show that the intensity of the peaks at the points $(\pm\pi/2, \pm\pi/2)$ decreases tenfold, while elsewhere $N(\mathbf{k})$ increases significantly. Note that the spread of the four-pocket structure of $N(\mathbf{k})$ with increasing temperature is caused not by the broadening of the quasiparticle peaks, as could be expected, but by the temperature shift of the quasiparticle energies $\omega_{\mathrm{QP}}(\mathbf{k})$. As mentioned earlier, at $\delta = 3\%$ and $T = 0$ we have $\omega_{\mathrm{QP}}(\mathbf{k}) < 0$, and the quasiparticle states form peaks in $N(\mathbf{k})$ in the neighborhood of point $\mathbf{k}^*$. However, for $T > T_{\mathrm{d}}$ quasiparticle peaks emerge above the chemical potential level, with the result that $\omega_{\mathrm{QP}}(\mathbf{k}) > 0$. The Fermi factor in (4.22) strongly suppresses the contribution of coherent states to $N(\mathbf{k})$ and leads to the disappearance of the four-pocket structure. Thus, Plakida et al. [49] established by their numerical calculations that the spectral density $A(\mathbf{k}, \omega)$ is weakly dependent on the hole concentration and temperature, while the momentum distribution function varies rapidly as the temperature increases to $T > T_{\mathrm{d}} \approx 1.5\delta J$.

How do various approximations limit the applicability of the magnetic-polaron theory [47 – 55]? First, it is assumed that there is long-range antiferromagnetic order. At the same time, it is known (see below) that this order disappears at low hole concentrations, of the order of several percent. At high concentrations, however, there is still a significant short-range order characterized by a correlation length ξ. Such a state of the t–J model is commonly called the spin-liquid state. Dagotto and Riera [43] have shown by their numerical calculations that the position of the minimum of the quasiparticle band at $\mathbf{k} = (\pi/2, \pi/2)$ does not depend on the type of system, i.e., the position is the same irrespective of whether we are dealing with a Néel antiferromagnet or a spin liquid. Richard and Yushankhai [50] found that the minimum in energy at the point $(\pi/2, \pi/2)$ is retained as long as $\xi \gg R_{\mathrm{p}}$, where R_{p} is the polaron radius. Only at $\xi \sim R_{\mathrm{p}}$ does a pattern emerge corresponding to a hole 'freely' propagating through a lattice with a large Fermi surface close to the edges of the magnetic Brillouin zone.

In another important approximation the renormalization of the magnon spectrum is ignored completely. However, for high concentrations δ one should expect a large renormalization of the spin-wave energy [57]. Such a renormalization can be taken into account in a totally self-consistent theory not only for the hole states but for the spin states as well. Thus, the magnetic-polaron theory under discussion is valid up to moderate hole concentrations δ, when the system is still in the spin-liquid state but renormalization of the magnon spectrum does not play too large a role.

As noted earlier, for an isolated impurity SCBA produces results that are in good agreement with those of numerical calculations for small clusters. Note that the success of this approximation is due to the fact that the renormalization of the vertex parts of Hamiltonian (4.7) proves unimportant. This aspect was specially studied by Liu and Manousakis [45] and Martinez and Horsch [48].

A magnetic polaron has a complicated structure and consists of a hole and the surrounding deformation of the Néel structure. The spatial distribution of this deformation was studied by Ramsak and Horsch [57] at absolute zero. They calculated a correlation function of the type

$$N_{\mathbf{R}} = \langle h_0^\dagger h_0 S_{\mathbf{R}}^z \rangle . \tag{4.27}$$

This function describes the correlation between a hole at site $\mathbf{0}$ and the spin deviations at site $\mathbf{R}$. Using the spin-wave approximation for $S_{\mathbf{R}}^z$, they found the following asymptotic formula for the function (4.27):

$$N_{\mathbf{R}} = 8\left[\gamma_{\mathbf{k}}^2 + 2(\mathbf{v}_{\mathbf{k}}\mathbf{n})^2\right] \frac{t^2}{JR^2} , \tag{4.28}$$

where $\mathbf{v}_{\mathbf{k}} = \nabla\gamma_{\mathbf{k}}$, and $\mathbf{n} = \mathbf{R}/R$. Thus, the spin deformation surrounding a hole falls off according to the power law $N_{\mathbf{R}} \sim 1/R^2$, so that there can be no concept of a polaron radius. Calculations of (4.27) via SCBA wave functions [58] for sites closest to the hole produce results that are in good agreement with those obtained by the method of exact diagonalization of small clusters.

4.4 Non-Fermi liquid behavior of holes

Here we discuss the results of SCBA calculations that ignore the renormalization of the spin-wave spectrum. A self-consistent approach that allows for mutual renormalization of the hole and spin-wave spectra was developed by Jian-Xin Li and Chang-De Gong [52], Igarashi and Fulde [53, 59], and Khaliullin and Horsch [54]. They defined the Green's functions of holes, G, and magnons, D, by similar relations

$$\langle\langle \beta_{\mathbf{k}}(t) | \beta_{\mathbf{k}}^\dagger(t') \rangle\rangle = -\mathrm{i}\Theta(t-t')\left\langle \left[\beta_{\mathbf{k}}(t), \beta_{\mathbf{k}}^\dagger(t')\right] \right\rangle . \tag{4.29}$$

Using Hamiltonian (4.7), an equation of motion for the magnon Green's function is set up and solved similarly to the case of holes. Let us write the Dyson equations for the Green's functions

$$G(\mathbf{k},\omega) = \left[\omega - \Sigma(\mathbf{k},\omega) + \mu\right]^{-1} , \tag{4.30}$$

$$D(\mathbf{k},\omega) = \left[\omega - \omega_{\mathbf{k}}^0 - \Pi(\mathbf{k},\omega)\right]^{-1} \tag{4.31}$$

with the self-energy parts Σ and Π given by the following expressions [52]:

$$\Sigma(\mathbf{k},\omega) = \sum_{\mathbf{q}} \int \frac{\mathrm{d}\omega_1}{\pi} \frac{\mathrm{d}\omega_2}{\pi} \left[\tanh\frac{\omega_1}{2T} + \coth\frac{\omega_2}{2T}\right] \mathcal{M}_{\mathbf{k}-\mathbf{q}}^2(\mathbf{k}) \times \frac{\operatorname{Im} G(\mathbf{q},\omega_1) \operatorname{Im} D(\mathbf{k}-\mathbf{q},\omega_2)}{\omega - \omega_1 - \omega_2 + \mathrm{i}\delta} , \tag{4.32}$$

$$\Pi(\mathbf{k},\omega) = -\sum_{\mathbf{q}} \int \frac{\mathrm{d}\omega_1}{\pi} \frac{\mathrm{d}\omega_2}{\pi} \left[\tanh\frac{\omega_1}{2T} - \tanh\frac{\omega_2}{2T}\right] \mathcal{M}_{\mathbf{k}}^2(\mathbf{q}) \times \frac{\operatorname{Im} G(\mathbf{q},\omega_1) \operatorname{Im} G(\mathbf{k}-\mathbf{q},\omega_2)}{\omega - \omega_1 + \omega_2 + \mathrm{i}\delta} . \tag{4.33}$$

We can easily verify that the expression (4.32) for the self-energy part of holes is a different form of (4.16). Both are obtained as a result of SCBA calculations and correspond to the emission of a spin wave by a hole or to the decay of the spin wave into an electron–hole pair.

To estimate expressions (4.32) and (4.33), we allow for the fact that the hole spectrum of a two-dimensional antiferromagnet has four minima at the points $\mathbf{k}^* = (\pm\pi/2, \pm\pi/2)$ and that in the neighborhood of a minimum the spectrum can be approximated by a quadratic form. If we ignore the spectrum's anisotropy (although numerical calculations show that the anisotropy is large), at a point $\mathbf{k}$ in the neighborhood of a minimum we have

$$E(\mathbf{k}) = E(\mathbf{k}_i^*) + \frac{1}{2m}\,\mathbf{k}'^2 . \tag{4.34}$$

The Green's function of holes in the pole approximation can be written as

$$G(\mathbf{k},\omega) = \frac{Z_{\mathbf{k}}}{\omega - E(\mathbf{k}) + \mu + \mathrm{i}\delta} , \tag{4.35}$$

where $Z_{\mathbf{k}} \sim J/t$ must remain small, and the effective hole mass $m \sim t/J$ must remain large. Estimates of (4.32) via the zeroth Green's function of spin waves yield [60]

$$Z_{\mathbf{k}}^2 \approx \frac{2}{\pi}\left(\frac{J}{t}\right)^2 . \tag{4.36}$$

Since both $\mathbf{k}'$ and $\mathbf{q}$ are small, the initial vertex part can be approximated by the function

$$\mathcal{M}_{\mathbf{q}}^2(\mathbf{k}) = \sum_{i=1}^{4} \mathcal{M}_{\mathbf{q}}^2(\mathbf{k}_i) \approx \frac{t^2}{2\sqrt{2}}\left[qk'^2 - 2\sqrt{2}(\mathbf{q}\mathbf{k}') + 2q\right] . \tag{4.37}$$

If we take all the approximations (4.34)–(4.47) into account, we have the following estimate for (4.33) [52]:

$$\operatorname{Im}\Pi(\mathbf{k},\omega) = \begin{cases} -\dfrac{Z_{\mathbf{k}}^2 t^2 m k_{\mathrm{F}}}{16\sqrt{2}\pi}\left(\dfrac{\omega}{T}\right), & \omega < T , \\ -\dfrac{Z_{\mathbf{k}}^2 t^2 m k_{\mathrm{F}}}{8\sqrt{2}\,\pi} , & \omega > T . \end{cases} \tag{4.38}$$

For the real part of $\Pi(\mathbf{k},\omega)$ we have the following expression when the momentum and energy transfers are small:

$$\operatorname{Re}\Pi(\mathbf{k},\omega) = -\frac{Z_{\mathbf{k}}^2 t^2 m k}{8\sqrt{2}\,\pi}\left(1 + \frac{k_{\mathrm{F}}}{2}\right) + \frac{Z_{\mathbf{k}}^2 t^2 m^2}{8\pi}\,\omega . \tag{4.39}$$

Let us now write the approximate expression for the imaginary part of the magnon Green's function in two limiting cases for the frequency-temperature ratio [52]:

$$\operatorname{Im} D(\mathbf{k},\omega) \approx \begin{cases} -\dfrac{Ck_{\mathrm{F}}}{\left\{(1-2\sqrt{2}mC)\omega-\left[\sqrt{2}J-C(2+k_{\mathrm{F}})\right]k\right\}^2}\dfrac{\omega}{T}, & \omega < T, \\ -\dfrac{2Ck_{\mathrm{F}}}{\left\{(1-2\sqrt{2}mC)\omega-\left[\sqrt{2}J-C(2+k_{\mathrm{F}})\right]k\right\}^2}, & \omega > T, \end{cases}$$

where $C = Z_{\mathbf{k}}^2 t^2 m/16\pi\sqrt{2}$. Using these relationships in formula (4.32) for $\Sigma(\mathbf{k},\omega)$, we obtain the following estimates for the imaginary part of the self-energy of a hole [52]:

$$\operatorname{Im}\Sigma(\mathbf{k},\omega) \approx \begin{cases} -\dfrac{mk_{\mathrm{F}}Jt}{2\sqrt{2}\,\pi^{5/2}\left[\pi^2 - mJ(2+k_{\mathrm{F}})\right]^2}\omega, & \omega > T, \quad (4.40a) \\ -\dfrac{mk_{\mathrm{F}}Jt}{2\sqrt{2}\,\pi^{5/2}\left[\pi^2 - mJ(2+k_{\mathrm{F}})\right]^2}(1+\ln 2)T, & \omega < T. \quad (4.40b) \end{cases}$$

These estimates show that holes behave like a non-Fermi liquid (in Fermi-liquid theory, quasiparticle damping is proportional to ω^2). The frequency and temperature behavior of damping described by (4.40a) and (4.40b) corresponds to a marginal Fermi liquid [61]. The result (4.40) immediately leads to a linear temperature dependence of resistance, which is characteristic of high-T_{c} materials.

The estimates (4.38) and (4.40) were made in the pole approximation for the Green's function. At the same time, we established earlier that the hole–quasiparticle spectrum contains a broad region of incoherent states. The first to discover this region below the quasiparticle spectrum were Igarashi and Fulde [53]. This part of the spectrum is weakly dependent on momentum, although it does exhibit a peculiar frequency dependence (see Fig. 9). Igarashi and Fulde [53] approximated the incoherent part of the spectrum by the function [see Eqn (4.19)]

$$A_{\mathrm{inc}}(\mathbf{k},\omega) = \frac{1}{2\Gamma}\,\Theta\big(\Gamma - |\omega|\big)\,, \qquad (4.41)$$

where $\Gamma \approx zt$ is the half-width of the initial band. Since $\Gamma \gg T$ and $J > T$, for frequencies ω below the cutoff frequency of the spin-wave spectrum the introduction of the incoherent part into the spectral density only slightly alters the results (4.40) that characterize the behavior of holes [52].

However, the contribution of incoherent states to the polarization operator $\Pi(\mathbf{k},\omega)$ of spin waves is extremely important. Equation (4.33) shows that three types of transitions contribute to $\Pi(\mathbf{k},\omega)$: between coherent states (Π_{cc}), between incoherent states (Π_{ii}), and mixed transitions (Π_{ic}). Estimates show [53] that

$$\Pi_{\mathrm{cc}} \approx -\frac{J}{t^2}\,\delta\,, \qquad \Pi_{\mathrm{ic}} \approx \frac{\delta}{t}\,, \qquad \Pi_{\mathrm{ii}} \approx \frac{\delta}{2t}\ln\frac{zt}{2J}\,. \qquad (4.42)$$

Thus, it is true that incoherent states contribute the most to polarizability. Because polarization is finite, the spin-wave spectrum undergoes renormalization. As the hole concentration rises, the spin-wave frequency (at a fixed $\mathbf{q}$) lowers, and at certain concentration δ_{c} vanishes. The numerical calculations made in Refs [53, 54] show that δ_{c} amounts to several percent. At $\delta = \delta_{\mathrm{c}}$ the long-range antiferromagnetic order is destroyed. The various aspects of spin dynamics in a two-dimensional antiferromagnetic system are discussed in detail in Section 5, where the critical hole concentration δ_{c} is calculated with an accuracy higher than that achieved in Refs [53, 54]. Here, we continue our general study of the hole spectrum.

4.5 Ferrons

As J becomes smaller, the tendency toward the formation of an antiferromagnetic state weakens, and at $J = 0$, according to Nagaoka's theorem, the system becomes ferromagnetic. But does this transition go directly from one phase to the other or through an intermediate (say, mixed) phase? Part of this general question is the problem of the structure of a single-particle hole state at small values of J. The idea that a hole introduced into an antiferromagnetic matrix can form a region of ferromagnetic order around itself (since this leads to a gain in kinetic energy, which for a weak exchange interaction may exceed the loss in exchange energy) has a long history [62]. Such an object, i.e., a hole in an antiferromagnetic matrix dressed in a ferromagnetically polarized region, was called a ferron [63]. The energetical advantage of a ferron was analyzed in the Ising limit of the exchange interaction. Allowance for the transverse components of spin leads, as it does in the magnetic-polaron problem, to a finite mobility of the ferron, and therefore, to the formation of a band of quasiparticle states for small values of J.

This problem has been studied by Sabczynski et al. [64, 65]. The researchers started with Hamiltonian (4.7), which describes a hole interacting with an antiferromagnetic matrix in the spin-wave approximation. Since the total spin commutes with the Hamiltonian, the eigenfunctions of a single-particle state can be characterized by the value of the total spin $S^z = 1/2, \ldots$ This value is the sum of the spin (1/2) of the hole and the flipped spins (with respect to the Néel state) of the nearest neighbors and those of the next-nearest neighbors. Since for a square lattice the number of nearest neighbors is even, only odd values $S^z = 1/2, 3/2, 5/2, \ldots$ are possible (from symmetry considerations). In accordance with the fixed value of S^z, the wave function of a single-particle state is written as a linear combination of wave functions with different numbers of spin deviations at the sites. In [64] the eigenfunctions and the energy eigenvalues were found for the $0.01 < J/t < 1.00$ interval by Lanczos's method with about 100 successive steps. This guaranteed a 2% accuracy in calculations. The results of the calculations of the energy of single-particle states for $S^z = 1/2$ and $3/2$ at $J/t = 0.15$ are depicted in Fig. 11.

The band spectrum for $S^z = 1/2$ has four minima at points X with $\mathbf{k} = (\pm\pi/2, \pm\pi/2)$, which agrees with the results of earlier calculations (see above). Near these minima the spectrum is quasi-one-dimensional: the effective mass in the direction perpendicular to the edges of the magnetic Brillouin zone is smaller than the effective mass in the parallel direction by a factor of ten. In the case opposite to $S^z = 1/2$, i.e., $S^z = 3/2$, the spectrum has a minimum at the point Γ, and the maxima are on the lines of the magnetic Brillouin zone. Clearly, these spectra overlap, and there is a region in the $\mathbf{k}$-space where states with $S^z = 3/2$ lie below (on the energy scale) the states with $S^z = 1/2$. Only for $J/t > 0.92$ does the ground state have spin $S^z = 1/2$. Near $J/t = 0.053$ the state with $\mathbf{k} = (\pm\pi/2, \pm\pi/2)$ and $S^z = 1/2$ changes to the ground state with $\mathbf{k} = \mathbf{0}$ and $S^z = 3/2$. Calculations show

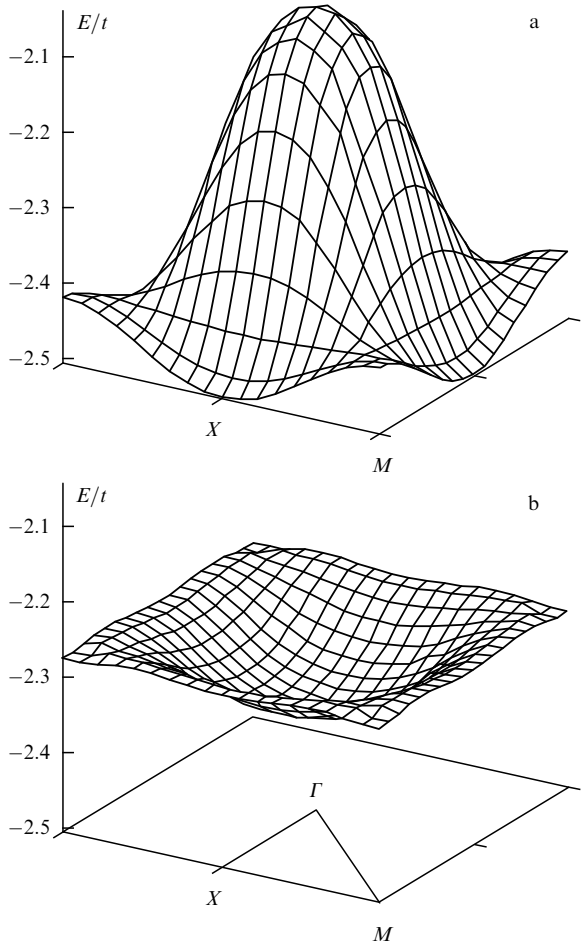

Figure 11. Band spectrum of holes in the magnetic Brillouin zone for two total-spin values: (a) $S^z = 1/2$, and (b) $S^z = 3/2$ [64].

that for fixed $\mathbf{k}$ the energy increases monotonically with S^z, so that the greater the value of S^z, the smaller the value of J/t at which the corresponding state is the ground state. Thus, we see that the hole state with total spin $S^z = 1/2$ is the ground state for $J/t > 0.053$. In the interval $0.02 < J/t < 0.053$ this state has a higher energy than the state with $S^z = 15/2$, and for $J/t < 0.02$ the ground state has $S^z > 15/2$. The ferron structure, i.e., the spatial distribution of the spin deviations near the hole, allowing for the symmetry of the square lattice, was discussed by Sherman and Schreiber [60] for several symmetry points of the Brillouin zone. As J diminishes, S^z grows, and so does the ferron radius. These numerical results reflect the tendency to the limit $J \to 0$, where the entire volume around the hole is filled by ferromagnetically oriented spins, which is required by Nagaoka's theorem [66].

4.6 The canonical form of the magnetic-polaron theory

The effective Hamiltonian in the form of (4.5) or (4.7), which describes a hole moving in an antiferromagnetic matrix, has the structure of the Fröhlich Hamiltonian for the electron–phonon model of metals. In the case of strong coupling between the electrons and the lattice, the Fröhlich Hamiltonian is used in the small-radius polaron problem, whose solution is based not on employing perturbation theory techniques but on using a canonical transformation (e.g., see [67]). This approach can also be applied to the Hamiltonian (4.5), in which magnons act as phonons [68–70]. Below, we single out the main steps in this canonical approach in magnetic-polaron theory.

First, we note that the problem has several integrals of motion. Among these is the number of fermions

$$\mathcal{N} = \sum_i h_i^\dagger h_i \tag{4.43}$$

and the total momentum

$$\mathbf{P} = \sum_{\mathbf{k}} \mathbf{k} h_{\mathbf{k}}^\dagger h_{\mathbf{k}} + \sum_{\mathbf{q}} \mathbf{q} b_{\mathbf{q}}^\dagger b_{\mathbf{q}} \equiv \mathbf{K} + \mathbf{Q}\,. \tag{4.44}$$

This means that a common basis consisting of the eigenvalues of the operators H and $\mathbf{P}$ can be chosen. In the ordinary polaron theory [67] this is achieved by employing the unitary Jost transformation $\mathrm{U} = \exp\bigl[-\mathrm{i}\mathbf{Q}\mathbf{r}\bigr]$, where $\mathbf{r}$ is the electron radius vector. A similar transformation can also be introduced for the magnetic polaron [70]:

$$\mathrm{U} = \exp\left[-\mathrm{i}\sum_i \mathbf{Q}\mathbf{R}_i h_i^\dagger h_i\right], \tag{4.45}$$

which can be considered a Jost transformation on a lattice. For a single hole the transformation can be written as follows:

$$\mathrm{U} = \sum_i \mathrm{T}_i h_i^\dagger h_i\,, \qquad \mathrm{T}_i = \exp\bigl[-\mathrm{i}\mathbf{Q}\mathbf{R}_i\bigr]\,. \tag{4.46}$$

Upon this transformation, the Fermi and Bose operators transform in the following manner:

$$\mathrm{U}^\dagger h_i^\dagger h_j \mathrm{U} = \mathrm{T}_{j-i} h_i^\dagger h_j\,, \qquad \mathrm{U}^\dagger b_i \mathrm{U} = \sum_j b_{i-j} h_j^\dagger h_j\,.$$

By transforming Hamiltonian (4.5) directly, we can easily show that the Hamiltonian becomes diagonal in the Fermi operators:

$$\mathrm{U}^\dagger H \mathrm{U} = \sum_{\mathbf{k}} H_{\mathbf{k}} h_{\mathbf{k}}^\dagger h_{\mathbf{k}}\,, \tag{4.47}$$

with $H_{\mathbf{k}}$ depending only on the Bose operators.

In diagonalizing $H_{\mathbf{k}}$, two additional unitary transformations must be made:

$$\mathrm{V} = \exp\left[\frac{1}{2}\sum_{\mathbf{q}} \theta_{\mathbf{q}} (b_{\mathbf{q}}^\dagger b_{-\mathbf{q}}^\dagger - \text{c.c.})\right], \tag{4.48}$$

$$\mathrm{W} = \sum_{\mathbf{k}} \mathrm{W}_{\mathbf{k}} h_{\mathbf{k}}^\dagger h_{\mathbf{k}}\,, \qquad \mathrm{W}_{\mathbf{k}} = \exp\left[\frac{1}{\sqrt{N}}\sum_{\mathbf{q}} \lambda_{\mathbf{q}}(\mathbf{k})(b_{\mathbf{q}} - b_{\mathbf{q}}^\dagger)\right]. \tag{4.49}$$

Provided that the parameters $\theta_{\mathbf{q}}$ are chosen correctly, the first transformation diagonalizes the purely magnon part of Hamiltonian (4.5) [transformation (4.48) is equivalent to the $u-v$ transformation (4.6) of the Bose operators]. The second transformation, (4.49), produces a linear shift in the Bose operators:

$$\mathrm{W}_{\mathbf{k}}^\dagger b_{\mathbf{q}} \mathrm{W}_{\mathbf{k}} = b_{\mathbf{q}} - \frac{1}{\sqrt{N}}\,\lambda_{\mathbf{q}}(\mathbf{k})\,. \tag{4.50}$$

The quantities $\lambda_{\mathbf{q}}(\mathbf{k})$ are interpreted as variational parameters, and they are selected from the condition that the terms in $(\mathrm{V}\mathrm{W}_{\mathbf{k}})^\dagger H_{\mathbf{k}} (\mathrm{V}\mathrm{W}_{\mathbf{k}})$ that are linear in the operators $b_{\mathbf{q}}$ vanish.

As a result of three unitary transformations the initial Hamiltonian becomes completely diagonalized in the spaces of states with one hole, i.e.,

$$(\mathrm{UVW})^{\dagger} H(\mathrm{UVW}) = \sum_{\mathbf{k}} E(\mathbf{k}) h_{\mathbf{k}}^{\dagger} h_{\mathbf{k}} , \tag{4.51}$$

where

$$E(\mathbf{k}) = -2z\Omega(\mathbf{k}) + \frac{1}{N}\sum_{\mathbf{q}} \omega_{\mathbf{q}} \lambda_{\mathbf{q}}^2(\mathbf{k}) \tag{4.52}$$

is the dispersion curve of a single-particle state (a magnetic polaron). Here,

$$\Omega(\mathbf{k}) = \frac{1}{N}\sum_{\mathbf{q}} \lambda_{\mathbf{q}}(\mathbf{k}) \mathcal{M}_{\mathbf{q}}(\mathbf{k}) F(\mathbf{k}) ,$$

$$F(\mathbf{k}) = \exp\left[-\frac{1}{N}\sum_{\mathbf{q}} \lambda_{\mathbf{q}}^2(\mathbf{k}) \right] , \tag{4.53}$$

and $\mathcal{M}_{\mathbf{q}}(\mathbf{k})$ is the hole–magnon interaction amplitude defined in (4.7).

The variational parameter is given by the following expression:

$$\lambda_{\mathbf{q}}(\mathbf{k}) = \frac{F(\mathbf{k}) \mathcal{M}_{\mathbf{q}}(\mathbf{k})}{\omega_{\mathbf{q}} + 2\Omega(\mathbf{k})} , \tag{4.54}$$

which is a complicated nonlinear equation in $\lambda_{\mathbf{q}}(\mathbf{k})$. The numerical solution of this equation for a given $\mathbf{k}$ and parameter J/t makes it possible, via (4.52), to calculate the dispersion curve for a magnetic polaron. The results are depicted in Fig. 7b for symmetry directions in the Brillouin zone. They are in good agreement with the results of SCBA numerical calculations made by Dagotto et al. [71] via the quantum Monte Carlo method with the same value of J/t, and with those of calculations done by Bulut et al. [72] using the Hubbard model. The calculations show that the results for the dispersion curves are only weakly sensitive to the value of J/t. Thus, the characteristic features of the spin–polaron spectrum, i.e., the absolute minimum at point $(\pi/2, \pi/2)$, the maximum at point $(0, 0)$, and the broad flat section at point $(\pi, 0)$, remain unchanged within a broad range of values of parameter J/t. It is these features that are observed in the hole spectrum of copper cuprates [71].

The quantity $\alpha = 2t/J$ is the dimensionless coupling parameter of the magnetic-polaron theory; in the t–J theory this parameter is much larger than unity. Comparison of the results of the canonical theory briefly discussed above with results of numerical calculations shows that the theory operates well when $\alpha \lesssim 5$, i.e., in the intermediate region inaccessible for standard perturbation theory.

4.7 t–t'–J Model

There are several reasons why allowing for electron hopping to a next-nearest-neighbor site is important. Firstly, the initial electron spectrum changes the topology of the Fermi surface near corresponding to the half-filled band [73–75]. Indeed, the dispersion law for free electrons in this case has the form

$$\varepsilon(\mathbf{k}) = -2t(\cos k_x + \cos k_y) - 2t'\left[\cos(k_x + k_y) + \cos(k_x - k_y)\right] . \tag{4.55}$$

The shape of the constant-energy surfaces depends on the sign of t', while in the model with electron hopping to the nearest site nothing depends on the sign of t. Near half-filling, the electron paths are open, at high hole concentrations they become closed, and at intermediate concentrations the curvature changes sign upon motion along the Fermi surface. This pattern is retained in the $-0.5t < t' < 0$ interval. In the model with $t' = 0$, the Fermi surface in the case of a half-filled band is flat, i.e., there is ideal nesting, which ensures that antiferromagnetic order is present. When $t' \neq 0$, the nesting is violated, and the occurrence of antiferromagnetism in such a system is under question. The anomalies in the initial magnetic susceptibility at different $t' < 0$ were studied by Benard et al. [74]. Of course, for $U \gtrsim W$ the Coulomb interaction has a strong effect on the behavior of the dc magnetic susceptibility and the shape of the true Fermi surface, but some anomalies originating from the initial spectrum (4.55) remain when we go over to the case of interacting electrons [74].

Another reason was pointed out by Lee [76], who especially emphasized that the hopping between next-nearest-neighbors couples the sites belonging to the same sublattice of a Néel antiferromagnet, with the result that such electron motion takes place without violating the magnetic order and must be taken into account in determining the phase boundaries of the antiferromagnetic state. Finally, Benard et al. [74] and Si et al. [75] stated that the experimental results of angle-resolved photoemission spectroscopy studies of high-T_c materials can be explained only on the basis of the lattice model with t' hopping. Tohyama and Maekawa [77] suggested that the sign of t' in copper cuprates depends on the carrier type. For the almost half-filled band, $t' < 0$ for hole carriers and $t' > 0$ for electron carriers.

The Hubbard model and the t–J model with hopping between next-nearest-neighbors became known as the U–t–t' and t–t'–J models, respectively. The U–t–t' model with weak Coulomb interactions was discussed in Refs [74, 75], and the t–t'–J model in Refs [73, 77–86]. Kotliar and Ruckenstein [87] studied the U–t–t' model numerically using the quantum Monte Carlo method at moderate values of $U \sim W$ in order to establish how the initial parameter t' renormalizes the Coulomb interaction. Their results suggest that there is considerable renormalization, so that determining the parameter t' by comparing the empirical photoemission data with the results of calculations involving the initial spectrum is a risky business. They also studied the effect of t' hopping on the magnetic properties of the system. Their findings revealed that for systems with low hole concentrations and $t' < 0$ the antiferromagnetic correlations weaken in comparison with the case where $t' = 0$. This result can be understood from the following simple qualitative reasoning. Hopping to a neighboring site induces an effective antiferromagnetic interaction $J \sim t^2/U$, while t' hopping induces an additional antiferromagnetic interaction $J' \sim t'^2/J$ between the sites that are next-nearest. This leads to frustration, which disrupts the Néel order to an extent determined by the ratio J'/J. Furthermore, earlier studies of the Hubbard model using the quantum Monte Carlo method have shown that deviations from half-filled states lead to the emergence of incommensurate magnetic structures with a wavevector of modulation of the Néel state that increases with hole concentration. Inclusion of the t' term facilitates the emergence of incommensurate structures at lower values of δ for $t' < 0$ in comparison with $t' > 0$.

But when we are dealing with a strong Coulomb interaction (for the $t-t'-J$ model), the effects of the t' term on the antiferromagnetic correlations are just the opposite. Deeg et al. [83] investigated the $t-t'-J$ model in the mean-field approximation for the effective Hamiltonian that emerges in the slave-boson representation technique (initially used with the Hubbard model by Kotliar and Ruckenstein [87] and Li et al. [88]). They studied a representation invariant with respect to spin rotation [81], in which the electron operators are expressed in terms of boson and pseudospin operators, which represent the charge and spin degrees of freedom, respectively. The phase diagram in Fig. 12 in the $(t'/t, \delta)$ plane was obtained by comparing the energies of several homogeneous phases. In the absence of a t' term, the incommensurate phases arise immediately after deviations from the half-filled state. Thus, in the $t-J$ model the antiferromagnetic Néel phase in this approximation proves unstable with respect to the formation of incommensurate spiral phases. However, we see that in the presence of even a small t' term there is a stable Néel phase near $n = 1$, and the region occupied by the phase broadens as $|t'|$ grows; at $|t'| > |t'_c| = 1.4t$, the phase becomes stable at any electron concentration.

The most exhaustive study of a quasiparticle state (a magnetic polaron) in the $t-t'-J$ model was carried out by Bala et al. [80], who used SCBA (the slave-fermion technique). Two terms were added to Hamiltonian (4.7) that describe the system of interacting holes and spin waves above the Néel state: the t' term, and the H_3 term, which takes into account the three-center interactions [see Eqn (2.8) obtained from the Hubbard Hamiltonian via a canonical transformation in the $U \gg W$ limit]. Usually the second term is discarded, although recently the important role of this term in the formation of the quasiparticle spectrum was demonstrated by Belinicher et al. [90] and Eskes and Oles [91]. The additional terms alter the fermion–magnon interaction amplitude, so that instead of (4.7) we have

$$\mathcal{M}_{\mathbf{q}}(\mathbf{k}) = zt(u_{\mathbf{k}}\gamma_{\mathbf{k}-\mathbf{q}} + v_{\mathbf{q}}\gamma_{\mathbf{k}}) + \frac{ztt'}{U}(1-\delta)(\eta_{\mathbf{k}-\mathbf{q}} - \eta_{\mathbf{k}})(u_{\mathbf{k}}\gamma_{\mathbf{k}-\mathbf{q}} - v_{\mathbf{q}}\gamma_{\mathbf{k}}) \,. \quad (4.56)$$

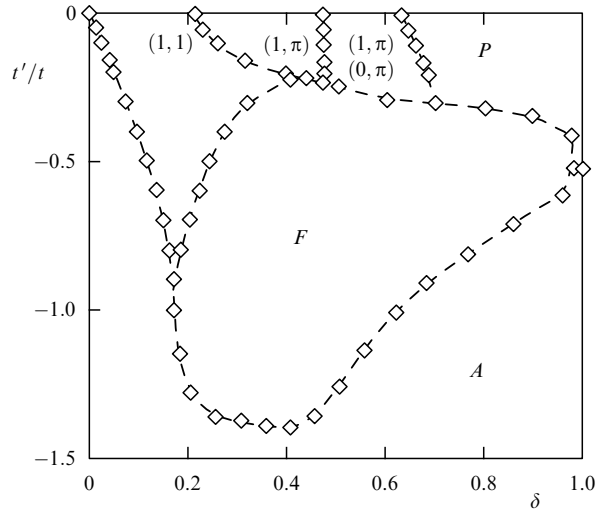

Figure 12. Phase diagram of the two-dimensional $t-t'-J$ model at $J/t = 0.4$ and $T = 0$ [83].

The second term on the right-hand side has its origin in the combined action of the t' term and the three-center interaction $\sim t^2/U$, with $\eta_{\mathbf{k}} = \cos k_x \cos k_y$. On the other hand, in contrast to the $t-J$ model, the Hamiltonian acquires the initial fermion spectrum with the dispersion law

$$\varepsilon(\mathbf{k}) = zt'\eta_{\mathbf{k}} + \frac{zt^2}{U}(1-\delta)\left(z\gamma_{\mathbf{k}}^2 - 1\right). \quad (4.57)$$

Here, the first term on the right-hand side describes the free fermion propagation caused by hops to neighboring sites of the same antiferromagnetic lattice, and the second term is caused by the three-center interaction, as a result of which two successive hops occur between nearest-neighbor sites. The factor $\gamma_{\mathbf{k}}^2$ can be written as the sum of two terms, $\propto \eta_{\mathbf{k}}$ and $\propto \gamma_{2\mathbf{k}}$, so that, as a result, a fermion may fall onto a next-nearest site (the term $\propto \eta_{\mathbf{k}}$) or onto a next-next-nearest site (the term $\propto \gamma_{2\mathbf{k}}$).

The results of numerical calculations of the SCBA equations with the new expressions for $\mathcal{M}_{\mathbf{q}}(\mathbf{k})$ and $\varepsilon(\mathbf{k})$ at $t' < 0$ show that in the $t-t'-J$ model the width of the band of quasiparticle states is determined not by the width $W = 2z|t'|$ of the initial fermion band, as one might expect, but exclusively by the effects of strong hole–spin-wave coupling. The coherent motion of quasiparticles in the $t-t'-J$ model is determined by the absorption and emission of spin waves (just as it is in the $t-J$ model). In other words, a hole propagates along an antiferromagnetic lattice due to local destruction of the antiferromagnetic order.

5. Spin dynamics of a quantum antiferromagnet

5.1 Spin-wave spectrum and damping

We start with the effective Hamiltonian (4.7), which describes the system of interacting spin waves and holes in an antiferromagnetic matrix. This interaction leads, on the one hand, to the formation of Fermi quasiparticles in the system (magnetic polarons), and on the other, to the renormalization of the initial spin-wave spectrum that characterizes the spin dynamics in the absence of holes. This renormalization proves so large that at absolute zero and at a hole concentration of the order of several percent, the spin-wave energy vanishes, and as a result, long-range antiferromagnetic order disintegrates. This effect is caused by the fact that a hole introduced into an antiferromagnetic matrix strongly distorts the magnetic order in the vicinity of the hole, which means that small hole concentrations (several percent) are sufficient for the deformed regions to overlap, with the result that long-range order completely disappears. The theory must have a method for calculating the dispersion curves of the spin waves and the wave damping and for establishing the dependence of the sublattice magnetizations and the Néel temperature T_N on the hole concentration δ.

All these problems (except the problem of calculating T_N) can be solved by the linear spin-wave theory. In view of this, we introduce a two-component operator of spin deviations,

$$\mathcal{A}_{\mathbf{q}} = \begin{pmatrix} \beta_{\mathbf{q}} \\ \beta^{\dagger}_{-\mathbf{q}} \end{pmatrix}, \qquad \mathcal{A}^{\dagger}_{\mathbf{q}} = (\beta^{\dagger}_{\mathbf{q}}, \beta_{-\mathbf{q}}) \quad (5.1)$$

and build a double-time retarded Green's function [92]

$$\langle\langle \mathcal{A}_{\mathbf{q}}(t) | \mathcal{A}^{\dagger}_{\mathbf{q}}(t') \rangle\rangle = -\mathrm{i}\Theta(t-t')\langle [\beta_{\mathbf{q}}(t), \beta^{\dagger}_{\mathbf{q}}(t')] \rangle \,. \quad (5.2)$$

Let us set up the equation of motion for this Green's function, differentiating (5.2) first with respect to t and then with respect to t'. The resulting equation for $\langle\langle \mathcal{A}_\mathbf{q}|\mathcal{A}_\mathbf{q}^\dagger\rangle\rangle_\omega$ can be transformed into a Dyson type equation

$$\langle\langle \mathcal{A}_\mathbf{q}|\mathcal{A}_\mathbf{q}^\dagger\rangle\rangle_\omega = \langle\langle \mathcal{A}_\mathbf{q}|\mathcal{A}_\mathbf{q}^\dagger\rangle\rangle_\omega^0 + \langle\langle \mathcal{A}_\mathbf{q}|\mathcal{A}_\mathbf{q}^\dagger\rangle\rangle_\omega^0 \Pi(\mathbf{q},\omega)\langle\langle \mathcal{A}_\mathbf{q}|\mathcal{A}_\mathbf{q}^\dagger\rangle\rangle_\omega , \tag{5.3}$$

where the 'zeroth' Green's function satisfies the equation

$$\omega\langle\langle \mathcal{A}_\mathbf{q}|\mathcal{A}_\mathbf{q}^\dagger\rangle\rangle_\omega^0 = \langle [\mathcal{A}_\mathbf{q}, \mathcal{A}_\mathbf{q}^\dagger]\rangle + \langle [\mathrm{i}\dot{\mathcal{A}}_\mathbf{q}, \mathcal{A}_\mathbf{q}^\dagger]\rangle\langle [\mathcal{A}_\mathbf{q}, \mathcal{A}_\mathbf{q}^\dagger]\rangle^{-1}\langle\langle \mathcal{A}_\mathbf{q}|\mathcal{A}_\mathbf{q}^\dagger\rangle\rangle_\omega^0 ,$$

and $\Pi(\mathbf{q},\omega)$ denotes a polarization operator specified by the following relationship [96]:

$$\Pi(\mathbf{q},\omega) = \langle [\mathcal{A}_\mathbf{q}, \mathcal{A}_\mathbf{q}^\dagger]\rangle^{-1}\Big\{\langle\langle \mathrm{i}\dot{\mathcal{A}}_\mathbf{q}|-\mathrm{i}\dot{\mathcal{A}}_\mathbf{q}^\dagger\rangle\rangle_\omega - \langle\langle \mathrm{i}\dot{\mathcal{A}}_\mathbf{q}|\mathcal{A}_\mathbf{q}^\dagger\rangle\rangle_\omega\langle\langle \mathcal{A}_\mathbf{q}|\mathcal{A}_\mathbf{q}^\dagger\rangle\rangle^{-1}\langle\langle \mathcal{A}_\mathbf{q}|-\mathrm{i}\dot{\mathcal{A}}_\mathbf{q}^\dagger\rangle\rangle_\omega\Big\}\langle [\mathcal{A}_\mathbf{q}, \mathcal{A}_\mathbf{q}^\dagger]\rangle^{-1} . \tag{5.4}$$

Taking into account the equation of motion for operators, $\mathrm{i}\dot{\mathcal{A}}_\mathbf{q} = [\mathcal{A}_\mathbf{q}, H]$, we see that $\Pi(\mathbf{q},\omega)$ can be expressed using the two-particle Green's function, which can be decoupled into a product of one-particle Green's functions. Then from (5.4) we find the matrix elements of the polarization operator

$$\begin{Bmatrix} \Pi_{11}(\mathbf{q},\omega) \\ \Pi_{12}(\mathbf{q},\omega) \end{Bmatrix} = \frac{1}{N}\sum_\mathbf{k}\begin{Bmatrix} \mathcal{M}_\mathbf{q}^2(\mathbf{k}) \\ \mathcal{M}_\mathbf{q}(\mathbf{k})\mathcal{M}_{-\mathbf{q}}(\mathbf{k}-\mathbf{q}) \end{Bmatrix} \times \int \mathrm{d}\omega_1\,\mathrm{d}\omega_2\,\big[f(\omega_1)f(-\omega_2) - f(-\omega_1)f(\omega_2)\big] \times \frac{A(\mathbf{k}-\mathbf{q},\omega_1)A(\mathbf{k},\omega_2)}{\omega+\omega_1-\omega_2+\mathrm{i}\delta} . \tag{5.5}$$

The other two matrix elements can be found from the following relationships:

$$\Pi_{22}(\mathbf{q},\omega) = \Pi_{11}(-\mathbf{q},-\omega) , \qquad \Pi_{21}(\mathbf{q},\omega) = \Pi_{12}(\mathbf{q},\omega) .$$

The Dyson equation (5.3) determines the Green's functions matrix

$$\langle\langle \mathcal{A}_\mathbf{q}|\mathcal{A}_\mathbf{q}^\dagger\rangle\rangle_\omega = \frac{1}{\mathcal{D}_\mathbf{q}(\omega)}\begin{pmatrix} \omega+\omega_\mathbf{q}^0+\Pi_{22}(\mathbf{q},\omega) & -\Pi_{12}(\mathbf{q},\omega) \\ -\Pi_{21}(\mathbf{q},\omega) & -\omega+\omega_\mathbf{q}^0+\Pi_{11}(\mathbf{q},\omega) \end{pmatrix}, \tag{5.6}$$

where

$$\mathcal{D}_\mathbf{q}(\omega) = \big[\omega+\omega_\mathbf{q}^0+\Pi_{22}(\mathbf{q},\omega)\big]\big[\omega-\omega_\mathbf{q}^0-\Pi_{11}(\mathbf{q},\omega)\big] + \Pi_{12}(\mathbf{q},\omega)\Pi_{21}(\mathbf{q},\omega) . \tag{5.7}$$

The spin-wave spectrum corresponds to the poles of the Green's function (5.6) or the zeros of (5.7). In calculating the matrix elements (5.5) of the polarization operator, we allow for the structure of the hole spectral density, more precisely, the pole and incoherent contributions [see Eqn (4.19)]

$$A(\mathbf{k},\omega) = Z_\mathbf{k}\delta\big(\omega-E(\mathbf{k})+\mu\big) + \frac{1}{W}\,\Theta(\omega-J)\Theta(W-\omega) , \tag{5.8}$$

where $W = 2zt$ is the width of the initial band. The sum rule

$$\int_{-\infty}^{\infty}\mathrm{d}\omega\;A(\mathbf{k},\omega) = 1 \tag{5.9}$$

determines the intensity of the coherent contribution $Z_\mathbf{k} = J/W$; we know that the width of the coherent-quasiparticle band is of the order of $J \ll W$.

The chemical potential μ can be found by solving the equation for the number of holes

$$\delta = \frac{1}{N}\sum_\mathbf{k}\int \mathrm{d}\omega\;A(\mathbf{k},\omega)f(\omega) . \tag{5.10}$$

Assuming that the Fermi surface consists of four spherical pockets centered at the points $(\pm\pi/2, \pm\pi/2)$, we find from (5.10) that

$$\mu = \frac{2\pi W}{mJ}\,\delta , \tag{5.11}$$

where m is the effective mass of holes.

If we substitute (5.8) into (5.5), we see that it can be represented by a sum of four terms. The term containing $A_\mathrm{coh}A_\mathrm{coh}$ is small because $Z_\mathbf{k} \ll 1$, with the result, as was first noted by Igarashi and Fulde [53], that the incoherent terms provide the main contribution to the polarizability. The greatest of these terms would be that containing $A_\mathrm{inc}A_\mathrm{inc}$ if not for the fact that in our approximations, which use (5.8), this contribution is simply zero [96] (Khaliullin and Horsch [54] overlooked this fact), with the result that the main contribution to the integrals in (5.5) is provided by terms containing $A_\mathrm{coh}A_\mathrm{inc}$ if we assume that $\mu < J$. Within this approximation and in the first order in δ, we arrive at the following expression for the spin-wave energy valid for small values of $\mathbf{q}$:

$$\omega_\mathbf{q} = vq , \qquad v = v_0\sqrt{1-\frac{\delta}{\delta_\mathrm{c}}} , \tag{5.12}$$

where $v_0 = \sqrt{2}\,J$ is the velocity of unrenormalized spin waves for an antiferromagnet at half-filling, and

$$\delta_\mathrm{c} = \frac{JW/4zt^2}{\ln(W/J)} \tag{5.13}$$

is the critical concentration at which the velocity becomes zero. At $t/J = 5$ we have $\delta_\mathrm{c} = 0.027$, which corresponds to the critical concentration at which antiferromagnetism in high-T_c materials disappears.

The numerical calculation of $\omega_\mathbf{q}$ and $\Gamma_\mathbf{q}$ yields the dispersion and damping of spin waves for different hole concentrations (Fig. 13). We see that the spin-wave energies 'soften' as δ increases, with the damping becoming stronger in the process. For very low hole concentrations, i.e., when the spin-wave velocity is much higher than the hole velocity at the Fermi surface, v_F, long-wavelength spin waves remain virtually undamped since they cannot split into an electron – hole pair. But short-wavelength spin waves are attenuated, as shown in Fig. 13. When $v < v_\mathrm{F}$, the spin-wave spectrum is entirely within the electron – hole pair continuum and the spin waves become overdamped. Under these conditions the antiferromagnetic order rapidly disintegrates.

As the velocity of the spin waves decreases with increasing δ, so does the sublattice magnetization m. The numerical

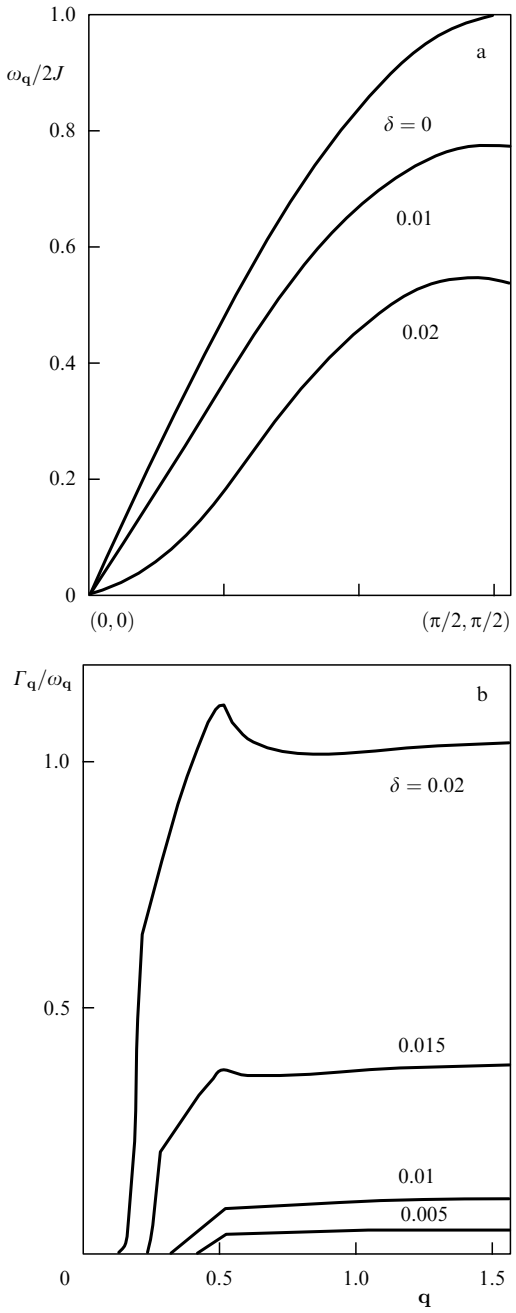

Figure 13. Spin-wave spectrum (a) and damping (b) along $\mathbf{q} = (q, q)$ for different hole concentrations at $J/t = 0.2$ [96].

calculations conducted by Belkasri and Richard [96] revealed that m becomes zero at the same concentration δ_c as the spin-wave speed does. This immediately implies that δ_c is the critical concentration for the disintegration of long-range order. The results of Belkasri and Richard [96] are in good agreement with the experimental data on high-T_c materials.

5.2 Antiferromagnet at a finite temperature

We have studied the renormalization of the spin-wave spectrum caused by the interaction between spin waves and holes at absolute zero and have determined the critical impurity concentration at which both the spin-wave velocity and the sublattice magnetization vanish. The problem was investigated by applying the linear spin-wave theory. In this section we examine the behavior of the system at finite temperatures using a self-consistent approach to the spin system, an approach similar to that employed in describing the Heisenberg model in a broad range of temperatures [92]. This approach produces self-consistent equations for the sublattice magnetization in the $t-J$ model that enable calculation of the Néel temperature. Here, we follow the work of Richard and Yushankhai [50, 93]. In the given situation we must start with the total Hamiltonian (4.4), which we write in a simplified form [93]

$$H = t\sum_{ij} h_i^{\dagger} h_j (s_i^+ + s_j^-) + J\sum_{ij}\left[\frac{1}{2}(s_i^+ s_j^+ + s_i^- s_j^-) - s_i^z s_j^z\right]. \tag{5.14}$$

Instead of (5.1), we introduce a two-component operator consisting of spin operators

$$\mathcal{B}_{\mathbf{q}} = \begin{pmatrix} s_{\mathbf{q}}^+ \\ s_{-\mathbf{q}}^- \end{pmatrix}, \qquad \mathcal{B}_{\mathbf{q}}^{\dagger} = (s_{\mathbf{q}}^-, s_{-\mathbf{q}}^+), \tag{5.15}$$

and then define the matrix (commutator) Green's function of magnetic excitations as

$$D(\mathbf{q}, \omega) = \langle\langle \mathcal{B}_{\mathbf{q}} | \mathcal{B}_{\mathbf{q}}^{\dagger} \rangle\rangle_{\omega}.$$

We write the equation of motion for the operator s_i^+ and linearize it in the same way as is done in the Heisenberg model [92] by replacing the operator s_i^z with its expectation value

$$s_i^z \to \langle s_i^z \rangle \equiv m. \tag{5.16}$$

Since at zero hole concentration the $t-J$ model reduces to the Heisenberg model, this approximation is more accurate the smaller the value of δ. We write the linearized equation in the Fourier representation as follows:

$$\mathrm{i}\frac{\partial s_{\mathbf{q}}^+}{\partial t} = 2m\left[\frac{1}{\sqrt{N}}\sum_{\mathbf{k}} \varepsilon(\mathbf{k}-\mathbf{q}) h_{\mathbf{k}-\mathbf{q}}^{\dagger} h_{\mathbf{k}} + J(\mathbf{0}) s_{\mathbf{q}}^+ + J(\mathbf{q}) s_{-\mathbf{q}}^-\right], \tag{5.17}$$

where $J(\mathbf{q}) = zJ\gamma_{\mathbf{q}}$ is the Fourier transform of the exchange interaction. Since in a two-dimensional magnetic material with a rotation-group symmetry (the $t-J$ model has such a symmetry), long-range order is possible only at $T = 0$, we must consider the quasi-two-dimensional case by incorporating into the picture a small exchange interaction $J_{\perp} \ll J$ in the direction perpendicular to the layers. Then, for the three-dimensional vector $\mathbf{q}$ in the equation of motion (5.17) we must put

$$J(\mathbf{q}) = zJ(\gamma_{\mathbf{q}} + \xi\cos q_z), \qquad \xi = \frac{J_{\perp}}{2J}. \tag{5.18}$$

We write the equation for the operator $\mathcal{B}_{\mathbf{q}}$ in the form

$$\mathrm{i}\frac{\partial \mathcal{B}_{\mathbf{q}}}{\partial t} = 2mI_{\mathbf{q}}\mathcal{B}_{\mathbf{q}} + j_{\mathbf{q}}, \tag{5.19}$$

where $I_{\mathbf{q}}$ is a two-row matrix and $j_{\mathbf{q}}$ is a two-component column

$$I_{\mathbf{q}} = \begin{pmatrix} J(\mathbf{0}) & J(\mathbf{q}) \\ -J(\mathbf{q}) & -J(\mathbf{0}) \end{pmatrix},$$

$$j_{\mathbf{q}} = \frac{2m}{\sqrt{N}}\sum_{\mathbf{k}} \begin{pmatrix} \varepsilon(\mathbf{k}-\mathbf{q}) h_{\mathbf{k}-\mathbf{q}}^{\dagger} h_{\mathbf{k}} \\ -\varepsilon(\mathbf{k}+\mathbf{q}) h_{\mathbf{k}}^{\dagger} h_{\mathbf{k}+\mathbf{q}} \end{pmatrix}.$$

Now we can construct the equation of motion of the spin-wave Green's function by differentiating the expression for $\langle\langle \mathcal{B}_{\mathbf{q}} | \mathcal{B}_{\mathbf{q}}^{\dagger} \rangle\rangle$ first with respect to t and then with respect to t'. In the Fourier representation this leads to a pair of coupled equations

$$(\omega - 2mI_{\mathbf{q}})\langle\langle \mathcal{B}_{\mathbf{q}} | \mathcal{B}_{\mathbf{q}}^{\dagger} \rangle\rangle_{\omega} = \langle [\mathcal{B}_{\mathbf{q}}, \mathcal{B}_{\mathbf{q}}^{\dagger}] \rangle + \langle\langle j_{\mathbf{q}} | \mathcal{B}_{\mathbf{q}}^{\dagger} \rangle\rangle_{\omega} ,$$

$$\langle\langle j_{\mathbf{q}} | \mathcal{B}_{\mathbf{q}}^{\dagger} \rangle\rangle_{\omega} (\omega - 2mI_{\mathbf{q}}) = \langle [j_{\mathbf{q}}, \mathcal{B}_{\mathbf{q}}^{\dagger}] \rangle + \langle\langle j_{\mathbf{q}} | j_{\mathbf{q}}^{\dagger} \rangle\rangle_{\omega} . \quad (5.20)$$

The equation for $\langle\langle \mathcal{B}_{\mathbf{q}} | \mathcal{B}_{\mathbf{q}}^{\dagger} \rangle\rangle$ can be transformed into a Dyson equation with the polarization operator expressed in terms of the Green's function of the currents as follows:

$$\Pi(\mathbf{q}, \omega) = \frac{1}{2m} \langle\langle j_{\mathbf{q}} | j_{\mathbf{q}}^{\dagger} \rangle\rangle_{\omega} \tau_z . \quad (5.21)$$

As a result we obtain

$$D(\mathbf{q}, \omega) = \frac{2m}{\omega - 2mI_{\mathbf{q}} - \Pi(\mathbf{q}, \omega)} \tau_z , \quad (5.22)$$

where

$$\Pi(\mathbf{q}, \omega) = 2m \frac{1}{N} \sum_{\mathbf{k}\mathbf{k}'} \chi_{\mathbf{q}\mathbf{k}\mathbf{k}'}(\omega) \times \begin{pmatrix} \varepsilon(\mathbf{k} - \mathbf{q})\varepsilon(\mathbf{k}' - \mathbf{q}) & \varepsilon(\mathbf{k} - \mathbf{q})\varepsilon(\mathbf{k}') \\ -\varepsilon(\mathbf{k})\varepsilon(\mathbf{k}' - \mathbf{q}) & -\varepsilon(\mathbf{k})\varepsilon(\mathbf{k}') \end{pmatrix} . \quad (5.23)$$

Here, we have introduced the two-particle Green's function of holes

$$\chi_{\mathbf{q}\mathbf{k}\mathbf{k}'}(\omega) = \langle\langle h_{\mathbf{k}-\mathbf{q}}^{\dagger} h_{\mathbf{k}} | h_{\mathbf{k}'}^{\dagger} h_{\mathbf{k}'-\mathbf{q}} \rangle\rangle_{\omega} . \quad (5.24)$$

The standard decoupling procedure yields

$$\chi_{\mathbf{q}\mathbf{k}\mathbf{k}'}(\omega) = \chi_{\mathbf{q}\mathbf{k}}(\omega)\delta_{\mathbf{k}\mathbf{k}'} ,$$

where

$$\chi_{\mathbf{q}\mathbf{k}}(\omega) = \int \mathrm{d}\omega_1 \, \mathrm{d}\omega_2 \, \frac{f(\omega_1) - f(\omega_2)}{\omega + \omega_1 - \omega_2 + \mathrm{i}\delta} A(\mathbf{k} - \mathbf{q}, \omega_1) A(\mathbf{k}, \omega_2) . \quad (5.25)$$

Thus, the self-energy part of the magnon, $\Pi(\mathbf{q}, \omega)$, is expressed in terms of integrals of the spectral density of the hole Green's function. The poles of the Green's function (5.22) determine the spin-wave frequencies $\omega_{\mathbf{q}}$ renormalized by the interaction with the holes.

5.3 Néel temperature

We have not yet defined the parameter m, the average sublattice magnetization. Just as in the theory of a Heisenberg magnet [92], this parameter should by defined as

$$m = \frac{1}{2} - \frac{1}{N} \sum_{\mathbf{q}} \langle s_{\mathbf{q}}^{-} s_{\mathbf{q}}^{+} \rangle , \quad (5.26)$$

where the spin correlator is expressed in terms of the corresponding element of the matrix Green's function

$$\langle s_{\mathbf{q}}^{-} s_{\mathbf{q}}^{+} \rangle = \int \mathrm{d}\omega \, \frac{-(1/\pi) \operatorname{Im} \langle\langle \mathcal{B}_{\mathbf{q}} | \mathcal{B}_{\mathbf{q}}^{\dagger} \rangle\rangle_{\omega}^{11}}{\exp(\beta\omega) - 1} . \quad (5.27)$$

Earlier we found that for a two-dimensional antiferromagnet, the incoherent states contribute to the hole spectral density. Now we employ approximation (4.41) for the spectral density and ignore the pole contribution. $\Pi(\mathbf{q}, \omega)$ becomes independent of $\mathbf{q}$ and Eqn (5.27) becomes

$$\frac{1}{(2m)^2} = \frac{1}{N} \sum_{\mathbf{q}} \frac{J(\mathbf{0}) - (zt/2)^2 \chi(T, \delta)}{\omega_{\mathbf{q}}} \coth\left(\frac{\omega_{\mathbf{q}}}{2T}\right) . \quad (5.28)$$

From equation (5.22), which determines the poles of the Green's function, we can easily derive an expression for the renormalized spin-wave frequencies of the lowest order in m

$$\omega_{\mathbf{q}} = 2m\omega_{\mathbf{q}}^{0} \left[1 - \frac{zt^2}{4J} \chi(T, \delta)\right] . \quad (5.29)$$

In both equations, (5.28) and (5.29), the quantity

$$\chi(T, \delta) = -\int \mathrm{d}\omega_1 \, \mathrm{d}\omega_2 \, \frac{f(\omega_1) - f(\omega_2)}{\omega_1 - \omega_2} A(\omega_1) A(\omega_2) \quad (5.30)$$

depends on the temperature and hole concentration. By substituting (5.29) into Eqn (5.28) and expanding the result in powers of m, we arrive at an equation for the sublattice magnetization

$$m^2 = \frac{3}{4C_{\xi}} \frac{T_{\mathrm{N}}(\delta) - T}{T_{\mathrm{N}}(\delta)} , \quad (5.31)$$

where the Néel temperature T_{N} is given by the equation

$$\frac{T_{\mathrm{N}}(\delta)}{T_{\mathrm{N}}(0)} = 1 - \frac{zt^2}{4J} \chi\big[T_{\mathrm{N}}(\delta), \delta\big] , \quad (5.32)$$

with $T_{\mathrm{N}}(0)$ the Néel temperature for the state where the band is exactly half-filled:

$$T_{\mathrm{N}}(0) = \frac{2J}{C_{\xi}} , \qquad C_{\xi} = \frac{1}{N} \sum_{\mathbf{q}} \left[1 - \frac{J(\mathbf{q})}{J(\mathbf{0})}\right]^{-1} . \quad (5.33)$$

For a two-dimensional antiferromagnet, C_{ξ} is logarithmically divergent and yields a zero Néel temperature, as expected. If we assume that the layers interact and select $J(\mathbf{q})$ in the form (5.18), for small values of ξ we have $C_{\xi} \sim \ln(1/\xi)$, which remains finite for all finite values of ξ.

Clearly, (5.18) vanishes for extremely low hole concentrations. Indeed, for an estimate we can set

$$\chi\big(T_{\mathrm{N}}(\delta), \delta\big) \sim \Pi_{\mathrm{ii}} \sim \frac{\delta}{zt} \ln \frac{zt}{2J} .$$

Then (5.32) immediately provides an estimate for the critical concentration

$$\delta_{\mathrm{c}} \approx \frac{J}{t} \frac{1}{\ln(zt/2J)} \ll 1 . \quad (5.34)$$

Using approximation (4.41) for the spectral density of incoherent states in evaluating the integrals in (5.30) and passing to the limit of extremely low concentrations $\Gamma\delta/T \ll 1$, we find that

$$\chi(T, \delta) \approx \frac{\delta}{\Gamma} \ln \frac{2\Gamma}{T} . \quad (5.35)$$

With this estimate in mind, we can write Eqn (5.32) for $T_N(\delta)$ as follows:

$$\delta = \frac{J\Gamma}{t^2}\,\frac{1 - T_N(\delta)/T_N(0)}{\ln\left[2\Gamma/T_N(0)\right] - \ln\left[T_N(\delta)/T_N(0)\right]}\,. \tag{5.36}$$

The results of solving this equation numerically are depicted in Fig. 14. We see that in the important region of the parameter the Néel temperature $T_N(\delta)$ decreases with increasing concentration. The critical hole concentration $\delta_c = 0.04$ for values of parameters typical of high-T_c materials. This is in good agreement with the experimental data of Rossat-Mignot et al. [94] and Shirane [95]. Finally, we note that the spin-wave spectrum in the $t-t'-J$ model was thoroughly studied by Onufrieva et al. [98].

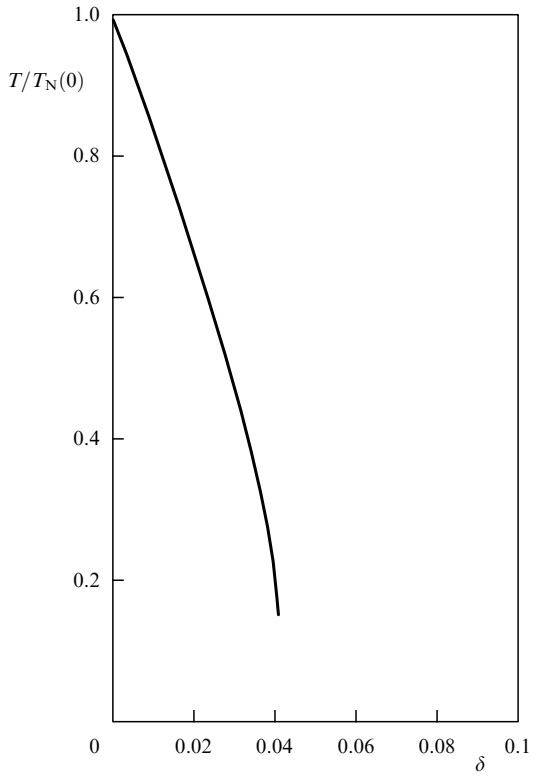

Figure 14. Dependence of the Néel temperature on hole concentration as obtained by solving Eqn (5.36) at $t = 0.5$ eV, $2J/t = 0.2$, $\Gamma = 2\sqrt{3}\,t$, and $T_N = 2J/3$ [50].

6. Gage fields for the two-dimensional $t-J$ model

6.1 Slave-boson representation for the spin liquid

When the hole concentration is above the critical value ($\delta > \delta_c$), the system loses its long-range antiferromagnetic order and becomes a spin liquid [100]. The system's ground state in this case may prove ferromagnetic, but at high temperatures the strongly correlated system falls into a state with large magnetic and charge fluctuations and behaves in an unusual manner. Several approaches to describing such a special state have been suggested, among which, we believe, the one based on introducing gage fields is the most consistent [101–113]. The idea of such an approach was proposed by Baskaran and Anderson [114].

In this case, researchers most often use the slave-boson representation for the X-operators describing the correlated motion of electrons in the lattice. We write the operator $X_i^{0\sigma}$ in the form of a product of the Fermi ($f_{i\sigma}$) and Bose (b_i) operators:

$$X_i^{0\sigma} = f_{i\sigma} b_i^{\dagger} \tag{6.1}$$

with the additional condition that

$$\sum_{\sigma} f_{i\sigma}^{\dagger} f_{i\sigma} + b_i^{\dagger} b_i = 1\,, \tag{6.2}$$

which guarantees that no 'doublons' appear at the sites. Since the spin label of the electron is transferred to the Fermi operator, the representation is called slave-boson, with the Bose operator describing the creation of a hole. The $t-J$ model becomes equivalent to a system of interacting fermions and bosons, and the partition function can be written in the form of a functional integral over Grassmann ($f_{i\sigma}$ and $f_{i\sigma}^*$) and complex-valued (b_i and b_i^*) fields [102]:

$$Z = \int \delta\lambda_i\,\delta b_i\,\delta b_i^*\,\delta f_{i\sigma}\,\delta f_{i\sigma}^* \exp\left[-\int_0^{\beta} (\mathcal{L}_0 + H)\,\mathrm{d}\tau\right], \tag{6.3}$$

$$\mathcal{L}_0 = \sum_{i\sigma} f_{i\sigma}^* \left(\frac{\partial}{\partial\tau} - \mu\right) f_{i\sigma} + \sum_i b_i^* \frac{\partial}{\partial\tau}\, b_i + \\ + \sum_i \lambda_i \left(\sum_{\sigma} f_{i\sigma}^* f_{i\sigma} + b_i^* b_i - 1\right), \tag{6.4}$$

$$H = -t \sum_{ij\sigma} f_{i\sigma}^* f_{j\sigma} b_i\, b_j^* + \frac{J}{2} \sum_{ij} f_{i\sigma}^* f_{j\sigma} f_{j\sigma'}^* f_{i\sigma'}\,. \tag{6.5}$$

Here (6.5) coincides with Hamiltonian (2.9) in the slave-boson representation. Below we ignore the fourth-order term $b_i^* b_i b_j^* b_j$, since the hole concentration is assumed to be low. $\mathcal{L}_0$ is the Lagrangian of a system of independent fermions and bosons; it incorporates the chemical potential μ, which takes into account the conservation of the number of holes, and the local Lagrangian multiplier λ_i, which takes into account constraint (6.2).

Further transformation of the functional integral is standard: the fourth-order terms f^*ff^*f and f^*fb^*b are transformed into the bilinear terms f^*f and b^*b by applying the Hubbard–Stratonovich identity, which introduces integration with respect to the complex variables χ_{ij} and η_{ij}. This yields the following result for Z:

$$Z = \int \delta\lambda_i\,\delta\chi_{ij}\,\delta\chi_{ij}^*\,\delta\eta_{ij}\,\delta\eta_{ij}^*\,\delta b_i\,\delta b_i^*\,\delta f_{i\sigma}\,\delta f_{i\sigma}^* \\ \times \exp\left[-\int_0^{\beta} \mathcal{L}(\tau)\,\mathrm{d}\tau\right] \tag{6.6}$$

with the linearized Lagrangian

$$\mathcal{L} = \mathcal{L}_0 - \frac{J}{2}\,\eta_{ij} f_{i\sigma}^* f_{j\sigma} + t\chi_{ij} b_i b_j^* + \text{c.c.} \\ + \frac{J}{2}\left(\eta_{ij}\chi_{ij}^* + \eta_{ij}^*\chi_{ij}\right) - J\chi_{ij}\chi_{ij}^*\,.$$

The gage-field integration is achieved by the stationary-point method. We start by representing the fields in the

following form:

$$\lambda_i = \mathrm{i}\lambda_0 + a_0(\mathbf{r}_i)\,,$$
$$\chi_{ij} = \chi_0 \exp(\mathrm{i}\vartheta_{ij})\,, \qquad \eta_{ij} = \eta_0 \exp(\mathrm{i}\vartheta_{ij})\,. \tag{6.7}$$

Thereby, we assume that we are dealing with a homogeneous state in which λ_0 and the amplitudes χ_0 and η_0 are independent of coordinates. The quantities $a_0(\mathbf{r}_i)$ and ϑ_{ij} describe a perturbation of the gage fields. The stationary point $(\lambda_0, \chi_0, \eta_0)$ corresponds to the mean-field approximation with a Lagrangian $\mathcal{L}_{\mathrm{MF}}$. We write the total Lagrangian in the form of a sum of two terms $\mathcal{L} = \mathcal{L}_{\mathrm{MF}} + \mathcal{L}_{\mathrm{f}}$, where $\mathcal{L}_{\mathrm{f}}$ describes the contribution of fluctuations above the mean field

$$\mathcal{L}_{\mathrm{f}} = \sum_{i\sigma} f_{i\sigma}^* \left[\frac{\partial}{\partial\tau} - \mu_{\mathrm{F}} + \mathrm{i}a_0(\mathbf{r}_i)\right] f_{i\sigma}$$
$$+ \sum_i b_i^* \left[\frac{\partial}{\partial\tau} - \mu_{\mathrm{F}} + \mathrm{i}a_0(\mathbf{r}_i)\right] b_i -$$
$$- \frac{J}{2}\eta_0 \sum_{ij} \exp(\mathrm{i}\vartheta_{ij}) f_{i\sigma}^* f_{j\sigma} + t\chi_0 \sum_{ij} \exp(\mathrm{i}\vartheta_{ij})\, b_i^* b_j\,. \tag{6.8}$$

Clearly, (6.8) is invariant under a gage transformation of the field on the lattice:

$$f_{i\sigma} \to f_{i\sigma} \exp(\mathrm{i}\phi_i)\,, \qquad b_i \to b_i \exp(\mathrm{i}\phi_i)\,,$$
$$\vartheta_{ij} \to \vartheta_{ij} + \phi_i - \phi_j\,, \qquad a(\mathbf{r}_i) \to a(\mathbf{r}_i) - \frac{\partial\phi_i}{\partial\tau}\,. \tag{6.9}$$

Later we will see that long-wavelength fluctuations play an important role in the system, so that in what follows we use the continuum approximation. Then instead of the phase ϑ_{ij} depending on two lattice sites that are nearest neighbors, we can introduce a vector $\mathbf{a}(\mathbf{r})$ depending on one point $\mathbf{r} = (\mathbf{r}_i + \mathbf{r}_j)/2$. We define this vector as follows:

$$\vartheta_{ij} = (\mathbf{r}_i - \mathbf{r}_j)\mathbf{a}\left(\frac{\mathbf{r}_i + \mathbf{r}_j}{2}\right).$$

As a result, the Lagrangian becomes [103, 104]

$$\mathcal{L} = \int \mathrm{d}^2\mathbf{r} \left[\sum_\sigma f_\sigma^*(\mathbf{r})\left(\frac{\partial}{\partial\tau} - \mu_{\mathrm{F}} + \mathrm{i}a_0\right) f_\sigma(\mathbf{r})\right.$$
$$+ b^*(\mathbf{r})\left(\frac{\partial}{\partial\tau} - \mu_{\mathrm{B}} + \mathrm{i}a_0\right) b(\mathbf{r})$$
$$- \frac{1}{2m_{\mathrm{F}}} \sum_{\sigma\alpha} f_\sigma^*(\mathbf{r})\left(\frac{\partial}{\partial x_\alpha} + \mathrm{i}a_\alpha\right)^2 f_\sigma(\mathbf{r})$$
$$\left. - \frac{1}{2m_{\mathrm{B}}} \sum_\alpha b^*(\mathbf{r})\left(\frac{\partial}{\partial x_\alpha} + \mathrm{i}a_\alpha\right)^2 b(\mathbf{r})\right]. \tag{6.10}$$

Here, we have introduced the effective fermion and boson masses (in place of the parameters t and J) according to the relations $1/m_{\mathrm{B}} = 2Ja^2$ and $1/m_{\mathrm{F}} = 2ta^2$, where a is the lattice parameter. The Lagrangian obtained as a result of the above transformations of the functional integral can be considered a phenomenological Lagrangian for a system of fermions and bosons interacting through the gage fields a_0 and $\mathbf{a}$. The gage invariance of the Lagrangian is of the type

$$f_\sigma \to f_\sigma \exp(\mathrm{i}\theta)\,, \qquad b \to b\exp(\mathrm{i}\theta)\,,$$
$$\mathbf{a} \to \mathbf{a} + \nabla\theta\,, \qquad a_0 \to a_0 - \frac{\partial\theta}{\partial\tau}\,, \tag{6.11}$$

where θ is a function of $\mathbf{r}$ and τ.

To clarify the physical meaning of the fluctuations described by the gage fields $\mathbf{a}$, we study the correlation function

$$P_{1234} = \left\langle f_{1\alpha}^\dagger f_{2\alpha} f_{2\beta}^\dagger f_{3\beta} f_{3\gamma}^\dagger f_{4\gamma} f_{4\delta}^\dagger f_{1\delta}\right\rangle$$

defined at four points, 1, 2, 3, and 4, that form a plaquette on a square lattice. We set up the following combination:

$$\left\langle P_{1234} - P_{1432}\right\rangle = \chi_0^4 \left\langle \exp\left[\mathrm{i}(\vartheta_{12} + \vartheta_{23} + \vartheta_{34} + \vartheta_{41})\right] - \text{c.c.}\right\rangle, \tag{6.12}$$

which, being a gage invariant, may serve as an order parameter. On the other hand, one can easily verify that

$$P_{1234} - P_{1432} = 2\mathrm{i}\left[(2-\rho_2)E_{134} + (2-\rho_4)E_{123}\right.$$
$$\left. + (2-\rho_3)E_{124} - \rho_1 E_{234}\right], \tag{6.13}$$

where $\rho_i = \sum_\alpha f_{i\alpha}^\dagger f_{i\alpha}$ is the fermion density operator, and

$$E_{123} = \mathbf{S}_1\left[\mathbf{S}_2 \times \mathbf{S}_3\right] \tag{6.14}$$

is the chirality operator for the triangular plaquette with vertices at points 1, 2, and 3. This operator violates spatial parity and invariance with respect to time reversal. It plays an important role in the chiral theory of spin liquid, where the average value of $\langle E_{123}\rangle$ in the ground state is finite. If $\langle E_{123}\rangle \neq 0$, then, in view of (6.13), the average over the square plaquette traversed clockwise and counterclockwise is also finite. Thus, (6.12) shows that the fluctuations of the gage fields in model (6.10) are related to the fluctuations in the chirality of plaquettes on a two-dimensional lattice.

Now, let us discuss the limits of model (6.10). This Lagrangian represents a system of fermions and bosons interacting via the gage fields a_0 and $\mathbf{a}$. It describes fluctuations above the homogeneous average field introduced by (6.7), in which the fluctuations of the quantities λ_0, χ_0, and η_0 are coordinate-independent. For these quantities, we derive the self-consistency equations from the condition that the Lagrangian at the stationary point is at its minimum [104]. Here, we assume that the Bose system, represented by the quantities b_i and b_i^*, is at a temperature that is higher than the temperature T_{B} of Bose–Einstein condensation, so that $b = 0$. At $T = 0$, we must allow for the fact that $b \neq 0$. Minimization yields

$$b^2 = \delta\,.$$

The homogeneous state under consideration is stable if $t\delta > cJ$, where c is a dimensionless quantity of order unity. Thus, at moderate hole concentrations and $T = 0$, the ground state is a Fermi liquid with large chirality fluctuations (as we know, at small values of δ a Néel type antiferromagnetic state arises). Lee and Nagaosa [104] called the state that exists at $T > T_{\mathrm{B}}$ a 'strange metal'. In this state, chirality fluctuations play the main role in the formation of the excited-state spectrum.

6.2 Collective mode

Let us now study the system at $T > T_B$ in greater detail. The integration in (6.10) over the Grassmann variables makes it possible to obtain an effective action that is gage-field-dependent. Isolating the term incorporating the vector fields $\mathbf{a}(\mathbf{r})$, and limiting discussion to the terms that are quadratic in these fields, we arrive at the following expression for the effective action:

$$\int_0^\beta d\tau\, \mathcal{L}_f(\tau) = T\sum_{\omega_n}\int d^2\mathbf{q}\; a_\alpha(\mathbf{q},\omega_n)\Pi_{\alpha\beta}(\mathbf{q},\omega_n)a_\beta(\mathbf{q},\omega_n)\,, \tag{6.15}$$

where

$$\Pi_{\alpha\beta}(\mathbf{q},\omega_n) = \int d^2\mathbf{k}\left\{\frac{f[\varepsilon(\mathbf{k}+\mathbf{q}/2)]-f[\varepsilon(\mathbf{k}-\mathbf{q}/2)]}{i\omega_n-\varepsilon(\mathbf{k}+\mathbf{q}/2)+\varepsilon(\mathbf{k}-\mathbf{q}/2)}\frac{\partial\varepsilon}{\partial q_\alpha}\frac{\partial\varepsilon}{\partial q_\beta} + \frac{\partial^2\varepsilon}{\partial q_\alpha\partial q_\beta}f[\varepsilon(\mathbf{k})]\right\}. \tag{6.16}$$

This result, obviously, corresponds to the random-phase approximation (RPA) in the theory of interacting fermions. At low frequencies and momenta, we have

$$\Pi_{\alpha\beta}(\mathbf{q},\omega_n) = \left(\delta_{\alpha\beta}-\frac{q_\alpha q_\beta}{q^2}\right)\left(\frac{\pi|\omega_n|}{v_F q}+\chi_F q^2\right), \tag{6.17}$$

where v_F is the velocity at the Fermi surface, and χ_F is the diamagnetic susceptibility in Landau's Fermi-liquid theory.

The functional integral (6.6) with the effective action (6.15) makes it possible to write the Green's function for the fluctuations of the gage field

$$D_{\alpha\beta}(\mathbf{r},\tau) = \langle Ta_\alpha(\mathbf{r},\tau)a_\beta(\mathbf{0},0)\rangle\,. \tag{6.18}$$

Combining (6.15) and (6.17), which determine the temperature Green's function, and performing the analytic continuation $i\omega_n \to \omega$, we arrive at the following expression for the retarded Green's function [101]:

$$D_{\alpha\beta}(\mathbf{q},\omega) = \frac{\delta_{\alpha\beta}-q_\alpha q_\beta/q^2}{i\pi\omega/v_F q+\chi_F q^2}\,. \tag{6.19}$$

This expression corresponds to a non-propagator relaxation collective mode, which is mediating the indirect fermion–boson interaction in the system. Already in the first-order approximation the interaction between the fermions and the fluctuation mode (6.19) leads to anomalies of the transport properties of the system, and in particular, to a linear temperature dependence of electrical resistivity, observed in the normal phase of high-T_c superconductors. We note for the sake of reference that the behavior of the system below the Bose-condensation temperature, and in particular, at $T = 0$ was studied in detail by Tikofsky and Laughlin [113], who applied the anion superconductivity technique.

6.3 Magnetic susceptibility

A detailed study of the magnetic properties of the two-dimensional $t-J$ model near the critical concentration was made by Tanamoto et al. [110]. They used the slave-boson representation of the electron operators (6.1) and then wrote the Hamiltonian in the mean-field approximation:

$$H_{MF} = \sum_{ij\sigma}(F_{ij}^* f_{i\sigma}^\dagger f_{j\sigma} + \text{c.c.}) - \lambda_F\sum_{i\sigma} f_{i\sigma}^\dagger f_{i\sigma} + \sum_{ij}(B_{ij}^* b_i^\dagger b_j + \text{c.c.}) - \lambda_B\sum_i b_i^\dagger b_i\,, \tag{6.20}$$

where

$$F_{ij} = -t\langle b_i^\dagger b_j\rangle + \frac{J}{2}\sum_\sigma\langle f_{i\sigma}^\dagger f_{j\sigma}\rangle\,, \qquad B_{ij} = -t\sum_\sigma\langle f_{i\sigma}^\dagger f_{j\sigma}\rangle\,, \tag{6.21}$$

$$\lambda_F = \mu+\lambda+(1-\delta)J\,, \qquad \lambda_B = \lambda\,. \tag{6.22}$$

This Hamiltonian describes a system of independent fermions (spinons) and bosons (holons) coupled by the effective parameters F_{ij} and B_{ij} of the hops of these particles on the lattice. The quantities λ_F and λ_B act as the chemical potentials of spinons and holons.

In approximating the initial Hamiltonian of the $t-J$ model by (6.20), we replaced the local constraint by a global one, with the result that the Lagrangian multiplier λ_i lost its dependence on the lattice site. We will deal below only with spatially homogeneous states corresponding to Hamiltonian (6.20). The energies of the spinons and holons, the quasiparticles of the model, then, are given by the following expressions:

$$\varepsilon_F(\mathbf{k}) = 2F(\cos k_x+\cos k_y)\,, \qquad \varepsilon_B(\mathbf{k}) = 2B(\cos k_x+\cos k_y)\,, \tag{6.23}$$

where F and B are the values of F_{ij} and B_{ij} for nearest neighbors. Thus, the relationships (6.21) written for the nearest neighbors constitute a system of self-consistent equations for the quantities F and B. These equations must be augmented by the equations that express the law of conservation of the number of electrons and constraint (6.2) averaged over the Gibbs ensemble. As is known, the mean-field approximation would be exact if we could label the electronic states by the index $\sigma = 1, 2, \ldots, N_F$ (color) in the $N_F \to \infty$ limit. In our case the spin index assumes only two values, with the result that Eqns (6.21) are certainly approximate. We are left to believe that their solutions belong to the same universal class as the solutions in the $N_F \to \infty$ limit. Equations (6.22) and (6.23) determine the large Fermi surface for quasiparticles (as well as for free particles). The reader will recall that in the case of low hole concentrations we used a different approximation, the slave-fermion representation (the magnetic-polaron concept), which yielded the small Fermi surface for quasiparticles: four pockets near the points $(\pm\pi/2, \pm\pi/2)$. At $\delta > \delta_c$ all antiferromagnetic correlations are suppressed, so that we are dealing with an entirely different state of the system (a spin liquid). Since δ_c amounts to several percent for meaningful values of the model parameters, we can assume that the slave-boson representation is correct (and this means that the mean-field approximation is correct, too) when $\delta \gtrsim 0.1$. The transitional region between the spin-polaron and spin-liquid states cannot be described in terms of auxiliary particles.

As in the case with the Hubbard model, the random-phase approximation makes it possible to apply the slave-boson representation to the Hamiltonian of the $t-J$ model and

obtain the dynamic magnetic susceptibility [110]

$$\chi(\mathbf{q},\omega)=\frac{\chi_0(\mathbf{q},\omega)}{1+J(\mathbf{q})\chi_0(\mathbf{q},\omega)}\,, \tag{6.24}$$

where

$$\chi_0(\mathbf{q},\omega)=\sum_{\mathbf{k}}\frac{f(\xi_{\mathbf{k}+\mathbf{q}})-f(\xi_{\mathbf{k}})}{\omega+\xi_{\mathbf{k}}-\xi_{\mathbf{k}+\mathbf{q}}+\mathrm{i}\delta}\,. \tag{6.25}$$

Here, $J(\mathbf{q})=J(\cos q_x+\cos q_y)$, and $\xi_{\mathbf{k}}=\varepsilon_{\mathrm{F}}(\mathbf{k})-\lambda_{\mathrm{F}}$. The quantity $\chi_0(\mathbf{q},\omega)$ is the dynamic susceptibility of the system described by Hamiltonian (6.20), i.e., a system of independent fermions. However, the width of their band depends on the temperature and hole concentration through the parameter F. Note that (6.24) has the same structure as the RPA susceptibility in the Hubbard model. In the latter case, instead of $J(\mathbf{q})$, we have the parameter U of Coulomb attraction at a site and the spectrum of independent electrons in the lattice instead of the fermion spectrum $\xi_{\mathbf{k}}$. These differences lead to substantial differences in the behavior of the magnetic susceptibility in the $t-J$ model and in the Hubbard model.

Here are the results of the numerical studies of Eqns (6.21)–(6.25) made by Tanamoto et al. [110]. Figures 15 and 16 depict the dc magnetic susceptibility as a function of the wave vector and temperature. In their numerical calculations, they used the typical ratio of the model parameters t and J, i.e., $t=4J$. Figure 15a clearly shows that there is a sharp increase in magnetic susceptibility near the point $\mathbf{q}=\mathbf{Q}$ for $\chi_0(\mathbf{q},\omega)$ in the concentration interval $\delta=0.10-0.15$, while Fig. 15b shows a sharp increase in susceptibility at $\mathbf{q}=\mathbf{Q}$, which suggests the onset of an unstable non-magnetic state.

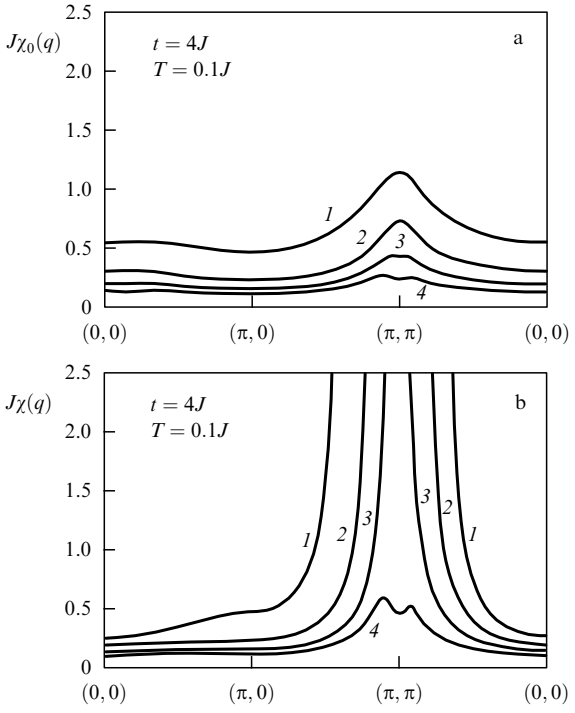

Figure 15. The **q**-dependence of the dc spin susceptibility (a) $\chi_0(\mathbf{q})$ and (b) $\chi(\mathbf{q})$ for different values of δ [110]: (*1*) $\delta=0$, (*2*) $\delta=0.05$, (*3*) $\delta=0.10$, and (*4*) $\delta=0.15$.

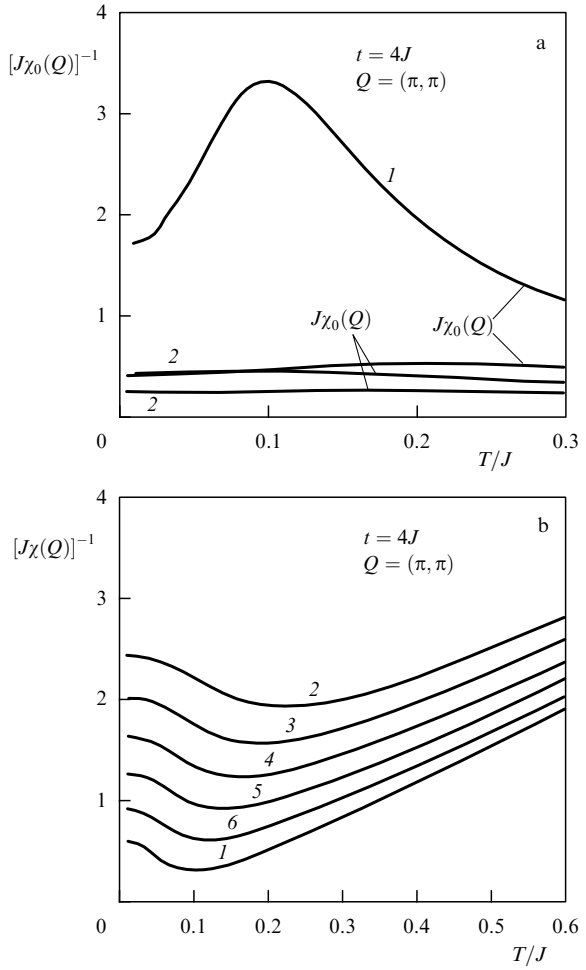

Figure 16. Temperature dependence of the dc spin susceptibility (a) $\chi_0(\mathbf{q})$ and (b) $\chi(\mathbf{q})$ at $\mathbf{q}=\mathbf{Q}$ for different values of δ [110]: (*1*) $\delta=0.10$, (*2*) $\delta=0.15$, (*3*) $\delta=0.14$, (*4*) $\delta=0.13$, (*5*) $\delta=0.12$, and (*6*) $\delta=0.11$.

At low δ and T, the magnetic susceptibility $\chi(\mathbf{q})$ diverges at a point near $\mathbf{q}=\mathbf{Q}$, which indicates instability with respect to the formation of an incommensurate antiferromagnetic structure. This divergence disappears as δ grows, although the maximum $\chi(\mathbf{q},0)$ rapidly decreases. Thus, in the concentration interval $\delta=0.10-0.15$ the system remains non-magnetic at low temperatures. Figure 16a shows that as T rises, the susceptibility reaches its peak value at $\delta=0.10$ but vanishes by $\delta=0.15$. The temperature dependence of the reciprocal susceptibility (Fig. 16b) agrees with the Curie–Weiss law $\chi\propto 1/T$ within a broad temperature range, but $\chi(\mathbf{q},0)$ at $\mathbf{q}=\mathbf{0}$ is virtually temperature-independent. Thus, in the spin-liquid state under consideration the system behaves like a Pauli magnet in a uniform field, while in a non-uniform field ($\mathbf{q}=\mathbf{Q}$) it behaves like a magnetic material with localized magnetic moments.

Now let us investigate the frequency dependence of $\chi(\mathbf{q},\omega)$. The spectral density of the spin excitations is determined by the quantity

$$\operatorname{Im}\chi(\mathbf{q},\omega)=\frac{\operatorname{Im}\chi_0(\mathbf{q},\omega)}{\left[1+J(\mathbf{q})\operatorname{Re}\chi_0(\mathbf{q},\omega)\right]^2+\left[J(\mathbf{q})\operatorname{Im}\chi_0(\mathbf{q},\omega)\right]^2}\,, \tag{6.26}$$

where

$$\operatorname{Im}\chi_0(\mathbf{q},\omega)=\pi\sum_{\mathbf{k}}\delta\big[\varepsilon_{\mathrm{F}}(\mathbf{k}+\mathbf{q})-\varepsilon_{\mathrm{F}}(\mathbf{k})-\omega\big]\times\big[f\big(\varepsilon_{\mathrm{F}}(\mathbf{k})-\lambda_{\mathrm{F}}\big)-f\big(\varepsilon_{\mathrm{F}}(\mathbf{k})+\omega-\lambda_{\mathrm{F}}\big)\big]\,. \quad (6.27)$$

Equation (6.27) shows that $\operatorname{Im}\chi_0(\mathbf{q},\omega)$ has a peak near $\mathbf{q}=\mathbf{q}_{\mathrm{M}}$, where $\mathbf{q}_{\mathrm{M}}$ is the nesting vector. The peak shifts as ω increases, and at $\omega\sim 2|\lambda_{\mathrm{F}}|$ the peak is at $\mathbf{q}=\mathbf{Q}$, so that in this case there is effective nesting at $\mathbf{q}=\mathbf{Q}$. The frequency dependence $\chi(\mathbf{q},\omega)$ at $\mathbf{q}=\mathbf{Q}$ the wave vector $\mathbf{Q}$ is depicted in Fig. 17 for two values of δ. In both cases at low temperatures there is no low-frequency branch of spin fluctuation, as if there were a gap in the spectrum of collective motions of the spin system. The phenomenon can be explained if we write (6.27) as

$$\operatorname{Im}\chi_0(\mathbf{q},\omega)=\frac{\pi}{2}\,\rho\left(\frac{\omega}{2}\right)\left[f\left(|\lambda_{\mathrm{F}}|-\frac{\omega}{2}\right)-f\left(|\lambda_{\mathrm{F}}|+\frac{\omega}{2}\right)\right], \quad (6.28)$$

where $\rho(\omega)$ is the spinon density of states. From this equation we find that at low temperatures $\operatorname{Im}\chi_0(\mathbf{Q},\omega)$ is extremely small when $|\omega|<2|\lambda_{\mathrm{F}}|$. When $\omega\sim 2|\lambda_{\mathrm{F}}|$, this quantity rapidly increases, as Fig. 17 suggests. As the temperature grows, the pseudo-gap in the spectrum becomes smeared. Moreover, as δ grows, the cut-off frequency in the spectrum increases but the peak's height decreases considerably.

Suppression of the low-frequency portion of the spectrum of fluctuations at low temperatures was discovered in the studies of inelastic neutron scattering in high-T_{c} materials. The problem has been intensively discussed in a number of theoretical papers, but, as suggested by Tanamoto et al. [110], the phenomenon is not related to a true pseudo-gap in the spectrum; rather it is a direct consequence of violation of nesting at $\mathbf{q}=\mathbf{Q}$ in the case of low hole concentrations.

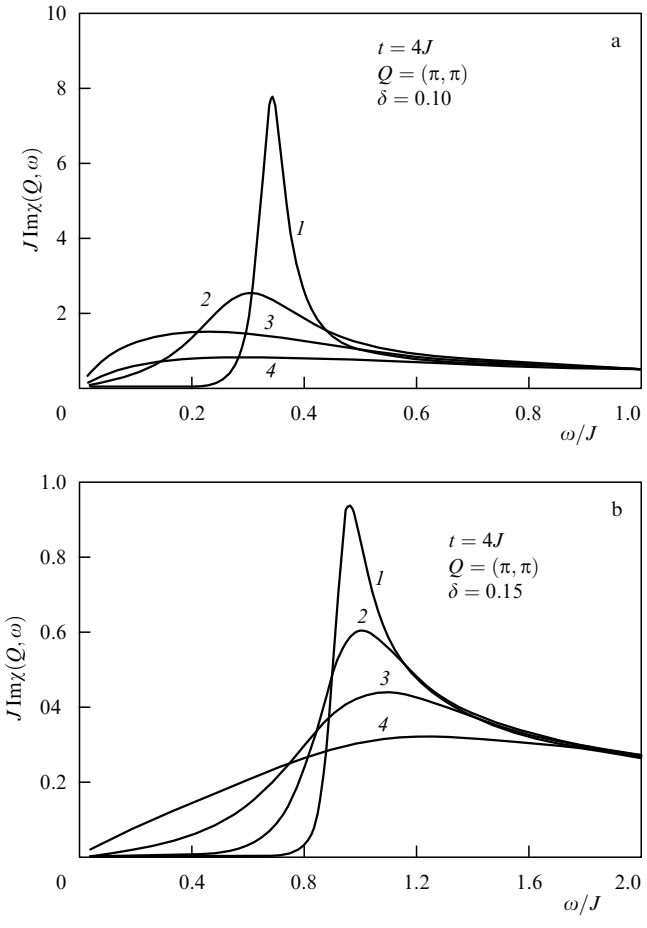

Figure 17. The ω-dependence of $\operatorname{Im}\chi(\mathbf{Q},\omega)$ at (a) $\delta=0.10$ and (b) $\delta=0.15$ [110]: (*1*) $T=0.02J$, (*2*) $T=0.05J$, (*3*) $T=0.10J$, and (*4*) $T=0.20J$.

7. Phase diagram

7.1 Phase separation

Up to this point we have assumed that spatially homogeneous phases are realized in the system, irrespective of the type of magnetic order; the electron density was assumed constant at each point. Simple physical considerations, however, suggest that separation of the system into phases with different electron (hole) densities is possible. The idea of phase separation in the Hubbard model was first suggested in the earlier works of Nagaev [115] and Visscher [116], and was then realized in the $t-J$ model by Ioffe and Larkin [117] and Emery et al. [118]. The tendency toward phase separation at large values of J can be realized from simple physical ideas. If a hole is introduced into an antiferromagnet, the exchange energy grows by zJ. For two holes separated by a large distance the energy variation amounts to $2zJ$, but for holes that are nearest neighbors the variation is only $2(z-1)J$, which implies that from the standpoint of exchange energy the presence of regions with enhanced hole concentrations is more favorable. Of course, the structure of a separated two-phase system is determined by the minimization of the total energy, i.e., allowing for the hopping energy in the lattice.

In view of the complexity of the problem, numerical results play an important role. The results of the first calculations are depicted in Fig. 18, which shows a phase diagram in the $(n, J/t)$ plane built for a two-dimensional $t-J$ model using an exact diagonalization of a 4×4-cluster [118] and high-temperature expansions up to the tenth order in $1/T$ [119]. The boundary separating the homogeneous and two-phase regions is marked by lozenges (the results of Emery et al. [118]) and by a solid line (the results of Putikka et al. [119]). Clearly, both methods show that the two-phase region occupies a large area in the phase diagram. But the methods yield different results in the region of small values of J and in the vicinity of $n=1$. According to Putikka et al. [119], near half-filling separation occurs at $J/t\gtrsim 1$, in contrast to the

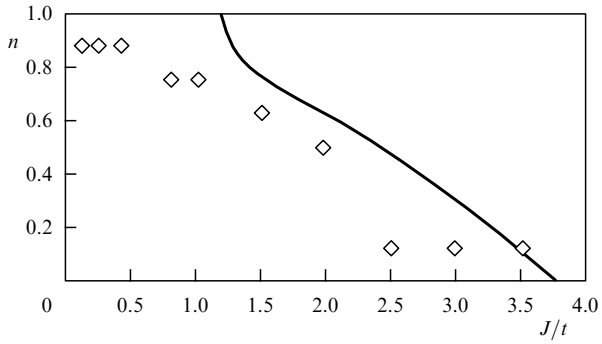

Figure 18. Phase diagram for the two-dimensional $t-J$ model [2].

results of Emery et al. [118]. Dagotto et al. [120] re-examined the calculations and concluded that the points in Fig. 18 should be interpreted not as a line that outlines the phase-separation region, but as the edge of the region where holes couple into pairs rather than into clusters, which is the case for large values of J. Fehske et al. [121] and Prelovsek and Zotos [122] arrived at similar conclusions using large clusters.

The results of studies of the problem of two or more holes forming bound states can be found in Refs [123 – 126]. Prior to the numerical calculations made in [123], Poilblanc [126] and Chernyshev et al. [127] studied the problem of the interaction of two holes in an antiferromagnetic matrix by variational methods, with the wave function incorporating five states: a hole at a site and at each of the four nearest neighbors. The solution of the two-particle Bethe – Salpeter equation revealed that there can be bound states of two holes of d and p types, with the binding energy (considered as a function of J/t) being in good agreement with Eder's results of numerical calculations [129]. For small values of J, such as $t/J \gtrsim 2-3$, there are no bound states. Poilblanc [123] showed, using clusters consisting of up to 26 sites, that below J_c ($J/t > 0.5$) four particles can form stable bound states; with a further decrease in J ($J/t > 0.02$), these bound states are replaced by bound states of hole pairs of d symmetry. Thus, within the $0.02 < J/t < J_c$ interval, a system of holes introduced into an antiferromagnetic matrix is a liquid consisting of bound aggregates of four or two holes, depending on the size of J. For $J/t < 0.02$, the hole liquid is in the paramagnetic state, which, at very small values of J, is replaced by the ferromagnetic state. Thus, if the hole concentration is kept constant and J increases starting at small values, the hole liquid first consists of bound pairs, of bound fours, etc., and finally phase separation sets in. The fact that there is a ferromagnetic state at extremely small values of J is corroborated by the high-temperature expansion [130] and by phase separation [119].

The results of Poilblanc [123] refer to the case of extremely high hole concentrations, $\delta \approx 0.15$, where at $T = 0$ there can be no long-range order. To establish the effect of short-range magnetic order, Poilblanc [123] calculated the dc magnetic susceptibility. A high peak near the point (π, π) was discovered, and it was found that this peak could be used to estimate the radius of short-wavelength magnetic correlations. This radius amounted to approximately three lattice constants; within such a length a pair of holes behaves as if it were in an antiferromagnetic matrix. These short-wavelength spin fluctuations generate an attraction between holes, binding them into pairs, fours, etc.

The question of whether bound states are formed in the $t-J$ model at extremely high hole concentrations (low electron densities) was studied by Hellberg and Manousakis [131], who used the quantum Monte Carlo method, and Kagan and Rice [132] and Chubukov [133], who used analytic methods. Phase separation emerges at $J/t \gtrsim 3.5$. As the J/t ratio becomes smaller, a phase with bound s type electron pairs emerges, which is replaced by a phase with d type pairs, and then, at $J/t \lesssim 1$, with p type pairs. No stable bound clusters with a larger number of particles appear at any values of J/t.

7.2 From the Hubbard model to the $t-J$ model

When dealing with the Heisenberg model, researchers often use a semiclassical approach based on investigating the limit of large atomic spin ($S \gg 1$), expanding the result in power series in $1/S$, and formally putting $S = 1/2$. One realization of this approach is the Goldstein – Primakoff formalism, in which the spin operators are approximately replaced by the Bose operators of spin deviations. A number of researchers [134 – 136] applied this formalism to the $t-J$ model, with the Hubbard X operators expressed approximately in terms of the Bose and Fermi operators via a formal expansion in powers of $1/\mathcal{N}$, where $\mathcal{N}$ is the number of electrons allowed at a site (in the $t-J$ model proper, this number is one). At the end of all calculations employing such expansions in powers of $1/\mathcal{N}$, one must set $\mathcal{N} = 1$. The problem of the spiral phase in the $t-J$ model was studied using this approach. Shraiman and Siggia [137] were the first to discover that under deviations from the half-filled state the Néel antiferromagnetic order may be distorted by long-wave modulations, so that there emerges a spiral structure with a wave vector $\mathbf{Q}$ diminished by a quantity proportional to the hole concentration. Similar results were obtained using other approaches [138 – 144]. We use the semiclassical approximation of Psaltakis and Papanicolaou [136] to examine this problem.

When discussing the magnetic phase diagram of the $t-J$ model, one must employ the phase diagram of the Hubbard model, since in the $U \gg W$ limit the two must correspond. Note that in deriving the $t-J$-model Hamiltonian from the Hubbard model the three-center terms, which may produce specific effects, are ignored.

Here we discuss only some aspects of the problem of comparing the phase diagram of the $t-J$ model with that region in the phase diagram of the Hubbard model where $U \gg W$. We begin by examining the question of how the Néel temperature T_N depends on the Coulomb repulsion U when the weak-correlation mode $U \ll W$ is transformed into the strong-correlation mode $U \gg W$. The studies of this question are numerous; here we list the numerical results for the half-filled state in the Hubbard model obtained through the exact diagonalization of small clusters [145] (the light circles in Fig. 19). The dark circles in Fig. 19 represent the results of earlier QMC calculations [146]. The dashed curve was obtained for $U \ll W$ by the mean-field method, which leads to an equation in T_N

$$\frac{1}{U} = \frac{1}{N}\sum_{\mathbf{k}} \frac{\tanh\left[\varepsilon(\mathbf{k})/2T_N\right]}{2\varepsilon(\mathbf{k})}\,, \tag{7.1}$$

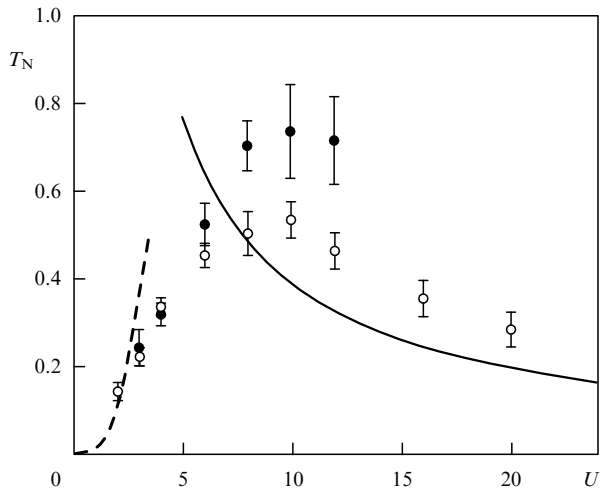

Figure 19. Néel temperature T_N as a function of U for the Hubbard model [145].

and the solid curve was obtained from high-temperature expansions for the Heisenberg model with the exchange integral $J = 2t^2/U$. All this leads to the following result:

$$T_N = 3.8\,\frac{t^2}{U}\,. \tag{7.2}$$

The theoretical curves may be interpreted as the asymptotes of the true curve describing the crossover from the weak-correlation mode to the strong-correlation mode. When $U \gg W$, Eqn (7.2), which refers to the $t-J$ model at $n = 1$, describes a behavior that agrees qualitatively with the behavior of the Hubbard model in the corresponding region.

Another aspect in which the two models must be compared is the phase diagram in the $(U/t, n)$ plane at $T = 0$ (Fig. 20) [138]. We selected this paper because, in addition to an antiferromagnetic phase, existing in particular at $n = 1$ for all U, a special phase was discovered in the $U \gg W$ region: the short-range-order paramagnetic (SRO-P) phase. Trapper et al. [138] used the slave-boson four-field representation of Kotliar and Ruckenstein [139] and the saddle-point method in the functional integral for the partition function. This approach yielded results for different electron and magnetic properties of the model that were found to be in good agreement with those yielded by the numerical methods of exact diagonalization of small clusters and the QMC method. Trapper et al. [138] developed a procedure for introducing a short-range order into the saddle-point method. This resulted in considerable changes in the phase diagram in the $U \gtrsim W$ range. Instead of the ferromagnetic phase that is often present when $U \gg W$ and $\delta \ll 1$, there is a paramagnetic phase with short-range order. This phase proves to be locally stable with respect to phase separation.

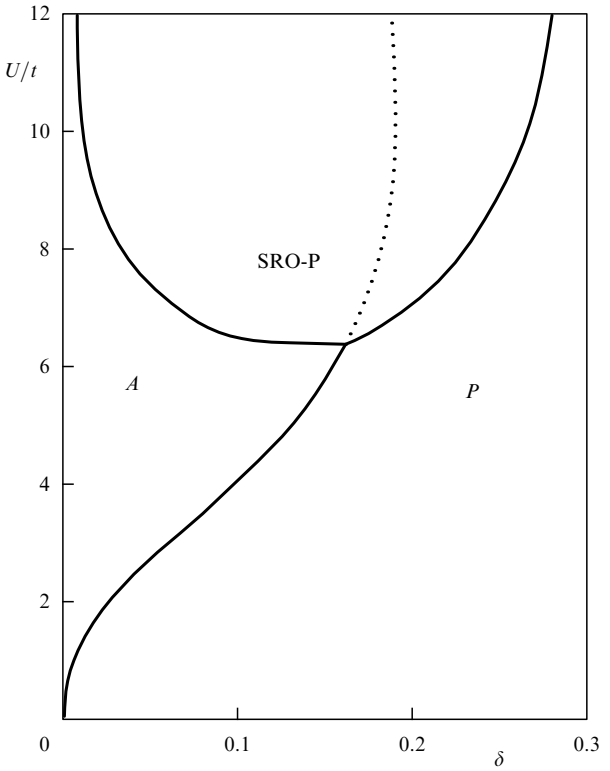

Figure 20. Phase diagram at $T = 0$ for the Hubbard model with a paramagnetic-phase with short-range order [138].

Because of the presence of this phase the antiferromagnetic region shrinks in comparison to the case where short-range order is ignored. However, the new boundary of the antiferromagnetic-phase region agrees with the results discussed in Section 5. For instance, at $U/t = 8$ the critical concentration is $\delta_c \sim 0.03$.

The phase diagram in Fig. 20 must be considered a typical example in which only the basic outlines have common features, which depend only a little on the adopted approximations. In other approximations other phases may emerge in the $(U/t, n)$ plane, e.g., a spiral phase, a ferromagnetic phase, or a region of phase separation. The question of the full phase diagram of the Hubbard model, or even the $t-J$ model, has yet to be resolved. In this situation one should rely more on numerical calculations, say, the method of exact diagonalization of small clusters or the QMC method, than on analytic methods.

8. Conclusion

This review's objective was to make a systematic study of the $t-J$ model chiefly near the half-filled states in two-dimensional space ($d = 2$). Such a choice of topic reflects the mainstream of research, which focuses primarily on studying high-T_c compounds of the metal-oxide group. The progress made in understanding the main properties of the model is due to the exhaustive nature of the studies, in which numerical methods, primarily the exact diagonalization of small clusters and the QMC method, are used together with analytic methods. The results of numerical studies can be found in Dagotto's well-known review [7], which also contains a detailed comparison with the experimental data on high-T_c compounds. For this reason the present review focuses on the analytic approaches.

It should be noted that, in view of the complexity of the Hamiltonian of the $t-J$ model, there can be no universal mathematical approach that describes the model over a broad range of the parameters t, J, n, and T. The model Hamiltonian can be expressed quite simply as a quadratic form of the Hubbard X operators. However, this simplicity is misleading because of the complexity of the commutation relations for the X operators. For this reason the X operators are usually expressed in the form of a product of Fermi and Bose operators augmented by certain constraints that reflect simple physical conditions: when U is large, each site can carry not more than one electron. This procedure realizes a specific representation of the algebra of X operators, but there can be many such representations, which means that the obtained effective Hamiltonians are ambiguous. Choosing a specific representation *a priori* is poorly justified; the meaningfulness of the choice is only determined by the soundness of the physical results. Experience has revealed that at low concentrations, $\delta < \delta_c$, i.e., when the antiferromagnetic state is realized, the slave-fermion representation is adequate, while at high concentrations, $\delta > \delta_c$, in the spin-liquid state, slave-boson representations are more effective.

In the first case the effective Hamiltonian is of the Fröhlich type, in which the fermions interact with spin waves. This leads to the formation of a magnetic polaron, a quasiparticle transferring electric charge. The second case usually leads to a representation in which fermions and bosons interact with each other through gage fields emerging from the constraints. In this case a collective relaxation mode emerges in the system; this mode determines the dynamics of

the entire system in the spin-liquid state. These two regions of the phase diagram, the antiferromagnetic state and the spin-liquid state, are the most firmly established regions for the $t-J$ model.

As for the magnetic-polaron problem, most researchers agree that the Fermi surface of the holes forms four pockets centered at the points $(\pm\pi/2, \pm\pi/2)$ of reciprocal space. The width of the band of quasiparticle states is of the order of J, and we have the following estimate for the intensity of the quasiparticle peaks: $Z \sim J/t$. Moreover, there exists a broad region of incoherent states, whose width is of order zt, which corresponds to the excitation of the internal structure of the polaron. These incoherent states provide the main contribution to one of the dynamic response functions, the magnetic susceptibility. This pattern appears in SCBA and is corroborated by numerical methods. The spin-liquid region corresponding to hole concentrations $\delta > \delta_c$, where antiferromagnetic order is suppressed, is characterized by the presence of chirality fluctuations. Both regions correspond to the doped states of high-T_c compounds. The different transport properties of the $t-J$ model in these states provide a satisfactory description of many physical properties of high-T_c compounds (see Dagotto's review [7]).

The above picture is true in the region where $\delta \ll 1$ and $J \ll t$. As J increases, new phenomena emerge: the holes begin to couple into pairs, then into fours, and finally, at $J \sim t$, phase separation sets in, with the holes grouping into clusters with ferromagnetic local order that are incorporated in the antiferromagnetic lattice free from holes. Thus, in a certain part of the phase diagram in the $(J/t, n)$ plane there exists a region with attraction between holes, which binds them into pairs. Condensation of these pairs would mean the emergence of a superconducting state. The problem of superconductivity in the $t-J$ model is under intense study. We do not discuss the problem here because it merits a separate large review. The results of early research can be found in reviews [9, 7], and the current results can be found in Refs [147 – 174]. An idea that is currently being developed is that the interaction between holes through spin fluctuations leads to a superconducting state in the $t-J$ model with a d type symmetry of the order parameter and a T_c of several tens of kelvins (see the most recent papers [175 – 180]).

Although the behavior of the $t-J$ model in a broad interval of electron concentrations $0 < n < 1$ is less important in the problem of high-T_c compounds, it is undoubtedly of interest from the theoretical standpoint. The central problem here is the description of the crossover, as the electron concentration increases, from itinerant magnetism to the mode with localized magnetic moments. The problem has been studied by applying the diagrammatic technique with X operators (see monograph [181]). The technique was used to develop a generalized random-phase approximation (GRPA) [182 – 185], with which it was shown that starting at a certain critical concentration $n_c \sim 0.6$, the dynamic magnetic susceptibility of the model contains both contributions: both the Pauli contribution, which is temperature-independent, and the Curie – Weiss contribution, which is proportional to $1/T$. The latter suggests that localized magnetic moments are formed in the process. The results were presented in our review [9]. We believe it important that other methods, especially molecular dynamics numerical methods or the method of exact diagonalization of small clusters, be used in corroborating these results.

References

1. Hubbard J *Proc. R. Soc. London Ser. A* **276** 238 (1963)
2. Hubbard J *Proc. R. Soc. London Ser. A* **281** 401 (1964)
3. Izyumov Yu A *Usp. Fiz. Nauk* **165** 403 (1995) [*Phys. Usp.* **38** 385 (1995)]
4. Herring C, in *Magnetism* IV (Eds G T Rado, H Suhl) (New York: Academic, 1966)
5. Anderson P W *Phys. Rev.* **115** 2 (1959)
6. Anderson P W *Science* **235** 1196 (1987)
7. Dagotto E *Rev. Mod. Phys.* **66** 763 (1994)
8. Zhang F C, Rice T M *Phys. Rev. B* **37** 3759 (1988)
9. Izyumov Yu A *Usp. Fiz. Nauk* **161** (11) 1 (1991) [*Sov. Phys. Usp.* **34** 935 (1991)]
10. Harris A B, Lange R V *Phys. Rev.* **157** 295 (1967)
11. Chao K A, Spalek J, Oles A M *J. Phys. C* **10** L271 (1977)
12. Gros C, Joynt R, Rice T M *Phys. Rev. B* **36** 381 (1987)
13. Hubbard J *Proc. R. Soc. London Ser. A* **285** 542 (1965); **296** 82 (1967)
14. Barnes S E *J. Phys. F* **6** 1375 (1976); **7** 2637 (1977)
15. Coleman P *Phys. Rev. B* **29** 3035 (1984)
16. Read N, Newns D M *J. Phys. C* **16** 3273 (1983)
17. Kotliar G, Ruckenstein A E *Phys. Rev. Lett.* **57** 1362 (1986)
18. Lee P A, Nagaosa N *Phys. Rev. B* **46** 5621 (1992)
19. Zou Z, Anderson P W *Phys. Rev. B* **37** 627 (1988)
20. Richard J L, Yushankhai V Yu *Phys. Rev. B* **47** 1103 (1993)
21. Wang Y R, Rice M J *Phys. Rev. B* **49** 4360 (1994)
22. Khaliullin G *Pis'ma Zh. Eksp. Teor. Fiz.* **52** 999 (1990) [*JETP Lett.* **52** 389 (1990)]
23. Wang Y R *Phys. Rev. B* **51** 234 (1995)
24. Loos J *Phys. Rev. B* **53** 12556 (1996)
25. Chang Z *Phys. Rev. B* **53** 1171 (1996)
26. Le Guillou J C, Ragoucy E *Phys. Rev. B* **52** 2403 (1995)
27. Arrigoni E, Strinati G C *Phys. Rev. B* **52** 2428 (1995)
28. Bulaevskiĭ L N, Khomskiĭ D I *Zh. Eksp. Teor. Fiz.* **52** 1603 (1967) [*Sov. Phys. JETP* **25** 1067 (1967)]
29. Bulaevskiĭ L N, Nagaev É L, Khomskiĭ D I *Zh. Eksp. Teor. Fiz.* **54** 1562 (1968) [*Sov. Phys. JETP* **27** 836 (1968)]
30. Brinkman W F, Rice T M *Phys. Rev. B* **2** 1324 (1970)
31. Metzner W, Schmit P, Vollhardt D *Phys. Rev. B* **45** 2237 (1992)
32. Metzner W, Vollhardt D *Phys. Rev. Lett.* **62** 324 (1989)
33. Strack R, Vollhardt D *Phys. Rev. B* **46** 13852 (1992)
34. Mohan M M *J. Phys.: Condens. Matter* **3** 4307 (1991)
35. Dagotto E et al. *Phys. Rev. B* **41** 9049 (1990)
36. Vlaming R, Vollhardt D *Phys. Rev. B* **45** 4637 (1992)
37. Lifshitz I M *Adv. Phys.* **13** 483 (1964)
38. Horsch P et al. *Physica C* **162 – 164** 783 (1989)
39. Horsch P *Helv. Phys. Acta* **63** 346 (1990)
40. Trugman S A *Phys. Rev. B* **41** 892 (1990)
41. von Szczepanski K J et al. *Phys. Rev. B* **41** 2017 (1990)
42. Sega I, Prelovsek P *Phys. Rev. B* **42** 892 (1990)
43. Dagotto E, Riera J *Phys. Rev. Lett.* **70** 682 (1993)
44. Inoue J, Maekawa S *J. Phys. Soc. Jpn.* **59** 2110 (1990)
45. Liu Z, Manousakis E *Phys. Rev. B* **45** 2425 (1992)
46. Marsiglio F et al. *Phys. Rev. B* **43** 10882 (1991)
47. Kane C L, Lee P A, Read N *Phys. Rev. B* **39** 6880 (1989)
48. Martinez G, Horsch P *Phys. Rev. B* **44** 317 (1991)
49. Plakida N M, Oudovenko V S, Yushankhai V Yu *Phys. Rev. B* **50** 6431 (1994)
50. Richard J L, Yushankhai V Yu *Phys. Rev. B* **50** 12927 (1994)
51. Richard J L, Yushankhai V Yu *Phys. Rev. B* **47** 1103 (1993)
52. Jian-Xin Li, Chang-De Gong *Phys. Rev. B* **51** 6343 (1995)
53. Igarashi J, Fulde P *Phys. Rev. B* **45** 12357 (1992)
54. Khaliullin G, Horsch P *Phys. Rev. B* **47** 463 (1993)
55. Schmitt-Rink S, Varma C M, Ruckenstein A E *Phys. Rev. Lett.* **60** 2793 (1988)
56. Tserkovnikov Yu A *Teor. Mat. Fiz.* **7** 250 (1971); **49** 219 (1981) [*Theor. Math. Phys.* **49** 993 (1981)]
57. Ramsak A, Horsch P *Phys. Rev. B* **48** 10559 (1993)
58. de Alcantara Bonfim O F, Reiter G, in *High Temperature Superconductivity* (Eds J Ashkenazi et al.) (New York: Plenum Press, 1991)
59. Igarashi J, Fulde P *Phys. Rev. B* **48** 998 (1993)
60. Sherman A, Schreiber M *Phys. Rev. B* **48** 7492 (1993)

61. Varma C M et al. *Phys. Rev. Lett.* **63** 1996 (1989)
62. Nagaev É L *Zh. Eksp. Teor. Fiz.* **54** 228 (1968) [*Sov. Phys. JETP* **27** 122 (1968)]
63. Nagaev É L *Fizika Magnitnykh Poluprovodnikov* (The Physics of Magnetic Semiconductors) (Moscow: Nauka, 1979)
64. Sabczynski J, Schreiber M, Sherman A *Philos. Mag. B* **65** 881 (1992)
65. Sabczynski J, Schreiber M, Sherman A *Phys. Rev. B* **48** 543 (1993)
66. Nagaoka Y *Phys. Rev.* **147** 392 (1966)
67. Pines D, in *Polarons and Excitons* (Eds C G Kuper, D Wkitfield) (Edinburgh: Oliver and Boyd, 1962)
68. Barentzen H *Phys. Rev. B* **53** 5598 (1996)
69. Barentzen H *Z. Phys. B* **94** 161 (1994)
70. Barentzen H, Wrobel P *Z. Phys. B* **93** 375 (1994)
71. Dagotto E, Nazarenko A, Boninsegni M *Phys. Rev. Lett.* **73** 728 (1994)
72. Bulut N, Scalapino D J, White S R *Phys. Rev. B* **50** 7215 (1994)
73. Tanamoto T, Kohno H, Fukuyama H *J. Phys. Soc. Jpn.* **62** 717 (1993)
74. Benard P, Chen L, Tremblay A M S *Phys. Rev. B* **47** 15217 (1993)
75. Si Q et al. *Phys. Rev. B* **47** 9055 (1993)
76. Lee P A *Phys. Rev. Lett.* **63** 680 (1989)
77. Tohyama T, Maekawa S *Phys. Rev. B* **49** 3596 (1994)
78. Gooding R J, Vos K J E, Leung P W *Phys. Rev. B* **50** 12866 (1994)
79. Lavagna M, Stemmann G *Phys. Rev. B* **49** 4235 (1994)
80. Bala J, Oles A M, Zaanen J *Phys. Rev. B* **52** 4597 (1995)
81. Deeg M, Fehske H, Buttner H *Europhys. Lett.* **26** 109 (1994)
82. Deeg M, Fehske H *Phys. Rev. B* **50** 17874 (1994)
83. Deeg M et al. *Z. Phys. B* **95** 87 (1994)
84. Chubukov A V, Musaelian K A *Phys. Rev. B* **50** 6238 (1994)
85. Lin H Q, Hirsch J E *Phys. Rev. B* **35** 3359 (1987)
86. Duffy D, Moreo A *Phys. Rev. B* **52** 15607 (1995)
87. Kotliar G, Ruckenstein A E *Phys. Rev. Lett.* **57** 1362 (1986)
88. Li T, Wolfle P, Hirschfeld P J *Phys. Rev. B* **40** 6817 (1989)
89. Horsch P, Stephan W *Phys. Rev. B* **48** 10595 (1993)
90. Belinicer V I, Chernyshew A L, Shubin V A *Phys. Rev. B* **53** 335 (1996)
91. Eskes H, Oles A M *Phys. Rev. Lett.* **73** 1279 (1994)
92. Tyablikov S V *Metody Kvantovoĭ Teorii Magnetizma* (Methods in the Quantum Theory of Magnetism) (Moscow: Nauka, 1964) [Translated into English (New York: Plenum Press, 1967)]
93. Richard J L, Yushankhai V Yu *Physica C* **235–240** 2193 (1994)
94. Rossat-Mignot J et al. *Physica C* **185–189** 86 (1991)
95. Shirane G *Physica C* **185–189** 80 (1991)
96. Belkasri A, Richard J L *Phys. Rev. B* **50** 12896 (1994)
97. Sherman A, Schreiber M *Phys. Rev. B* **50** 12887 (1994)
98. Onufrieva F P, Kushnir V P, Toperverg B P *Phys. Rev. B* **50** 12935 (1994)
99. Tusch M A, Szczech Y H, Logan D E *Phys. Rev. B* **53** 5505 (1996)
100. Ioffe L B, Larkin A I *Int. J. Mod. Phys. B* **2** 203 (1988)
101. Ioffe L B, Larkin A I *Phys. Rev. B* **39** 8988 (1989)
102. Grilli M, Kotliar G *Phys. Rev. Lett.* **64** 1170 (1990)
103. Nagaosa N, Lee P A *Phys. Rev. Lett.* **64** 2450 (1990)
104. Lee P A, Nagaosa N *Phys. Rev. B* **46** 5621 (1992)
105. Liu Yu-Liang, Su Zhao-Bin *Phys. Rev. B* **48** 13018 (1993)
106. Ioffe L B, Kalmeyer V *Phys. Rev. B* **44** 750 (1991)
107. Ioffe L B, Wiegmann P *Phys. Rev. Lett.* **65** 653 (1990)
108. Ioffe L B, Kotliar G *Phys. Rev. B* **42** 10348 (1990)
109. Wen X G, Wilczek F, Zee A *Phys. Rev. B* **39** 11413 (1989)
110. Tanamoto T, Kuboki K, Fukuyama H *J. Phys. Soc. Jpn.* **60** 3072 (1991)
111. Sa de Melo C A R, Wang Z, Doniach S *Phys. Rev. Lett.* **68** 2078 (1992)
112. Raykin M *Phys. Rev. B* **51** 3856 (1995)
113. Tikofsky A M, Laughlin R B *Phys. Rev. B* **50** 10165 (1994)
114. Baskaran G, Anderson P W *Phys. Rev. B* **37** 580 (1988)
115. Nagaev É L *Zh. Eksp. Teor. Fiz.* **54** 228 (1968) [*Sov. Phys. JETP* **27** 122 (1968)]
116. Visscher P B *Phys. Rev. B* **10** 943 (1974)
117. Ioffe L B, Larkin A I *Phys. Rev. B* **37** 5730 (1988)
118. Emery V J, Kivelson S A, Lin H Q *Phys. Rev. Lett.* **64** 475 (1990)
119. Putikka W O, Luchini M, Rice T M *Phys. Rev. Lett.* **68** 538 (1992)
120. Dagotto E et al. *Phys. Rev. B* **45** 10741 (1992)
121. Fehske H et al. *Phys. Rev. B* **44** 8473 (1991)
122. Prelovsek P, Zotos X *Phys. Rev. B* **47** 5984 (1993)
123. Poilblanc D *Phys. Rev. B* **52** 9201 (1995)
124. Hasegawa Y, Poilblanc D *Phys. Rev. B* **40** 9035 (1989)
125. Poilblanc D, Riera J, Dagotto E *Phys. Rev. B* **49** 12318 (1994)
126. Poilblanc D *Phys. Rev. B* **49** 1477 (1994)
127. Chernyshev A L, Dotsenko A V, Sushkov O P *Phys. Rev. B* **49** 6197 (1994)
128. Sushkov O P *Solid State Commun.* **83** 303 (1992)
129. Eder R *Phys. Rev. B* **45** 319 (1992)
130. Putikka W O, Luchini M U, Ogata M *Phys. Rev. Lett.* **69** 2288 (1992)
131. Hellberg C S, Manousakis E *Phys. Rev. B* **52** 4639 (1995)
132. Kagan M Yu, Rice T M *J. Phys.*: *Condens. Matter* **6** 3771 (1994)
133. Chubukov A V *Phys. Rev. B* **48** 1097 (1993)
134. Marder M, Papanicolaou N, Psaltakis G C *Phys. Rev. B* **41** 6920 (1990)
135. Angelucci A, Sorella S *Phys. Rev. B* **47** 8858 (1993)
136. Psaltakis G C, Papanicolaou N *Phys. Rev. B* **48** 456 (1993)
137. Shraiman B T, Siggia E D *Phys. Rev. Lett.* **62** 1564 (1989)
138. Trapper U, Ihle D, Fehske H *Phys. Rev. B* **52** R11553 (1995)
139. Kotliar G, Ruckenstein A E *Phys. Rev. Lett.* **57** 1362 (1986)
140. Zhou C, Schulz H J *Phys. Rev. B* **52** R11557 (1995)
141. Yoshioka D *J. Phys. Soc. Jpn.* **58** 1516 (1989)
142. Jayaprakash C, Krishnamurthy H R, Sarker S *Phys. Rev. B* **40** 2610 (1989)
143. Flensberg K et al. *Phys. Rev. B* **40** 850 (1989)
144. Chakraborty B et al. *Phys. Rev. B* **42** 4819 (1990)
145. Scalettar R T et al. *Phys. Rev. B* **39** 4711 (1989)
146. Hirsch J E *Phys. Rev. B* **35** 1851 (1987)
147. Puig-Puig L, Lopez-Aguilar F *Phys. Rev. B* **52** 17143 (1995)
148. Abrahams E et al. *Phys. Rev. B* **52** 1271 (1995)
149. Mierzejewski M, Zielinski J *Phys. Rev. B* **52** 3079 (1995)
150. Batista C D, Lema F, Aligia A A *Phys. Rev. B* **52** 6223 (1995)
151. Altshuler B L, Ioffe L B, Millis A J *Phys. Rev. B* **53** 415 (1996)
152. Belinicher V I et al. *Phys. Rev. B* **51** 6076 (1995)
153. Quinlan S M, Hirschfeld P J, Scalapino D J *Phys. Rev. B* **53** 8575 (1996)
154. Brawner D A, Ott H R *Phys. Rev. B* **53** 8249 (1996)
155. Maly J, Liu D Z, Levin K *Phys. Rev. B* **53** 6786 (1996)
156. Franz M et al. *Phys. Rev. B* **53** 5795 (1996)
157. Radtke R J et al. *Phys. Rev. B* **53** 5137 (1996)
158. Beal-Monod M T, Maki K *Phys. Rev. B* **53** 5775 (1996)
159. Xu J H, Ren Y, Ting C S *Phys. Rev. B* **53** R2991 (1996)
160. Nazarenko A, Dagotto E *Phys. Rev. B* **53** R2987 (1996)
161. Zeyher R, Kulic M L *Phys. Rev. B* **53** 2850 (1996)
162. Normand B, Kohno H, Fukuyama H *Phys. Rev. B* **53** 856 (1996)
163. Tanaka Y, Kashiwaya S *Phys. Rev. B* **53** R11957 (1996)
164. Shimahara H, Matsuo S, Nagai K *Phys. Rev. B* **53** 12284 (1996)
165. Xu W, Ren Y, Ting C S *Phys. Rev. B* **53** 12481 (1996)
166. Hayn R et al. *Phys. Rev. B* **53** 11714 (1996)
167. Kuklov A B, Krakovsky A, Birman J L *Phys. Rev. B* **52** R7002 (1995)
168. Hwang E H, Das Sarma S *Phys. Rev. B* **52** R7010 (1995)
169. Xu J H, Ren Y, Ting C S *Phys. Rev. B* **52** 7663 (1995)
170. Bulut N, Scalapino D J *Phys. Rev. B* **53** 5149 (1996)
171. Onufrieva F, Rossat-Mignod J *Phys. Rev. B* **52** 7572 (1995)
172. Carbotte J P et al. *Phys. Rev. B* **51** 11798 (1995)
173. Nazarenko A et al. *Phys. Rev. B* **54** R768 (1996)
174. Heeb R et al. *Phys. Rev. B* **54** 9385 (1996)
175. Terrmann T, Nolting W *Phys. Rev. B* **53** 10579 (1996)
176. Sushkov O P *Phys. Rev. B* **54** 9988 (1996)
177. Khaliullin G, Horsch *Phys. Rev. B* **54** R9600 (1996)
178. Change Z *Phys. Rev. B* **54** 10046 (1996)
179. Zeyher R, Kulic M L *Phys. Rev. B* **54** 8985 (1996)
180. Bala J, Oles A M, Zaanen J *Phys. Rev. B* **54** 10161 (1996)
181. Izyumov Yu A, Katsnel'son M I, Skryabin Yu N *Magnetizm Kollektivizirovannykh Elektronov* (Itinerant Electron Magnetism) (Moscow: Fizmatlit, 1994)
182. Izyumov Yu A, Letfulov B M *J. Phys.*: *Condens. Matter.* **2** 8905 (1990)
183. Izyumov Yu A, Letfulov B M, Shipitsyn E V *J. Phys.*: *Condens. Matter.* **4** 9955 (1992)

184. Izyumov Yu A, Letfulov B M, Shipitsyn E V *J. Phys.: Condens. Matter*. **6** 5137 (1994)
185. Izyumov Yu A, Henderson J A *Int. J. Mod. Phys. B* **8** 1877 (1994)